NTNU – Trondheim
Norwegian University of
Science and Technology

Quantative Analyzes of Seismic Inversion in Terms of Acquisition and Interpretation

Example From Southwest Haltenbanken Area
in the Norwegian Continental Shelf

Haakon Hannasvik Dyrnes

Earth Sciences and Petroleum Engineering
Submission date: June 2012
Supervisor: Egil Tjåland, IPT

Norwegian University of Science and Technology
Department of Petroleum Engineering and Applied Geophysics

Preface

This master`s thesis was carried out by the work of the author from January to June 2012 and constitutes the final work of a 5 year Master of Science education program within the field of Petroleum Technology and Applied Geophysics.

The thesis was made possible by the Leader of the Geophysical Reservoir Monitoring department at Statoil`s research-center (Rotvoll), Mr. Mark Thompson, and by the Principal Researcher Geophysics at Statoil`s research center (Rotvoll), Mr. Andrew Morton. The thesis is a continuation of the work done by the author, autumn 2011. Mr. Thompson acknowledged the need for both the acquisition with the over/under cable combination streamer, and the quantification of the inversion of the different lines and the differences between them. Generous research assistance was provided to the author by numerous persons at the department through the entire extent of the master`s thesis. A special thanks to Dr. Ulrich Theune for great guidance and help in every aspect of the thesis, Mr. Thompson for good ideas and great guidance, Dr. Joachim Mispel for helpful discussions and clarifications on various subjects and to Mr. Andrew Langridge for all your effort in processing of the data and guidance throughout the extent of the thesis.

My formal adviser at NTNU, Associate Professor, Dr. Egil Tjåland has given me continuous feedbacks and help during the project, and has been helpful in with both the academical work and with the motivation for all the other areas of the project. I am grateful for your inputs during the project.

During the last two months of the work, the finishing touches to the thesis were done at an abandoned desk in reading room number 100. Despite the fact that I had forced myself into a reading area where I didn't belong, all the people here welcomed me with open arms and made the end of my career at NTNU the two most memorable months of my study. Thanks to all of you!

A special thanks to the greatest inspiration in my life, and the one person that always believed in me. You have encouraged and motivated me more times then you are aware of. I will always be grateful for what you have done for me and for who you are. Thank you, Kirsti Jektvik.

Trondheim, June 7, 2012

_____

Haakon Dyrnes

Abstract

In regular marine acquisition configuration, shallow sources and shallow streamers are used. Because of this configuration the high-frequency content of the seismic is favored, which is needed for sufficient vertical resolution. If the receivers were deployed at a larger depth the low-frequency content would be favored. The low frequencies are needed for inversion, deep penetration and visualization. However, this configuration would attenuate the higher frequencies and would suffer from poor vertical resolution. The attenuation of either high or low frequencies is a result of the receiver ghost, which attenuates higher frequencies for the deep tow, and lower frequencies for the shallow tow.

Over/under acquisition method allows the wavefield to be separated into upgoing and downgoing wavefields. The configuration consists of 2 receiver-cables in vertical alignment with each other. By detecting only the upgoing wavefield, we are removing the receiver ghost and hence the frequency bandwidth should be broadened. These cables are towed at 18 and 25 meters, respectively. Regular receiver-cables are normally towed at 7 to 9 meters. Because of the deeper tow, the noise levels should also be lowered and result in a better signal to noise ratio.

Post-stack seismic inversion is the process where we analyze the stacked seismic traces and try to reconstruct the velocity structure, or the acoustic impedance, of the sub-surface covered by the seismic. Inversion is sensitive to various parameters and small improvements in the seismic would result in improvements in the inversion volume. In the inversion configuration of this thesis, we are using a background model based on a-priori information from one known well. The a-priori information is used as an initial guess for the inversion to follow.

To keep the inversion volumes as data-driven as possible, the inversions were processed with a weight factor on the initial model as low as possible, to enhance the changes made by the differences in the seismic volumes.

Quantification of the difference in the inversion volumes based on different acquisition methods for the input seismic resulted in various comparisons of the acoustic impedance volumes. Difference in vertical resolution has been investigated and identified to have a relative difference in favor of the single cable seismic. The differences were due to a change in the wavelet shape and width and also change in dominating frequency of the respective time interval. Comparing the inversion volumes, based on the acquisition method, to their respective average inversion volumes identified changes in the inversion volumes due to feathering of the receiver cables. Further tests illustrated that the feathering had a significant impact on the inversion volumes. Since the feathering causes the receiver

cables to deviate from a straight line astern of the vessel, the seismic volume is slightly changed compared to a volume where there is no feathering.

Experiments illustrated that the frequency spectra are different. However, the frequency spectrum is not broadened, but shifted and shortened prone to lower frequencies. Dominating frequency was hence lower for cable combination seismic volumes compared to single cable seismic volumes. This resulted also in difference in the seismic wavelet as previously explained.

Results indicate a significant change in inversion volumes due to fold, acquisition direction and feathering. Changes caused by the cable combination method were not as first anticipated. Since the method is used with a deeper tow, we were anticipating a significant change in the signal to noise ratio, also considering that receiver ghost is removed when evaluating only the upgoing wave. Results indicate that there was no significant change in signal to noise ratio. However, significant changes in the ratio were found when using the split spread method versus the single direction method (both single cable and cable combination method).

This work concludes that the largest impact on the inversion volume is found where we have identified poor alignment of feathering, different acquisition direction and increased fold. The cable combination method doesn't have significant impact on the inversion volume. Identified changes are quantified in this work and will verify these results.

Sammendrag

I vanlig marin seismisk innsamlings-konfigurasjon blir det brukt grunne kilder og grunne streamere. På grunn av denne konfigurasjonen er det høyfrekvente innholdet av seismikken favorisert, noe som er nødvendig for vertikal resolusjon. Dersom mottakerne ble tauet ved en større dybde ville det lavfrekvente innholdet bli favorisert, noe som er nødvendig for inversjon, dypere penetrering og visualisering. Denne konfigurasjonen ville imidlertid dempe de høyere frekvensene og lide av dårlig vertikal oppløsning. Demping av enten høye eller lave frekvenser er et resultat av mottaker-ghosten, som demper høye frekvenser ved dyp tauing av streamerne, og lavere frekvenser ved grunn tauing av streamerne.

Over/under innsamlingsmetoden gjør at bølgefeltet kan deles inn oppadgående og nedadgående bølgefelt. Konfigurasjonen består av 2 mottaker-kabler i vertikal linje med hverandre. Ved å motta kun det oppadgående bølgefeltet, fjerner vi mottaker ghosten og utvider bredden på frekvensspekteret. Disse kablene er slept på henholdsvis 18 og 25 meter. Ved vanlig seismisk innsamlings-konfigurasjon er mottaker-kablene normalt tauet ved 7 til 9 meter. På grunn av dypere slep blir støynivået også senkes og resulterer i et forbedret signal til støyforhold.

Post-stack seismisk inversjon er prosessen der vi analyserer de stackede seismiske traser og prøver å rekonstruere hastighet-strukturen, eller den akustiske impedansen, av undergrunnen dekket av seismikken. Inversjonsprosessen er følsom for flere parametere, og små forbedringer i seismikken resulterer til forbedringer i inversjonsvolumet. Inversjons-konfigurasjonen i denne oppgaven, bruker en bakgrunnsmodell basert på a-priori informasjon fra en kjent brønn. Denne a-priori informasjonen blir brukt som et første gjett som inversjonen følger.

For å holde inversjons-prosessen så datadrevet som mulig ble inversjonene prosessert med en vektfaktor på bakgrunns-modellen så lav som mulig. Dette for å forsterke endringene forskjellene forårsaket av endringene i de seismiske volumene.

Kvantifisering av forskjeller i inversjon-volumene basert på ulike innsamlingsmetoder for input seismikk, resulterte i ulike sammenligninger av de akustisk impedans-volumene. Forskjellen i vertikal resolusjon har blitt undersøkt og identifisert til å ha en relativ forskjell i favør av enkel-kabel seismikk. Forskjellene var på grunn av en endring i bølgeformens form og bredde, og også endring i dominerende frekvens i det aktuelle tidsintervallet. Sammenligning av inversjon volumer, basert på innsamlingsmetode, til deres respektive ”gjennomsnitts-inversjons-volum” identifiserte endringer i inversjon volumene på grunn av at mottakeren-kablene avvek fra en rett linje bak det seismiske fartøyet. Ytterligere tester viste at dette avviket hadde en betydelig innvirkning på inversjon-

volumene. Siden dette forårsaker kablene til å avvike fra en rett linje aktenom fartøyet, er det seismiske volumet litt endret i forhold til et volum der det ikke er observert et slik avvik.

Eksperimenter illustrerte at frekvensområdene for seismiske volumer basert på forskjellig innsamlingsmetode er forskjellige. Imidlertid er frekvensspekteret ikke utvidet, men forskjøvet og forkortet mot lavere frekvenser. Dominerende frekvens er dermed lavere for det seismiske volumet basert på kabelkombinasjons-konfigurasjonen sammenliknet med det seismiske volumet basert på enkelkabel konfigurasjonen. Dette resulterte også i forskjell i den seismiske bølgeformen som tidligere forklart.

Resultatene tyder på en betydelig endring i inversjon-volumer på grunn fold, innsamlings-retning og avvik av mottakerkablene fra en rett linje akterut det seismiske fartøyet. Endringer forårsaket av kabelkombinasjons-konfigurasjonen var ikke som først antatt. Siden metoden er utført med en dypere tauing forventet vi en betydelig endring i signal til støyforholdet, også med tanke på at mottaker-ghosten fjernes ved vurdering av kun den oppadgående bølgen. Resultatene tyder på at det ikke var noen signifikant endring i dette forholdet. Det ble imidlertid funnet betydelige endringer i signal til støyforholdet ved bruk av ”split spread” metoden kontra ”èn retning” metode (både enkel-kabel og kablekombinasjons metoden inngår her).

Dette arbeidet konkluderer med at den største innvirkningen på inversjonsvolumet er funnet der vi har identifisert dårlig overlapping av ”feathering”, motsatt innsamlingsretning og økt fold. Kabel-kombinasjonsmetoden har ikke vesentlig innvirkning på inversjons-volumet. Endringene som er funnet er kvantifisert i dette abeidet og vil verifisere disse resultatene.

Table of Contents

Chapter 1 Introduction

The Kristin Field lies in the south-west area of the Haltenbank, in the Norwegian Sea. It straddles block 6406/2 and block 6505/11 (Technology, 2007). The field is a gas and condensate field and has 12 production wells. The reservoir is located approximately 5000 meter below the seafloor.

The pressure and temperature in the reservoir are higher than any field so far developed off the Norwegian shore, with initial pressure and temperature at 900 bars and 170°C respectively. Because of the high pressure/high temperature conditions of the field, this comes with a great concern regarding production and further development, also taken into account that the field has experienced a higher pressure drop than first precipitated.

Since the reservoir is located at such great depth, the seismic surveys and acquisition of the data is a crucial factor for further development of the field, and the amount of insight to the field`s interior setting. Even though the field is widely covered by prior seismic surveys, there are improvements potential in the seismic. The frequency bandwidth could be improved, the signal to noise ratio could also be better and there are improvement potential in the multiple attenuation. These improvement potentials were part of the reason why the 2008 survey, by Statoil, with an over/under cable combination streamer was completed. The possible benefits of this survey were many. In this paper the author will focus on the benefits of the survey in terms of inversion improvement from regular seismic, and if these are significant.

Throughout the completion of this theses, the different lines from the survey has been inverted, and here we will give attention to difference in frequency bandwidth of the seismic, and to what extent this would benefit the process or not.

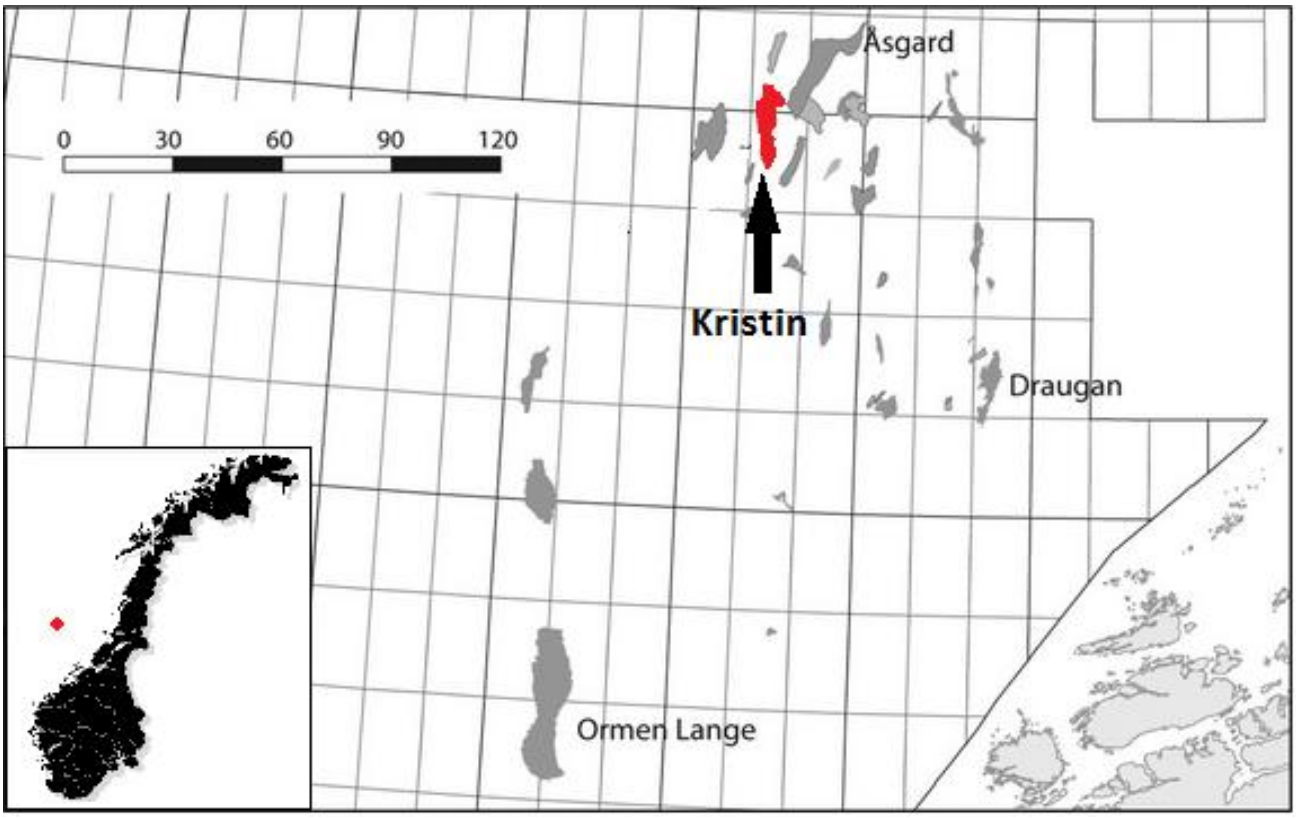

Figure 1 - 1: *Kristin Field`s location in the Norwegian Sea. The biggest island in the bottom right corner is Hitra, which is located in the mid-west coast of Norway.*

1.1 Geology of the area

The Kristin Field is a high-pressure, high-temperature gas condensate field that lies about 200 km off the mid-Norwegian coast, which is in the south-western part of the Halten Bank in the Norwegian Sea. The field came on stream on November 3rd 2005, and has so far been developed with 12 production wells (Statoil, 2007).

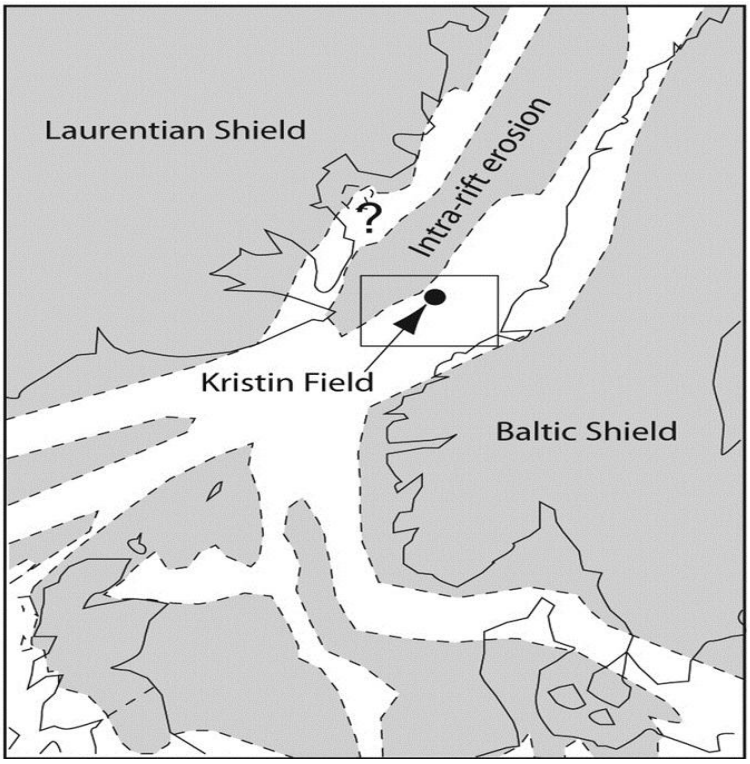

Figure 1 - 2: *The Kristin Field illustrated in a Middle Jurassic Paleographic map* ***(Quin, et al., 2010)****.*

The reservoir of the field is located almost 5000 meter below the sea floor, and pressure and temperature is higher than on any other field so far developed on the Norwegian continental shelf.

The field is a conventional structural trap compromising an elongated north-south horst block. The structure is partly eroded along the northern part of the western margin by the Base Cretaceous Unconformity (BCU) and dips to some extent to the east. The field has gas condensate in three sandstone units, which are Lower to Middle Jurassic age. These three are the Garn Formation, the Ile formation (Fangst Group) and the Tofte Formation (Baat Group) (see Figure 1-2).

From the early Carboniferous through the opening of the Atlantic in the early Eocene, there was a long period of tectonic extension on the Norwegian continental margin. There were different phases from Carboniferous to the Cenozoic. From Carboniferous to Permian there were active rifting, which were continued by a phase of thermal relaxation from Middle Triassic to the Early Jurassic. From Middle Jurassic to the Cenozoic the activity were continued with intermitted tectonic activity (Quin, et al., 2010). In the area were the Kristin Field is located, faulting took place as a result of rifting during shallow burial of the reservoir formations from the late Middle Jurassic to the early Cretaceous (Zweigel, et al., 2009). The reservoir section (Jurassic of age) is capped by the BCU.

As earlier mentioned, the field is a high-pressure field, and there is a theory that both the overpressure and the hydrocarbon generation came as a pulse of subsidence in the Pliocene. There

are two different hypotheses about this overpressure. These are either by a response to local mechanical compaction of shales, or through pressure-transfer from the deep and hughly over-pressured Raas Basin to the west. However, since the overpressure was developed late in the burial history, this has minor influence upon the reservoir quality of the sandstones.

The Kristin Field reservoirs are quartz cemented with best reservoir quality associated with intervals of coarser grain size, favorable packing chlorite/illite grain coats (Christoffersen, et al., 2008). The sand-dominated Garn Formation is approximately 100 meters thick and of rather poor quality, with permeability on average ca 5 mD. Deposition of the Garn Formation was most likely in a shoreface environment. The heterolithic Ile Formation is approximately 85 meters thick with permeability ranging from 40 to 2000 mD. The Ile Formation was probably deposited in a tidal setting with river flow from west to east. The sand-dominated Tofte Formation is approximately 125 meters thick with average permeability of ca 200 mD (Zweigel, et al., 2009).

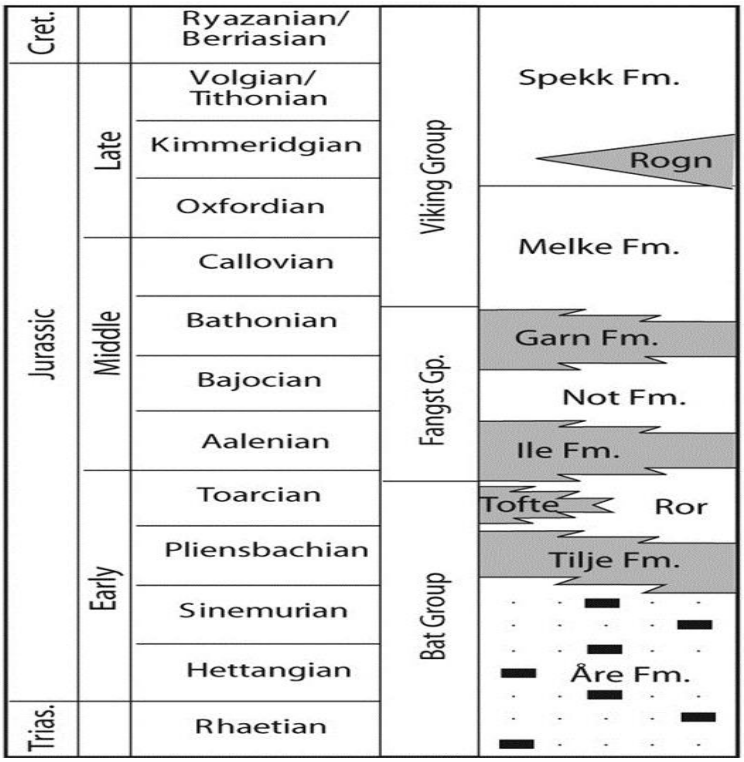

Figure 1 - 3: *Haltenbanken stratigraphic column* ***(Quin, et al., 2010)****.*

1.2 Over/under acquisition and theory

As an experiment to try to enhance the frequency bandwidth of the seismic data, optimize the multiple-attenuation, obtain deeper penetration of the signal, increased the weather window for the survey and enhance the signal to noise ratio, Statoil has performed a seismic survey of a line in the Kristin Field with a new acquisition tool: Over/under seismic streamers. The survey was performed in June 2008.

In regular marine acquisition configuration, there are used both shallow streamers and shallow sources. Because of this configuration the high-frequency content of the seismic data needed for resolution is favored. However, the shallow source and streamer attenuates the low frequencies, which are important for the absolute trend needed for inversion, deep penetration and visualization. The opposite effect happens with deep sources and streamers. This configuration enhances the low frequencies, but attenuates the high frequencies. Due to the more benign environment, the signal to noise ratio is also improved for the data recorded via a deep tow. To optimize both the signal to noise ratio and the bandwidth for a specific target depth, regular seismic must therefore try to adjust the depth of both the streamer and source. This often happens at expense of shallower or deeper objectives (Hill, et al., 2006).

Another phenomenon that is playing a role in the extent of the frequency spectra of the seismic is the free-surface reflections, or the source-/receiver-ghost. They strongly modulate the spectrum, reducing the energy at the so-called notch frequencies

$$f_n = \frac{iv}{2z} \quad \{i = 0, 1, \dots, \infty\} \tag{1-1}$$

where v is the water velocity and z is the source or receiver depth. A result of this is that there is a loss of low and high frequency energy. As mentioned earlier we have both source and receiver ghost. At the receiver, the upgoing wavefield reflected from the underlying rocks are reflected off the free surface (water surface), with inverted polarity, before it continues down to the receiver again. At the source, the upgoing part of the wavelet is reflected off the free surface (water surface), with inverted polarity, before it continues its propagation into the underlying rocks (Moldoveanu, et al., 2007).

Because the source-ghost and the receiver-ghost attenuates high and low frequencies, these reduces the bandwidth of the seismic and damage the vertical resolution power. The effect of the ghost is depth dependent of the source and receiver. Deeper sources or deeper receiver (or both) modulates the spectrum more frequently but has a better response at the lowest frequencies, while the opposite effect happens for shallow sources and/or receivers. Both of these cases would almost be similar to applying a bandpass filter in the frequencies the ghost does not modulate (Moldoveanu, et al., 2007).

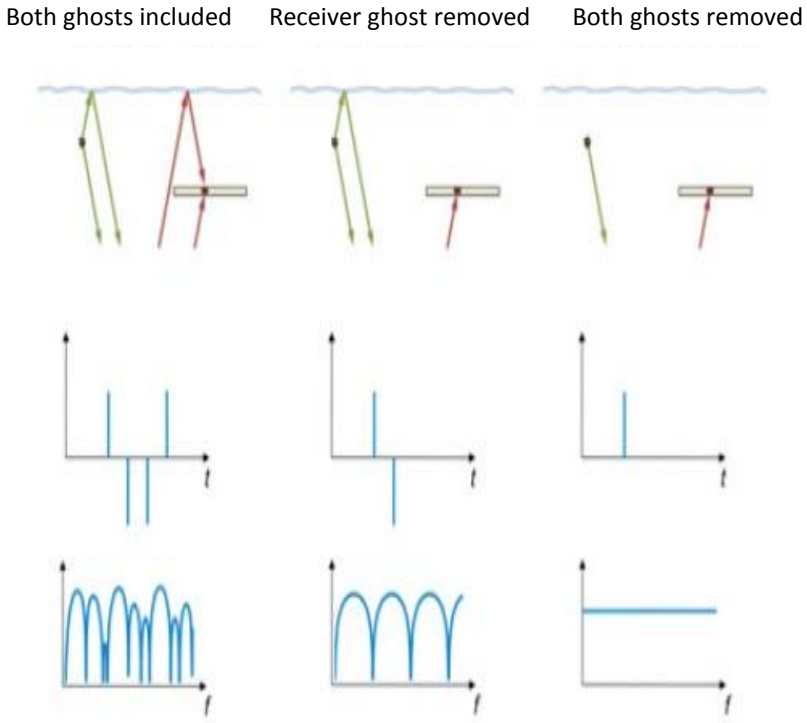

Figure 1 - 4: *Sea surface reflections that cause ghosts on both the source and receiver side. The individual ghost functions and their spectra are shown in the centre along with the combined function and amplitude spectra on the right* ***(PGS, 2011)****.*

Deconvolution (deghosting) can to some extent remove the effect of the ghost. However, the notches in the ghost spectrum cannot be completely removed because they contain no signal. Also, the signal to noise ratio is very low near the notch, which prevents a successful deconvolution of the ghost. The method we are using with the over/under process is that we are combining the two ghosts at different depths to exploit their respective advantages.

The over/under acquisition method allows separation of the upgoing and downgoing wavefields at the source (or receiver) using a vertical pair of sources (or receivers as in the seismic survey of 2008 at Kristin) to determine wave direction. Since the weather- and wave-noise is significantly better at deeper deployment (15-25 meter), the deeper receivers experience a better signal-to-noise ratio. To separate the up- and downgoing wavefields, we need to accurately maintain the 2 lower streamers in exactly the same vertical plane. This is done by both two cables at both sides of the cables in the horizontal plane and the steerable streamers. Even though the over/under cable combination is an old technology (1980`s), the advantage of it has not been of use until newer dates after the introduction of steerable streamers.

1.2.1 Wavefield separation

The technology of the cable combination streamers and its advantages is widely described in the literature, and under we will take a closer look at Sonneland`s method from 1986 (Moldoveanu, et al., 2007), which in a simple way illustrates the overall principle of wavefield separation.

We have here 2 different versions of the seismic wavefield, based on that we have 2 different cables at 2 vertical depths, respectively S_1 and S_2. These wavefields are recorded at their respective streamer, Streamer 1 (over cable) and Streamer 2 (under cable). By the basis that the seismic wavefield is a sum of the upgoing and downgoing wavefields, we may express each of them as;

$$\begin{aligned} S_1 &= U_1 + D_1 \\ S_2 &= U_2 + D_2 \end{aligned} \tag{1-2}$$

Since *U* is the upgoing wavefield, *D* is the downgoing wavefield and the ghost is the reflection off the free surface, then *U* is the unghosted part of the wavefield. As mentioned earlier, Streamer 1 lies above Streamer 2 in the vertical direction, hence the upgoing wavefield, *U*, is received later at Streamer 1, since the wavefield has traveled through an extra thickness of the water layer, Δz. The opposite effect happens for the downgoing wavefield, where it is received later at Streamer 2. By applying wave extrapolators (angle dependent time shifting filters), we may relate to the wavefields at different depths. Then we would have;

$$\begin{aligned} WU_2 &= U_1 \\ D_2 &= WD_1 \end{aligned} \tag{1-3}$$

Here, *W* is the wave extrapolator that depth delay *D* over a thickness $|\Delta z|$, or depth advances *U* over a thickness of $|\Delta z|$. W is also equivalent to the dip dependent time delay;

$$W = e^{ik_z|\Delta z|} \tag{1-4}$$

Where k_z denotes spatial frequency over the depth axis, and $i = \sqrt{-1}$. We can now specify the separated wavefields (*U* and *D*) by inserting (1-3) into (1-2). We here prefer the complex conjugate $\bar{W}$ to W^{-1};

$$\begin{aligned} U_1 &= +\frac{S_2 - WS_1}{\bar{W} - W} \\ D_1 &= -\frac{S_2 - \bar{W}S_1}{\bar{W} - W} \end{aligned} \tag{1-5}$$

The numerator tells us that the depth-shifted shallow wavelet gets subtracted from the deeper wavefield, but it still contains an effective ghost equivalent to a streamer at depth $|\Delta z|$, i.e. a ghost that is equivalent to the separation between the two streamers (Moldoveanu, et al., 2007). The effect of the equation is that it removes one ghost, but creates another one. Still, this new created ghost is preferable to either of the original ghost, since the deconvolution of the new ghost is an easier task for the bandwidth of interest.

1.2.2 The acquisition and possible advantages

The layout for the over/under acquisition is outlined in the figure below. Please note that the outermost horizontal cables are for positioning purposes only.

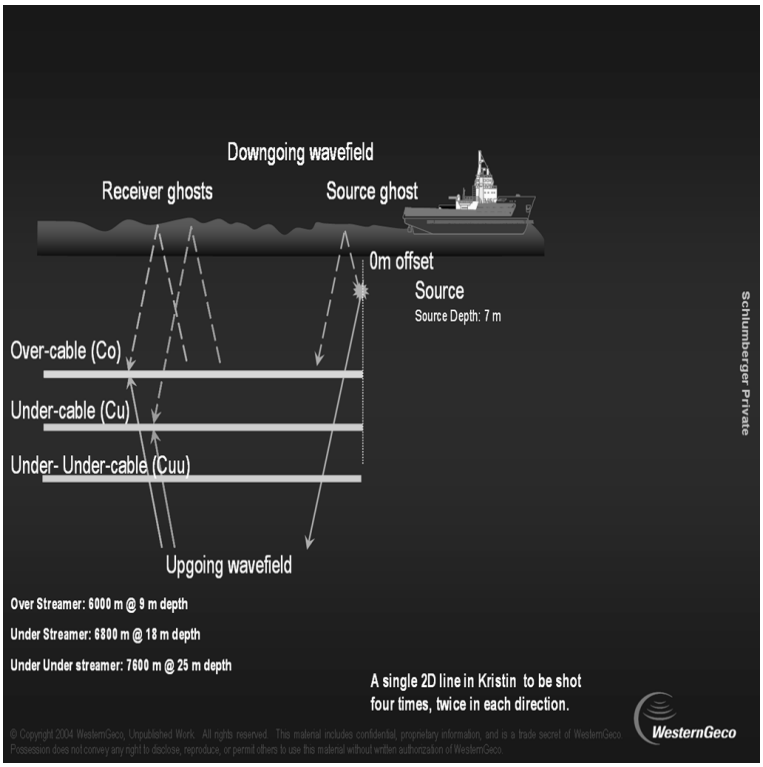

Figure 1 - 5: *Streamer and shot configuration of the cable combined seismic survey. There are also two cables horizontally aligned with the "Under-cable" which are only used for positioning of the cables* ***(Langridge, 2010)****.*

The possible benefits of over/under data compare with conventional data are various, which include (Hill, et al., 2006);

- A broader signal bandwidth, where the low-frequency content give deeper penetration, and therefore improved imaging of deeper prospects (as in the Kristin Field), imaging beneath salt, basalt and highly absorptive overburdens. Also the seismic inversion is less dependent upon model-based methods with the lower frequencies
- A simpler signal wavelet with the bandwidth extension to higher frequencies giving enhanced resolving power, allowing for a more detailed stratigraphic interpretation
- Improved signal-to-ambient-noise ratio as a consequence of the deeper towed-cable pairs
- An extended weather window enabled by the deeper towed-cable pairs

1.3 Datasets

Initially, 12 different datasets (SEG-Y) to work with from the seismic survey were available. For the quantification of the difference between the acquisition methods, the need for all the datasets to be consistent in the processing of the seismic was important. The different datasets were therefore all Kirchhoff Time Migrated and Post-Stack seismic.

The quality of the datasets was good, and the only difference of the processing between them is for the split-spread volumes. The comparison between them, regarding the respective results, was therefore conducted without any further conversion or adjustments.

These were the different inputs of the process of inversion (seismic lines):

Line number	Cable type	Tide	Direction
001_02	Single	High	296 degrees
002_02	Single	High	116 degrees
003_02	Single	Low	296 degrees
004_02	Single	Low	116 degrees
001_03	Cable Combined	High	296 degrees
002_03	Cable Combined	High	116 degrees
003_03	Cable Combined	Low	296 degrees
004_03	Cable Combined	Low	116 degrees
a5_001	Single	High	Split-spread
a5_003	Single	Low	Split-spread
a6_001	Cable Combined	High	Split-spread
a6_003	Cable Combined	Low	Split-spread

Table 1 - 1: *Table of the available datasets. Note that the single cable was towed at a depth of 9 meters, while the "cable combination"-cables were towed respectively at depths of 18 and 25meters.*

Chapter 2 Methodology

"*What hopes and fears does this scientific method imply for mankind? I do not think that is the right way to put the question. Whatever this tool in the hand of man will produce depends entirely on the nature of the goals alive in this mankind. Once the goals exist, scientific method furnishes means to realize them. Yet it cannot furnish the very goals. The scientific method itself would not have led anywhere, it would not even have been born without passionate striving for clear understanding*." – Albert Einstein, *Out of My Later Years*.

This thesis was carried out after the research and calculations done by the author between January and June 2012 using quantitive methods. The objectives of the study were to invert all the seismic lines of the different acquisition methods earlier mentioned, and quantify the difference between inversion with the conventional seismic as input and the seismic acquired with the over/under cable combination streamer as input. Key questions: were there any differences, and were these differences significant or not?

By quantifying the differences between the two acquisition methods, it were hoped that the thesis would be of interest for further development of the Kristin Field. Several methods have been used to achieve the results from the study, these methods will be introduced and explained in the following chapter, and also the theory behind it (see Chapter 3: Theory).

These are the programs which are to be introduced in the chapter:

1. Hampson-Russell STRATA
2. OpenWorks
3. IRAP RMS
4. MatLab

2.1 Hampson-Russell STRATA

STRATA is a program package in the main program Hampson-Russell GeoView (Hampson-Russell, 1999). STRATA are optimized for both *post-stack* and *pre-stack inversion*. In this paper, the only version used is *model-based post-stack inversion*. STRATA analyzes 2D and 3D post-stack seismic volumes to produce an acoustic impedance (AI) volume. The program package can be linked with other programs packages that are compatible with GeoView, e.g. OpenWorks which will be introduced in the next subchapter (see 2.2 OpenWorks).

The program let the user change input seismic volumes, different parameters in the process and some mathematical formulas for analyzing the output. The process itself is run automatically without any interactions during in the progress. To understand the process, the user will have to read and link the theory to the progress itself. This is crucial, since the program can be viewed as a “black-box” process, where the user is forced to fully trust the rightfulness of the programs inversion process.

The theory behind the inversion of the STRATA program is explained in Chapter 3 (see Chapter 3: Theory).

2.1.1 Introduction to the inversion process

For the area covered by the different seismic lines, there was one well available (well 6406/2-3 T3) which was used in the inversion process. From OpenWorks (see 2.2 OpenWorks) there were extracted 3 different logs, respectively P-wave velocity (DT), density (RHOB) and a corrected depth-time conversion log (see 2.2 OpenWorks).

For the data to have the best possible fit with the well, there were applied some small corrections to the log to best fit the reference datum (shift and stretch) and also a check-shot correction to optimize the correlation in time between the well log and the seismic. Illustration of the well correlation can be seen in the figure below (figure 2-1).

For the correlation to be optimized, we need to extract a correct wavelet for the data it represents. In STRATA there are two different options to extract the wavelet, one extraction in conjunction with the well and one extraction from the seismic data alone. Since the paper want to illustrate the difference between the two different acquisition methods, we need the inversion to be as data-driven as possible, which implies that as much as possible of the inversion should be driven by the input data itself, and not on the a-priori information. Hence, all the wavelets are statistical (extracted from the seismic). An illustration of the wavelet can be seen in figure 2-2.

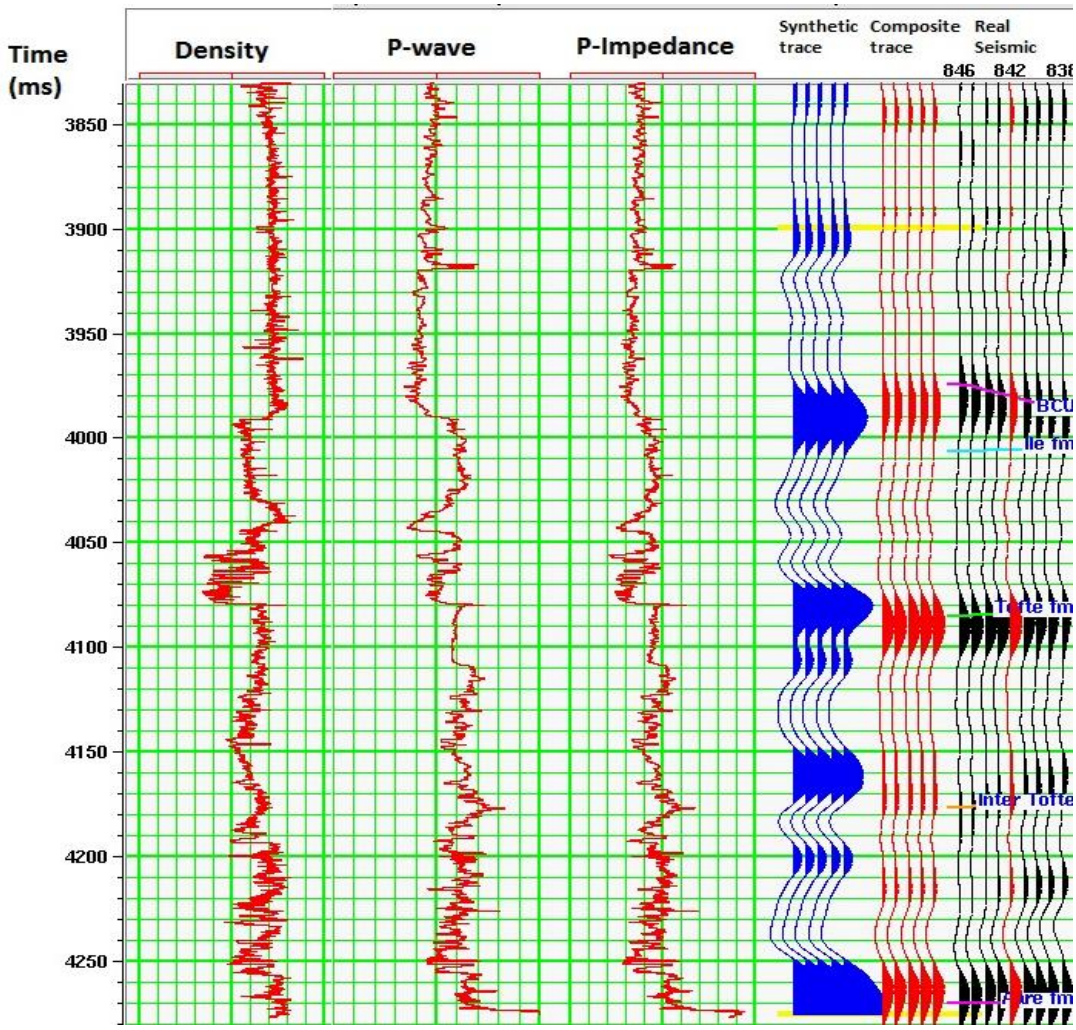

Figure 2 - 1: *Correlation window in STRATA. The three red traces to the left is the different well logs, the synthetic traces in blue, the composite traces in red and the real seismic as black traces. The correlation is between the blue traces and the red traces (composite traces of the seismic in the well location) in the program.*

The background model represents the a-priori information, and are build by interpolating the impedance values form the well-logs into the reservoir by following the interpreted horizons. Typically, only the low-frequency (less than 10 Hz) components are used in the background model (or initial model). Based on the frequency spectra of the seismic input data in the reservoir depth, the background model had a high cut filter of 6 Hz.

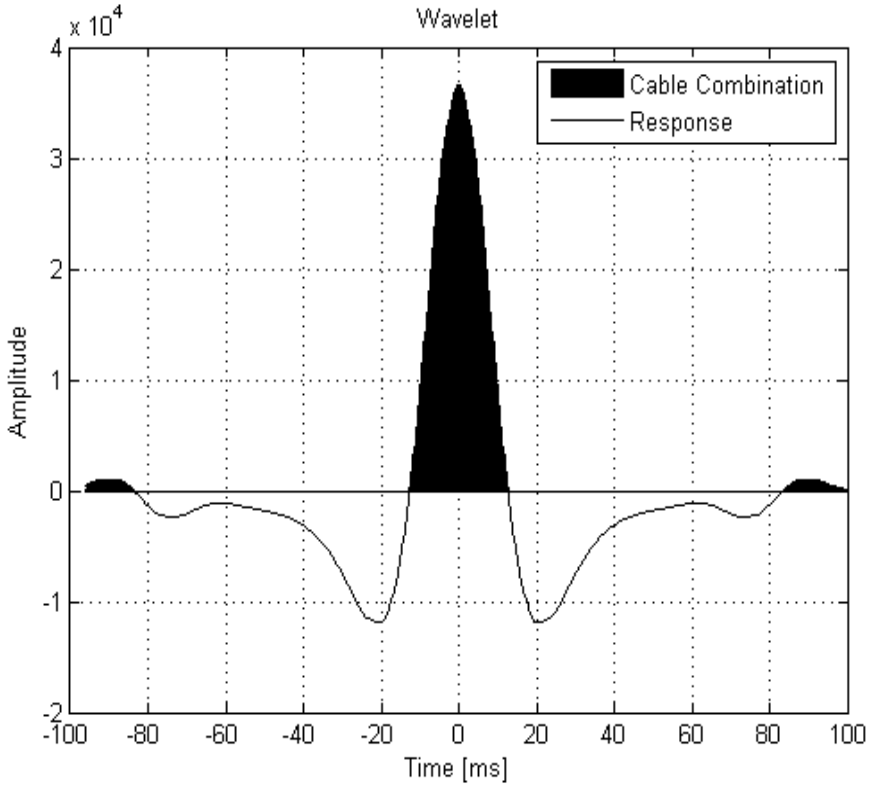

Figure 2 - 2: *Wavelet response for one of the cable combination lines. The Amplitude scale is not normalized, while the time-axis is from -100 to 100 ms.*

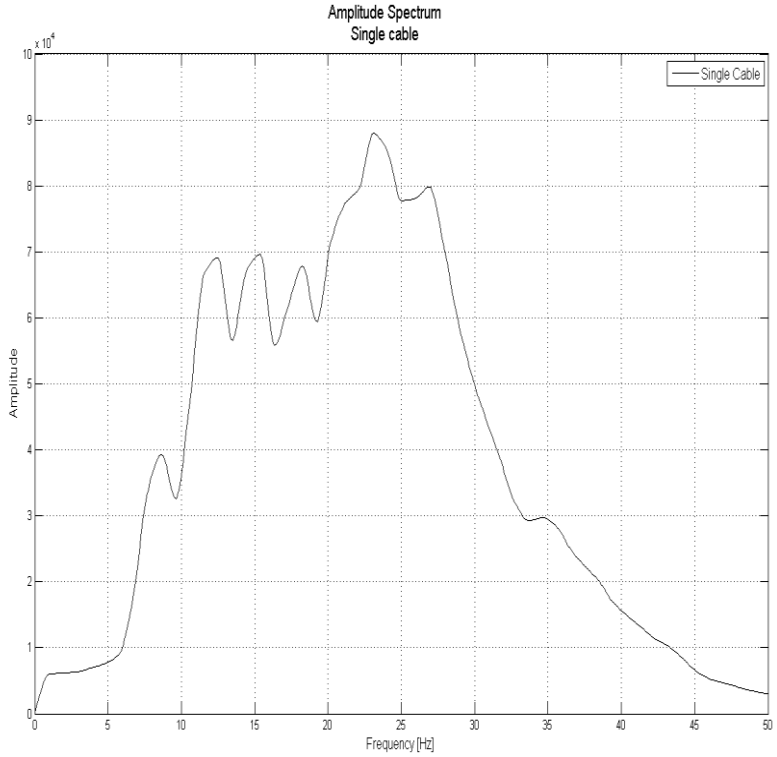

Figure 2 - 3: *An amplitude spectrum from one of the seismic lines in the reservoir depth (3852-4352 ms). The spectrum is known as the frequency response.*

In the STRATA program there are built-in tools that have been useful to confirm the validity of the results with, these two is the *Error Plot* and the *Inversion Analysis*. The Error Plot shows the difference between the original input seismic and the synthetic volume calculated from the inversion result. This should show very little unpredicted energy. The Inversion Analysis illustrates an overlay of the resulting inversion trace at the well location and the original impedance log.

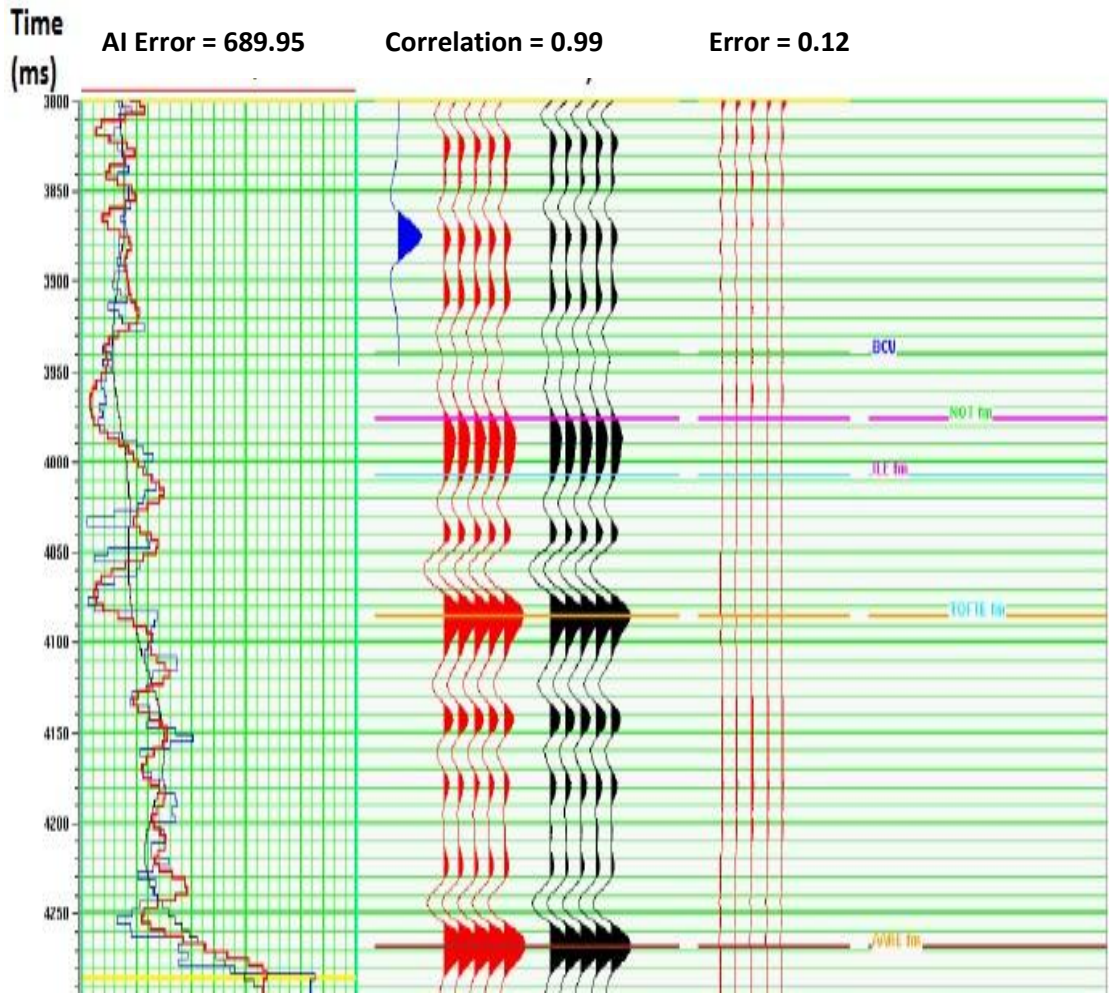

Figure 2 - 4: *Inversion analysis window in Hampson-Russell STRATA. Figure illustrates the inverted trace at the well location (red trace) overlying the original well log acoustic impedance trace (blue trace) and the background model trace (black trace). In the middle of the figure, we can observe the corresponding wavelet (blue), the synthetic seismic (red traces) and the original seismic (black traces). To the right is the error between them.*

2.2 OpenWorks

OpenWorks® software is the most widely used exploration and production project data management system in the oil and gas industry, with more than 1100 customer sites worldwide. The software is compatible with many open system standards, and offers E&P professionals a broad range of oilfield data in a single database (Halliburton, 2008).

As a new 3rd party application, OpenWorks has opened a new calibration with Hampson-Russell GeoView. This turned out useful for my work, since the different well-logs inputs to the workflow needed to be extracted from OpenWorks.

When a DT-log (P-wave velocity in $\mu s/ft$) is applied to the program, a time-depth correction curve is automatically created by the program. In most cases, this correction is incorrect, and results in that the logs are placed at the wrong depth, given the seismic as background image. The solution to this problem is a check-shot correction, which takes in a check-shot of the travel-time and corrects the logs due to the correct time-depth correlation. Import of the check-shot correction from OpenWorks (OW) was then easily done with the calibration between the two software packages.

2.3 IRAP RMS

"*IRAP RMS Suite is a software toolkit for geomodelling and designing reservoirs. It is primarily for use in the oil industry, helping engineers gather data from a wide variety of sources to efficiently build reliable reservoirs. In the program, the workflow consists of Internal Programming Language scripts, which execute emulations of certain models, varying one parameter, whilst keeping the rest consistent* " (Geomatic, 2009).

Through earlier work (Dyrnes, 2011), the use of IRAP RMS was used to better interpret the horizons in the reservoir and also to obtain a better understanding of the geology in terms of deposition and faulting. Another usable feature of the program was to cross-correlate the correct depths of the horizons with data from the fact pages of the Norwegian Petroleum Directorate (NPD, 2012). From NPD, these results were obtained;

Topp dyp [m]	Navn
396	NORDLAND GP
396	NAUST FM
1518	KAI FM
1954	HORDALAND GP
1954	BRYGGE FM
2300	ROGALAND GP
2300	TARE FM
2364	TANG FM
2425	SHETLAND GP
2425	SPRINGAR FM
2549	NISE FM
2838	KVITNOS FM
3429	CROMER KNOLL GP
3429	LYSING FM
3440	LANGE FM
4620	LYR FM
4629	FANGST GP
4629	GARN FM
4716	NOT FM
4751	ILE FM
4837	BÅT GP
4837	ROR FM
4877	TOFTE FM
5028	TILJE FM
5210	ÅRE FM

Figure 2 - 5: *Litostratigraphic reservoir section of well 6406/2-3 T3. Note that the Garn Formation in the thesis` datasets is not covered by the well log, this due to the fact that the well is a small distance south of the seismic lines. Picture is captured from* ***(NPD, 2002)****.*

The figure below illustrates the geomodel of the Kristin Field`s reservoir. The vertical line approximately in the middle of the image is the well, respectively 6406/2-3 T3. The different horizons, from top to bottom, are;

- Garn Formation – sand colored
- Not Formation – red and orange layers
- Ile Formation – blue lines
- Tofte Formation – yellow and green layers

The Aare Formation is the end of the reservoir, and contains no interesting hydrocarbon reserves. In an economical point of view the formation is not interesting and is excluded from the model. Yet in the actual inversion of the reservoir this formation is still a part of the reservoir, since the top of the formation is recognized as the end of the reservoir formations and the well logs ends here.

As we can see from the figure below, there are two major faults, one on each flank, which restricts the reservoir area. Even though the easterly fault does not cut through the reservoir section, the horizons has been faulted at an earlier stage in the geological timeline since we can find these layers on a deeper part east of the reservoir. The fault on the westerly part of the reservoir cut directly through the section, and we can find these sections again in a deeper part, west of the fault. All the faults in the Kristin Field are normal faults.

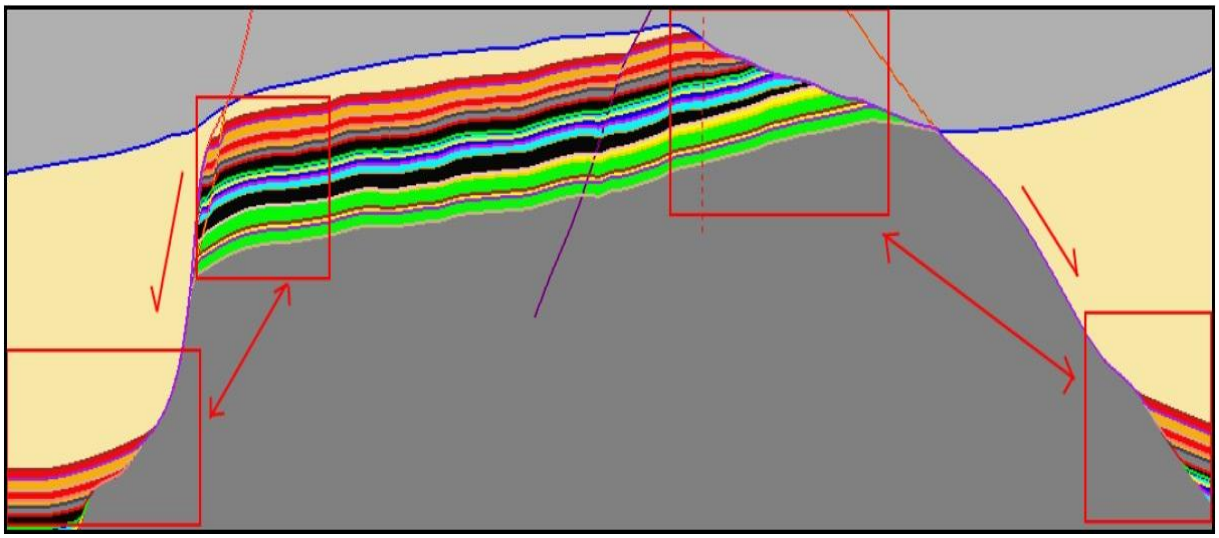

Figure 2 - 6: *A geomodel of the Kristin Field`s reservoir. There are two major faults, one on each section flank, and both are normal faults. The dark red line cutting the reservoir is a possible fault which can explain the unexpected pressure drop. At each bottom corner of the image, the faulted blocks are highlighted.*

The unexpected pressure drop from the Kristin Field has raised some concerns about the interpretation of the faults from the area. Since the drop in pressure was faster and larger than anticipated, an interpretation of a fault within the reservoir might be valid. As seen in the geomodel of the reservoir in the figure above, this fault is illustrated as the dark red cutting line inside the reservoir. The interpretation comes as a respond to the pressure drop, and may be a more correct interpretation of the field. However, any evidence of this is difficult to observe in the seismic.

2.4 MatLab

MatLab is a programming environment for algorithm development, data analysis, visualization, and numerical computation (MatLab, 2012). As earlier mentioned in (see 2.1 Hampson-Russell STRATA), the process for inversion in the program is considered to be a black box process, where the user has limited access. This caused limitations to the extent of analyses I could perform to the data. The solution was to export the different inversion volumes, and analyze the datasets in MatLab, where the user has full access and creates the further process himself.

Matlab has been of great use both to plotting, linear regression, probability analyses and complex mathematical computation.

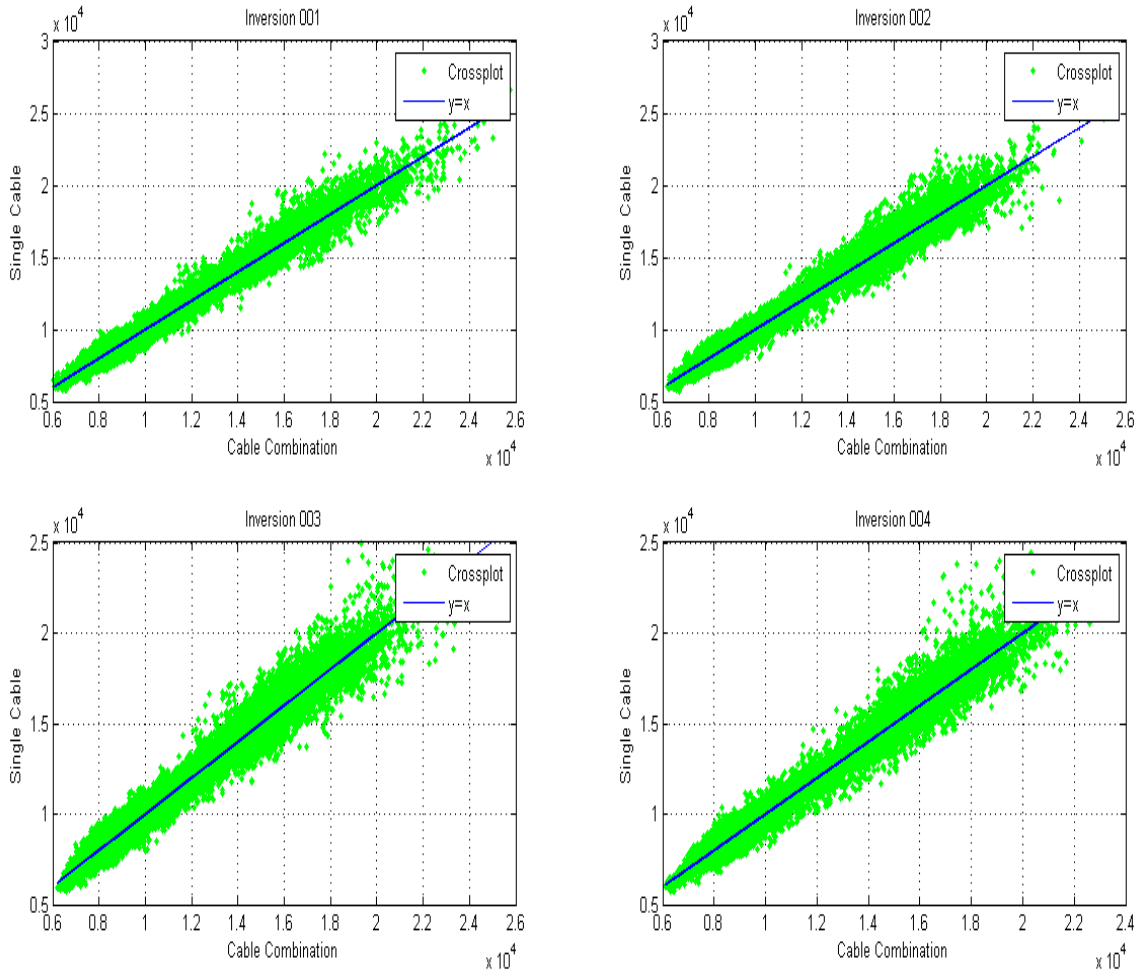

Figure 2 - 7: *Single cable versus cable combination crossplot created through MatLab. Similar illustrations will be explained in detail in chapter 4 and 5.*

Chapter 3 Theory

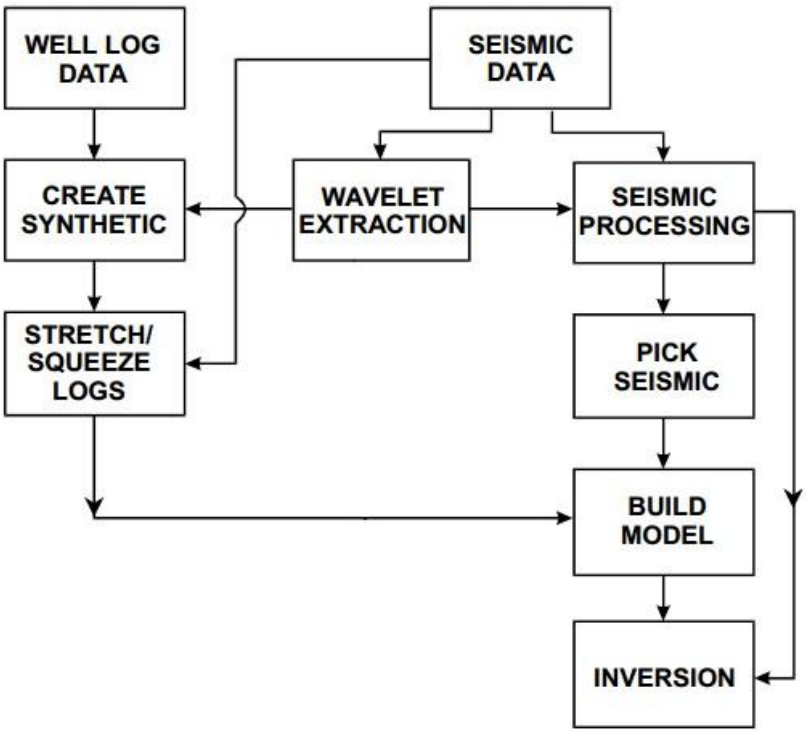

Figure 3 - 1: *Interrelationship of the components of Hampson-Russell STRATA, and the main procedure for the inversion of this thesis* ***(Hampson-Russell, 1999)****.*

The workflow of inversion contains many different steps which are more or less done automatically in the used program, Hampson-Russell STRATA. The importance of understanding the theory behind the workflow is therefore crucial. Not only is it important to understand what the output is, but also to be able to optimize the process in order to obtain the correct parameter values. Finally, in what manner we should vary the parameters in order to study the most important effects.

As mentioned, the inversion volumes are calculated using the Hampson-Russell STRATA program. The probability calculations are programmed in MathWorks MatLab.In this chapter we will cover the theory behind both the workflow of the inversions and the probability used in the thesis.

Before introducing the theory behind the workflow of inversion, it is important to illustrate the procedure of how this is done step by step. To what extent of understanding the concept of the

inversion required, often depends on how much we can follow the procedure when introducing the theory. The procedure of the workflow in this work for the inversion is illustrated in figure 3-1.

Since Strata is used for the inversion, and because STRATA in many cases has its own nomenclature for various parameters, most of the theory behind the workflow in STRATA is collected from (Hampson-Russell, 2009).

3.1 Convolutional model

The convolutional model is used to explain how the seismic trace is formed, and it approximates the earth by a linear system. The convolutional model can be written as

$$T(i) = \sum_{i} r(j)W(i - j + 1) + n(i) \tag{3-1}$$

- $r(j)$ is the zero-offset reflectivity
- $W(i)$ is the seismic wavelet
- $n(i)$ is the noise

As a result of this, we are illustrating that the inversion is the procedure of determining the reflectivity, $r(j)$, given the seismic trace $T(i)$. The reflectivity in (3-1), is related to the acoustic impedance or the velocity and density of each layer by the formula

$$r(j) = \frac{AI(j) - AI(j-1)}{AI(j) + AI(j-1)} \tag{3-2}$$

- $AI(j) = \rho(j)V(j)$ (acoustic impedance)
- ρ is the density
- V is the P-wave velocity

All the volumes used in the inversion process are volumes of acoustic impedance, hence the objective is to determine the reservoir velocities given the seismic traces. An estimate of the reflectivity is therefore the next step, before we can move into the process of deconvolution.

3.2 Seismic wavelet

We have 2 types of deconvolution; *Statistical deconvolution* and *deterministic deconvolution*. The difference between them is that deterministic deconvolution uses the basis that the precise shape of the source is known, and we may then use inverse in the deconvolution process. Most of the time, we don't have this information. To estimate the source shape, we then have to use statistical deconvolution, which is the case for the work done.

"*The seismic wavelet is the link between seismic data (traces) on which interpretations are based, and the geology (reflection coefficient) that is being interpreted"* (Henry, 2001). Accurate wavelet estimation is critical to the process of seismic inversion, since the seismic wavelet strongly influences the seismic inversion result, and subsequent assessments of the reservoir quality. The wavelet is defined by its phase and amplitude spectra. The four different terms in the figure below, refers to the characteristics of the signal shape and location in the data; *Minimum phase, maximum phase, mixed phase* and *zero phase*.

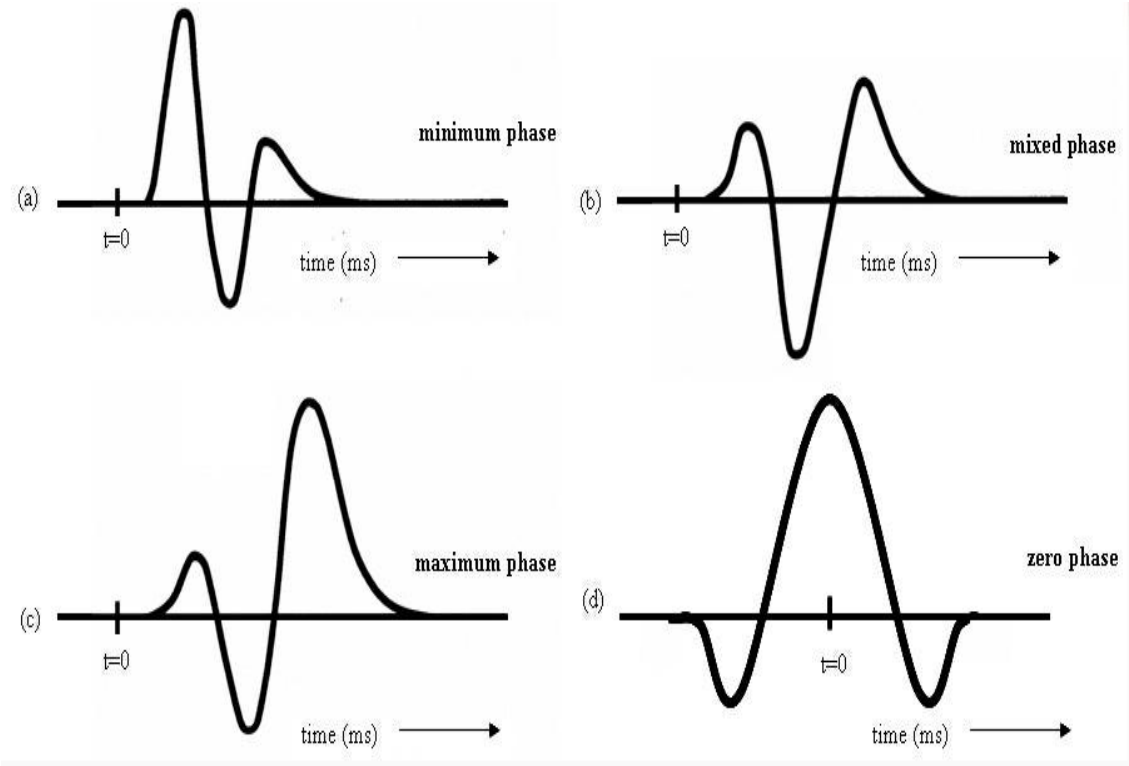

Figure 3 - 2: *Illustration of the 4 different phases of the seismic wavelet. Here we have a) minimum phase, b) mixed phase, c) maximum phase and d) zero phase* ***(Ikele, et al.)****.*

Since the inversion process used in this thesis is consistent with the use of the zero-phase wavelet, the other terms is not included in this subchapter, thus it is widely described in the literature, and for further reading the author recommends the work by Ikele and Amundsen (Ikele, et al.)

A zero-phase wavelet, as illustrated in Figure 2-4(d), is symmetrical with a maximum at time zero. The zero-phase wavelet is of shorter duration than the minimum phase equivalent (XSGeo, 1999). Since the signal has the shortest duration and it contains the same amount of energy as the other wavelets, the zero-phase signal has the narrowest duration and the largest peak amplitude of any signal with the same amplitude spectrum. As illustrated in the figure above, the zero-phase wavelet

has energy arriving before time zero, which is not physically realizable. Anyhow, the wavelet is useful for increased resolving power and ease of picking reflection events (peak or through). Another helpful feature of the zero-phase signal is that the phase is zero for all frequency components contained in the signal.

3.3 Deconvolution

"The objective of deconvolution is to find a filter that will transform an input wavelet into some 'desired' output shape." (Hampson-Russell, 2009)

What we would like from the output wavelet is often a single spike, but the output can be set to whatever we like. There are several solutions to this problem, and under this sub-chapter we will look into 3 different types;

1. The Wiener-Levinson Shaping Filter
2. Minimum Phase Statistical Deconvolution (Spiking Deconvolution)
3. Two Sided Spiking Deconvolution

3.3.1 Wiener-Levinson shaping filter

Filtering algorithms that are based on the optimum Wiener filter theory are known as Wiener-Levinson algorithms. The algorithms then assume least-squares fit between the desired output and the actual output, which are just a special case of the Wiener filter. A short description of Wiener filtering is designing a filter, $f(t)$, so that the least-squares error between the actual outputs is minimum (Sah, 2003).

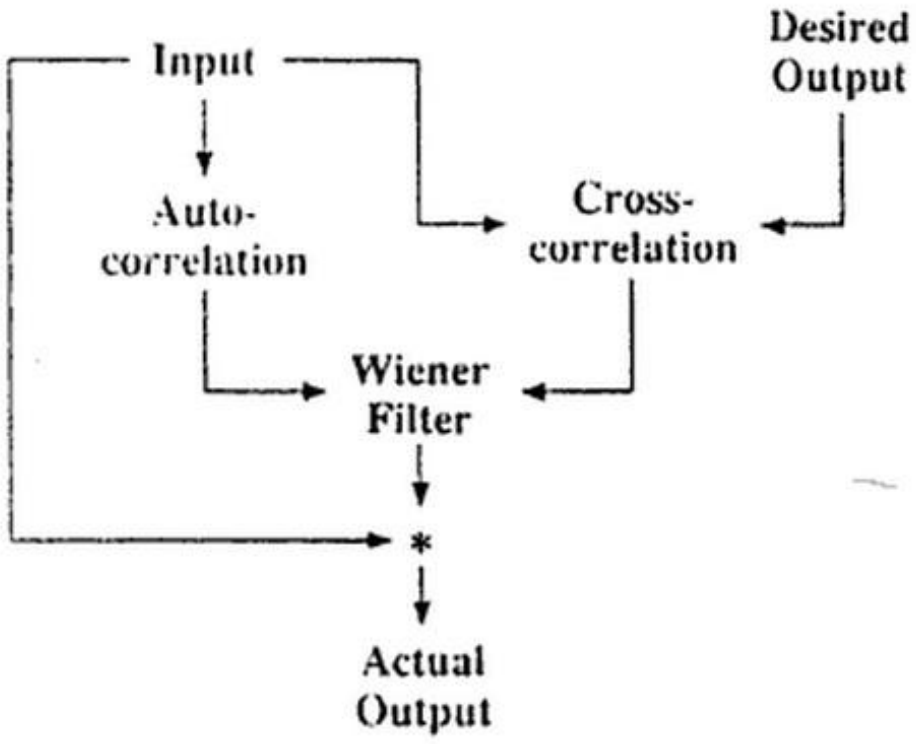

Figure 3 - 3: *A flowchart for Wiener Filter design and application* ***(Sah, 2003)****.*

A special case where the Wiener-Levinson filter is identical to the least-squares inverse filter is occurring when the desired output is the zero-lag spike (1, 0, 0,…, 0). The determination of the Wiener-Levinson filter coefficients can be found by solving the equation

$$\begin{bmatrix} r_0 & r_1 & \cdots & r_{n-1} \\ r_1 & r_0 & \cdots & r_{n-2} \\ \vdots & \vdots & \ddots & \vdots \\ r_{n-1} & r_{n-2} & \cdots & r_0 \end{bmatrix} \begin{bmatrix} a_0 \\ a_1 \\ \vdots \\ a_{n-1} \end{bmatrix} = \begin{bmatrix} g_0 \\ g_1 \\ \vdots \\ g_{n-1} \end{bmatrix} \tag{3-3}$$

Where r_i, a_i and g_i, (i=0, 1, 2,…, n-1) are the autocorrelation lags of the input wavelet, the Wiener-Levinson coefficients and the cross correlation lags of the desired output with the input wavelet, respectively. From the equation matrix (3-3), we can observe that the autocorrelation matrix is symmetric, and can be solved with Levinson recursion. We then need a two-point filter, from which we will derive a three-point filter, and so on, until the n-point filter is derived.

3.3.2 Spiking deconvolution

The process with zero-lag spike is often called spiking deconvolution. If we have the desired spike in the form of (1, 0, 0,…, 0) and convolves this with the input wavelet ($x_0, x_1, x_2, \ldots, x_{n-1}$) this will yield the series (x_0, 0, 0,…, 0). Then the matrix of (3-3) will have the form of;

$$\begin{bmatrix} r_0 & r_1 & \cdots & r_{n-1} \\ r_1 & r_0 & \cdots & r_{n-2} \\ \vdots & \vdots & \ddots & \vdots \\ r_{n-1} & r_{n-2} & \cdots & r_0 \end{bmatrix} \begin{bmatrix} a_0 \\ a_1 \\ \vdots \\ a_{n-1} \end{bmatrix} = \begin{bmatrix} 1 \\ 0 \\ \vdots \\ 0 \end{bmatrix} \tag{3-4}$$

The problem of (3-4) has the same form as the least-squares inverse filter. In the case of spiking deconvolution, the autocorrelation matrix on the left side of (3-4) is computed from the input seismogram (statistical deconvolution), while in the case of least-squares inverse filtering it is computed directly from the known source wavelet (deterministic deconvolution) (Sah, 2003).

However, it is important to notice that the previous problems do not take into account that the seismogram always contain some noise in a normal acquisition, and this noise is additive in both the frequency and time domains. Even during processing there is generated some noise, which is known as numerical noise. So, to ensure numerical stability, we add a level of *white noise* (evenly distributed noise) to the amplitude spectrum of the input seismogram before deconvolution. This process is called *prewhitening*. We are now adding a constant value to the zero-lag of the autocorrelation function (3-5). The percentage of the prewhitening is given by a scalar between 0 and 1 (ε), and the added value (β) to the autocorrelation function is then equal to 1+ε. As illustrated in (2-5) we are by adding this constant value to the autocorrelation function, adding white noise to the spectrum;

$$\begin{bmatrix} \beta r_0 & r_1 & \cdots & r_{n-1} \\ r_1 & \beta r_0 & \cdots & r_{n-2} \\ \vdots & \vdots & \ddots & \vdots \\ r_{n-1} & r_{n-2} & \cdots & \beta r_0 \end{bmatrix} \begin{bmatrix} a_0 \\ a_1 \\ \vdots \\ a_{n-1} \end{bmatrix} = \begin{bmatrix} 1 \\ 0 \\ \vdots \\ 0 \end{bmatrix} \tag{3-5}$$

We would have the best result if no prewhitening was added, but then the process would be unstable. So, to keep the operation stable, we are adding a small amount of prewhitening, and in this thesis the operation were stable at 1%.

3.3.3 Two-sided spiking deconvolution

When we are looking at the spiking deconvolution, the desired effect is to put the spike at time zero. However, we have also the opportunity to put the spike at a greater time. By adding the spike at a greater time we would make the error term more symmetrical;

$$\begin{bmatrix} r_0 & r_1 & r_2 & r_3 & r_4 \\ r_1 & r_0 & r_1 & r_2 & r_3 \\ r_2 & r_1 & r_0 & r_1 & r_2 \\ r_3 & r_2 & r_1 & r_0 & r_1 \\ r_4 & r_3 & r_2 & r_1 & r_0 \end{bmatrix} \begin{bmatrix} a_0 \\ a_1 \\ a_2 \\ a_3 \\ a_4 \end{bmatrix} = \begin{bmatrix} 0 \\ 0 \\ 1 \\ 0 \\ 0 \end{bmatrix} \tag{3-6}$$

This is referred to as *two-sided spiking deconvolution* (Hampson-Russell, 2009). Even though the solution may not be symmetrical for all cases of the two-sided spiking deconvolution, the solution will still be more symmetrical than the first solution. However, in this approach, the input wavelet must be known, which isn't a criteria for one-sided spiking deconvolution.

3.4 Inversion

The purpose of seismic inversion is to recover the subsurface elastic properties (e.g. acoustic impedance and velocity) from seismic data (Y. Quan). Post-stack seismic inversion is the process where we analyze the stacked seismic traces and try to reconstruct the acoustic impedance or the velocity structure of the earth.

The model that seismic inversion is based on is the 1-D convolutional model from (3-1). In this model, multiples are assumed to be negligible.

3.4.1 Soft constrained model based inversion

For this project, the inversion method used for all the different datasets have been consistent. For the datasets to be comparable at the end, this was necessary. The inversion method used is *"Soft Constrained Model based Inversion",* which will be explained in detail hereunder.

Constrained model based inversions

Since the term Soft Constrained Model based Inversion comes from the Hampson Russell program, much of the theory about this inversion method is collected from the built-in program assistant itself, (Hampson-Russell, 2009).

In a constrained inversion we are using the initial guess (background model) as a starting point for the inversion and sets absolute boundaries for how far the calculated acoustic impedance may deviate from the initial guess. As the process runs, any parameter may be set freely as long as it stays within the fixed boundaries.

As a boundary for the inversion, we set a maximum impedance change, which sets the maximum allowable deviation in impedance as a percentage of the constraint log. For instance, if we here use the number 0.30 (or 30%), the final Impedance at sample I, I(i), must be within

$$I(i) = I_0(i) \pm 0.30\, I_{AV} \tag{3-7}$$

- $I_0(i)$ = the initial guess at sample i
- I_{AV} = the average impedance of the input constraint, I_0

As we can tell from the formula, the Inversion is tightened when the number is reduced, and if we set the number to be 0, the initial guess model is returned from the Inversion.

We want to take a closer look at the reflectivity series, and how it is connected to the initial guess, or the logarithm of the initial guess impedance. We then need to take a closer look at the mathematics behind the inversion form.

If we now let the initial guess impedance be

$$Z_{oi}, i = 1, N_{SAMP} \tag{3-8}$$

Then we can define the logarithm of the impedance as

$$L_i = \log [Z_{oi}] \tag{3-9}$$

Within each layer we can define the impedance to be

$$Z_j = Z_{j-1}\left[\frac{1+r_j}{1-r_j}\right] \tag{3-10}$$

Keeping in mind that the process is started with an estimate of the impedance in the first layer, this equation can be generalized for *i* layers. Then the generalized equation would be

$$Z_j = Z_1 \prod_{j-2}^{i}\left[\frac{1+r_j}{1-r_j}\right] \tag{3-11}$$

As we can tell from the formula, each impedance value depends on all the reflection coefficients for the layers above. We can now rewrite the formula in the manner of

$$Z_{0i} \cong L_1 + \sum_{j-2}^{i} 2\left[r_j + \frac{r_j^3}{3} + \frac{r_j^5}{5} + \cdots\right] \tag{3-12}$$

And for small reflection coefficients it can be approximated as

$$L_i - L_1 \cong \sum_{j-2}^{i} 2r_j \tag{3-13}$$

Formula (3-12) and (3-13) can then be transformed to

$$L_i \cong L_0 + \sum_{j-1}^{i} 2\left[r_j + \frac{r_j^3}{3} + \frac{r_j^5}{5} + \cdots\right] \tag{3-14}$$

$$L_i \cong L_0 + \sum_{j-1}^{i} 2r_j \tag{3-15}$$

We are then assuming that we are working with an earth model with m+1 number of layers, where the logarithm of the respective impedances is;

$L_0, L_1, L_2, L_3, L_4, \ldots, L_m$

Then we can define a vector, **L**, with length m+1;

$$\boldsymbol{L} = \begin{bmatrix} L_0 \\ L_1 \\ \vdots \\ L_m \end{bmatrix} \tag{3-16}$$

Since there are m+1 layers, there would be m reflection coefficients, since there is no boundary at the end of the last layer where we could have a reflection. The reflection coefficients will then be represented by the formulas;

$$\begin{aligned} r_1 &= \frac{1}{2}[L_1 - L_0] \\ r_2 &= \frac{1}{2}[L_2 - L_1] \\ r_m &= \frac{1}{2}[L_m - L_{m-1}] \end{aligned} \tag{3-17}$$

As we defined the vector for the logarithm of the different impedances, we can now define a vector for the various reflection coefficients. This vector then has length m

$$\boldsymbol{r} = \begin{bmatrix} r_1 \\ r_2 \\ \vdots \\ r_m \end{bmatrix} \tag{3-18}$$

The relationship between the reflection coefficient vector **r** and the impedance vector **L** is then represented as

$$\begin{bmatrix} r_1 \\ r_2 \\ \vdots \\ r_m \end{bmatrix} = \frac{1}{2}\begin{bmatrix} -1 & 1 & 0 & \dots \\ 0 & -1 & 1 & \ddots \\ 0 & 0 & -1 & \ddots \\ \vdots & \ddots & \ddots & \ddots \end{bmatrix}\begin{bmatrix} L_0 \\ L_1 \\ \vdots \\ L_m \end{bmatrix} \tag{3-19}$$

or

$$\boldsymbol{r} = \boldsymbol{DL} \tag{3-20}$$

Here we have to notice that the **D** matrix has m+1 columns and m rows. We now want to find the **L**-vector that minimizes the function

$$\boldsymbol{J} = (\boldsymbol{S} - \boldsymbol{WDL})^{\boldsymbol{T}}(\boldsymbol{S} - \boldsymbol{WDL}) \tag{3-21}$$

Where **W** is the wavelet matrix and **S** is the seismic traces. We can determine this as an optimization function, which can easily be solved directly, given the standard normal equations

$$\boldsymbol{L} = (\boldsymbol{D^T W^T DW})^{-1}\boldsymbol{D^T W^T S} \tag{3-22}$$

However this direct solution would not allow us to impose hard bounds on the inversion, which would result in low frequency instability. Instead of this direct solution, we then use a conjugate-gradient algorithm. Then for the constrained conjugate-gradient, we create 3 different vectors:

- One vector for the upper bound
- One vector for the lower bound
- One vector for the "initial guess" impedance

The final impedance can then freely vary between the upper and lower bound, but never exceed these values. If the final impedance exceeds these values, the value for that point will be the initial guess.

$$\boldsymbol{L_L} = \begin{bmatrix} L_L(0) \\ L_L(1) \\ \vdots \\ L_L(m) \end{bmatrix} \quad \boldsymbol{L_0} = \begin{bmatrix} L_0(0) \\ L_0(1) \\ \vdots \\ L_0(m) \end{bmatrix} \quad \boldsymbol{L_U} = \begin{bmatrix} L_L(0) \\ L_L(1) \\ \vdots \\ L_L(m) \end{bmatrix} \tag{3-23}$$

For each of the different layers, the algorithm solves for the final impedance ($\boldsymbol{L_i}$) with the starting point at $\boldsymbol{L_{0i}}$, so that the following is always maintained:

$$\boldsymbol{L_{Li} \leq L_i \leq L_{Ui}}$$

Weight factor

Since, in this thesis, we want to enhance the differences between inversions with different acquisition methods, the inversions should be as data-driven as possible, but still put as much weight on the initial model that the process is stable. To illustrate this method, we are adding a *weighting factor* to the problem.

Since we now have a weighting factor in the problem, the combined least-squares problem consists of minimizing the total objective function;

$$\boldsymbol{J} = w_1(\boldsymbol{L} - \boldsymbol{Hr})^{\boldsymbol{T}} + (1 - w_1)(\boldsymbol{T} - \boldsymbol{Wr})^{\boldsymbol{T}}(\boldsymbol{T} - \boldsymbol{Wr}) \tag{3-24}$$

Where w_1 is a weight factor between 0 and 1 which determines the factor that weighing the two types of measurement, **T** and **L**. If we set w_1 to 0, we are neglecting the initial guess and the second term of the equation (3-24) dominates completely. The opposite effect is obtained by setting w_1 to 1 (Hampson-Russell, 1999).

3.5 Inversion and probability

This chapter will basically introduce the linear regression where we are using 2 different inversion volumes as input. To analyze the data, a linear regression was performed and added to the cross-plots. To illustrate the deviations in the plot, two new lines (one above and one under the linear regression line) was added, representing the standard deviations.

3.5.1 Linear regression on different inversion data

By using one inversion volume as X-value, and another inversion volume as Y value, we can analyze the relationship between the by using linear regression. For every data point, we know both the X- and Y-value, and we want to find the best straight line through the data. In this paper, both the slope and the intercept have a scientific meaning.

The goal is to find the line that best predicts Y from X. This is done by finding the line that minimizes the sum of squares of the off-diagonal elements of the line.

Minimizing sum of squares

Vertical least squares fitting, which we are interested in here, go on by finding the sum of squares of the vertical deviation R^2 of n data points. This procedure uses the sum of the squared deviations from each point and then the sum is minimized to find the best fit line. From (Weisstein) we have that;

$$R^2 \equiv \sum [Y_i - f(X_i, a_1, a_2, \dots, a_n)]^2 \tag{3-25}$$

Where R^2 is the sum of the squares of the vertical deviations. Then the conditions for R^2 to be minimized is;

$$\frac{\partial R^2}{\partial a_i} = 0 \qquad i = 1, \dots, n \tag{3-26}$$

For a linear fit where the function $\boldsymbol{f}$ would be of the form a+bX, then the derivate of $\boldsymbol{R^2}$ would take the form of

$$\frac{\partial R^2}{\partial a_i} = -2 \sum_{i=1}^{n} [Y_i - (a + bX_i)] = 0$$

$$\frac{\partial R^2}{\partial b_i} = -2 \sum_{i=1}^{n} [Y_i - (a + bX_i)] X_i = 0 \tag{3-27}$$

This has the solution

$$\begin{bmatrix} a \\ b \end{bmatrix} = \begin{bmatrix} n & \sum_{i=1}^{n} X_i \\ \sum_{i=1}^{n} X_i & \sum_{i=1}^{n} X_i^2 \end{bmatrix}^{-1} \begin{bmatrix} \sum_{i=1}^{n} Y_i \\ \sum_{i=1}^{n} X_i Y_i \end{bmatrix} \tag{3-28}$$

By taking the 2x2 matrix inverse, we can find the unknown a and b;

$$a = \frac{\bar{Y}(\sum_{i=1}^{n} X_i^2) - \bar{X}\,(\sum_{i=1}^{n} X_i Y_i)}{\sum_{i=1}^{n} X_i^2 - n\,\overline{X^2}}$$

$$b = \frac{\sum_{i=1}^{n} X_i Y_i - n\bar{X}\bar{Y}}{\sum_{i=1}^{n} X_i^2 - n\,\overline{X^2}} \tag{3-29}$$

By defining the sums of squares, these equations can be rewritten

$$\boldsymbol{ss}_{xx} = \left(\sum_{i=1}^{n} X_i^2\right) - n\bar{X}^2$$

$$\boldsymbol{ss}_{yy} = \left(\sum_{i=1}^{n} Y_i^2\right) - n\bar{Y}^2 \tag{3-30}$$

$$\boldsymbol{ss}_{xy} = \left(\sum_{i=1}^{n} X_i Y_i\right) - n\bar{X}\bar{Y}$$

Now we can define the regression coefficient, b, and that a is given;

$$b = \frac{\boldsymbol{ss}_{xy}}{\boldsymbol{ss}_{xx}}$$

$$a = \bar{Y} - b\bar{X} \tag{3-31}$$

We can now define the correlation coefficient, which is the overall quality of the fit. The correlation coefficient is defined by;

$$r^2 = \frac{\boldsymbol{ss}_{xy}{}^{\mathbf{2}}}{\boldsymbol{ss}_{xx}\boldsymbol{ss}_{yy}} \tag{3-32}$$

Chapter 4 Results

"But the reason I call myself by my childhood name is to remind myself that a scientist must also be absolutely like a child. If he sees a thing, he must say that he sees it, whether it was what he thought he was going to see or not. See first, think later, then test. But always see first. Otherwise you will only see what you were expecting." – Douglas Adams, *So Long, and Thanks for all the Fish.*

Since the goal of the thesis were to identify and quantify the difference in inversion between the seismic acquired with a single cable receiver and a cable combination receiver, we wanted the inversion to be as *data-driven* as possible. By keeping the inversion as data-driven as possible, we can best identify the differences in inversion, which are caused by the data itself.

By data-driven we mean that the inversion should have as much weight on the input seismic (input data) as possible. All the inversion were processed in the program package Hampson-Russell STRATA (see 2.2 Hampson-Russell STRATA), and here we have some tools to help us keeping the inversion weighted more on the input than the a-priori information (background model);

- *Prewhitening*
- *Statistical wavelet*
- *Weight factor*

Inversion itself is actually very much like the deconvolution, where we derive the reflection coefficient based on the known wavelet. As the deconvolution, this process can be unstable if the wavelet is band limited, as in the case for this thesis. The solution is to add white noise to the spectrum to stabilize the process. This process is known as *prewhitening*. We would have the best result if no prewhitening was applied, but some prewhitening is needed for stabilization. We therefore have to add an amount of prewhitening, but to keep the deconvolution and inversion as driven as possible on the data, we want the prewhitening to be as small as possible. The inversion was computed with different prewhitening factors to see how low the prewhitening could be, to still have a stabile process and an inversion result that was more or less consistent with the inversion done with the added prewhitening plus a fraction of the prewhitening to the autocorrelation matrix;

$$\begin{bmatrix} (\beta+\partial\varepsilon)r_0 & r_1 & \cdots & r_{n-1} \\ r_1 & (\beta+\partial\varepsilon)r_0 & \cdots & r_{n-2} \\ \vdots & \vdots & \ddots & \vdots \\ r_{n-1} & r_{n-2} & \cdots & (\beta+\partial\varepsilon)r_0 \end{bmatrix} \begin{bmatrix} a_0 \\ a_1 \\ \vdots \\ a_{n-1} \end{bmatrix} = \begin{bmatrix} 1 \\ 0 \\ \vdots \\ 0 \end{bmatrix} \quad (4\text{-}1)$$

Here, β is equal to $1 + \varepsilon$, where ε is the prewhitening and $\partial\varepsilon$ is a fraction of ε. If the two results are more or less equal, we can conclude that the process was stable. We used a prewhitening of 1% to the autocorrelation matrix, or $\varepsilon = 0.01$.

In Hampson-Russell STRATA, we have 2 different methods for extracting the wavelet, respectively one method based on the well logs and one method were we extract the wavelet from the input seismic alone (both uses the basis that the precise shape of the source is not known). Because of the basis that all wavelets for any input seismic would be equal if we used the well logs for extracting the wavelet, the wavelet was extracted using the input seismic alone. The result was that we had 8 different wavelets which were data-driven (based on the input data), for the comparison between the cable combination seismic and the single cable seismic, 1 for each line. The wavelets for the cable combination seismic in the reservoir section were more or less equal, and the wavelets for the single cable seismic in the reservoir section were more or less equal. The basic shape and the difference between them can be observed in the figure below.

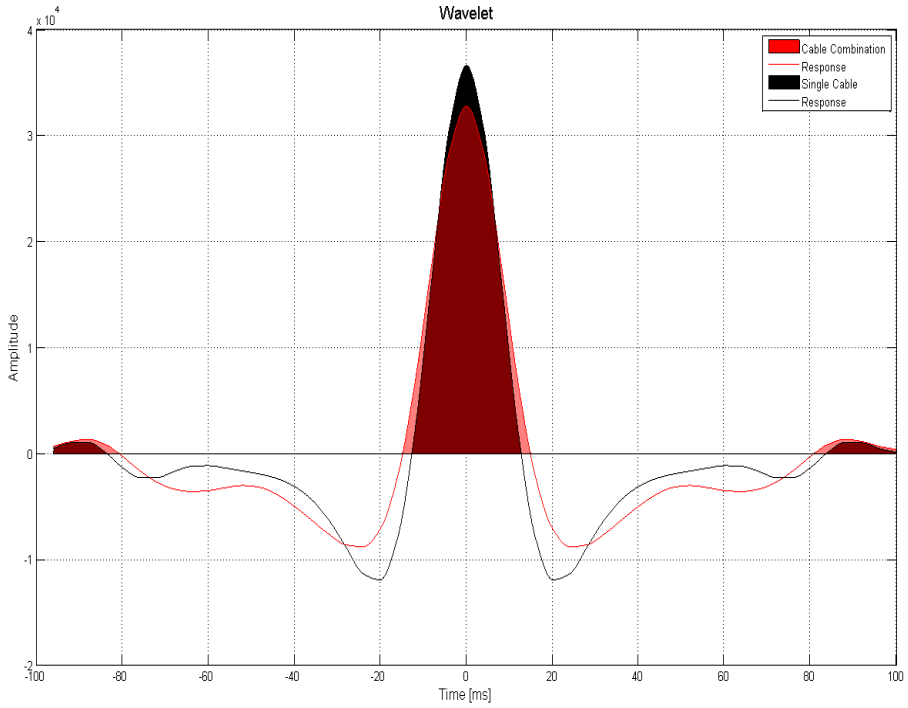

Figure 4 - 1: *Basic shape of the wavelet for the single cable seismic and for the cable combination seismic, both extracted from a time window equivalent to the reservoir section of the Kristin Field, respectively from [3852-4352ms].*

The weight factor controls how much weight the user wants to put on the background model (a factor between 0 and 1), the weight on the input seismic would then be 1 minus "the weight on the background model" (see Chapter 3.4.1 Soft constrained model-based inversion). This factor is the one that has the best control if the inversion is data-driven. There were tried with different weight factors prior to the result, to find out how much the data changed by changing the weight factor, and if the process of inversion were stabile for a low weight factor on the background model (<5%).

The result were that the process were stabile down to a weight factor of 0.8% on the background model, hence the used weight factor for all the different inversion were set to 1%. I would also like to

add, that if we had a weight factor of over 90% on the background model, the inversion output would be more or less similar to the background model itself, which is not wanted.

4.1 Inversion process in Hampson-Russell

As mentioned earlier, the inversion process used is Soft Constrained Model based Inversion, with post-stack seismic as input. For comparison reasons, we have used one common background model for all inversions.

One of the reasons for using one common background model is based on the fact that before creating the model, we need to extract a wavelet and correlate the synthetic seismic against the input seismic. After extracting the wavelet we are to correlate with the well, which correlates the well log to the real seismic and creates the basis on which the background model can be created. When we are correlating, by stretch and time-shift, we are actually stretching the original P-wave log. By keeping the stretch equal for all input seismic and only extracting their respective wavelets, we are keeping the background model (and original log) equal for all inversions. This was important, so that the logs didn't vary from inversion to inversion.

Before making a background model, the correlation between the original log synthetic traces and the seismic in the well location, were tried for all input seismic to find out which one that correlated the best (had the highest value). The input seismic with the best correlation was then used as a reference to the stretch and time-shift, and also a reference for the background model. The input seismic that obtained the best correlation was;

*003_03 -> **Cable combination** seismic acquired in **low tide** with vessel direction of **296 degrees**.*

The background model was then created based on the original logs (P-wave and density), and followed the horizons interpreted by the author. An illustration of the model can be seen in the figure below (Figure 4-2). The background model is a low frequency model and represents the a-priori information. It consists of frequencies ranging from 0-6 Hz, with an overlying interval from 6-8 Hz.

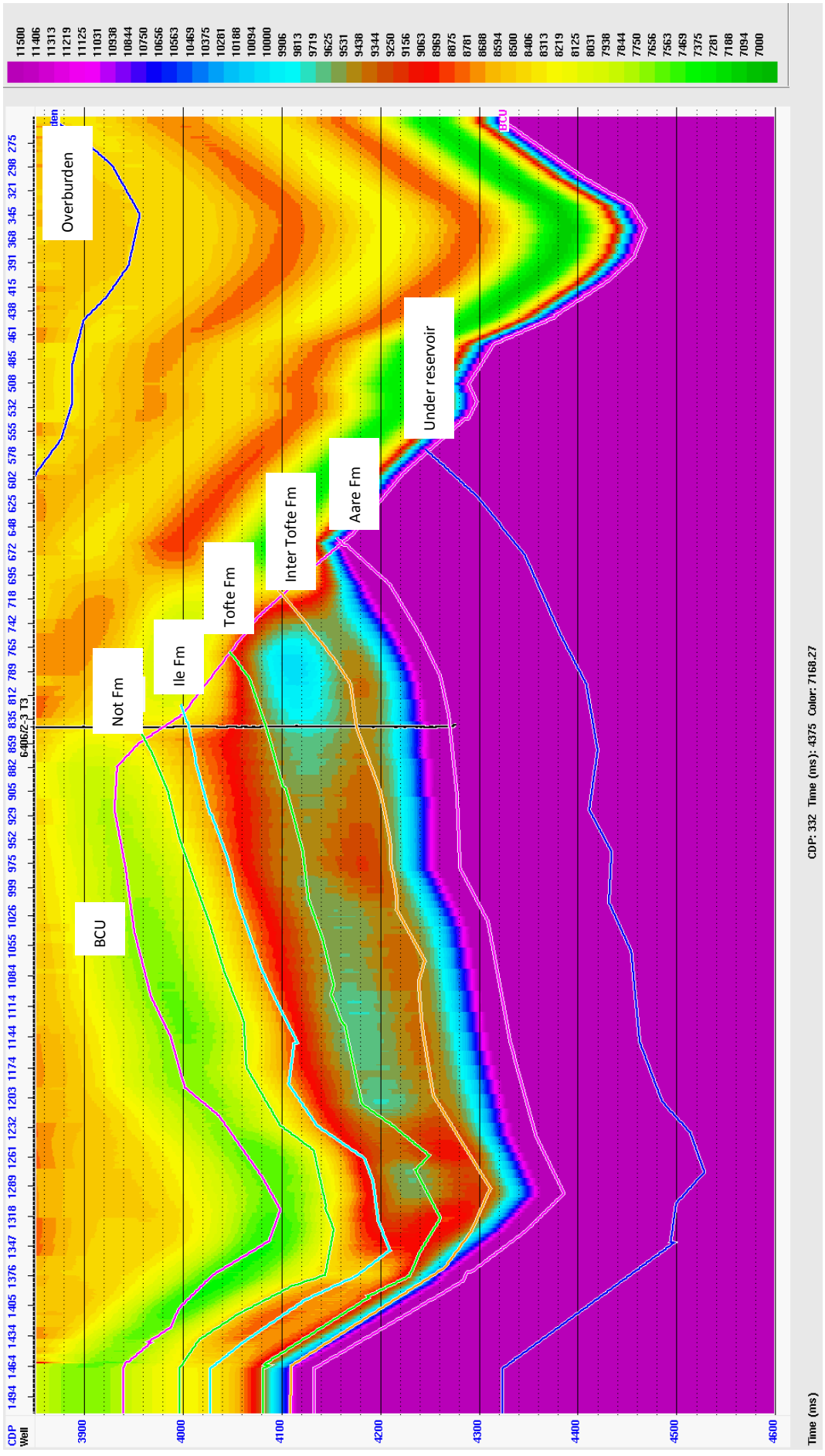

Figure 4 - 2: *The background model used for all inversions. The horizons are described earlier, whilst the blue horizon at the top, is an interpreted horizon which is consistent for the overburden. The scale on the right is in acoustic impedance.*

4.1.1 Inversion analysis

Hampson-Russell has some built-in tools to help the user confirm the validity of the inversion, one of them is *the inversion analysis*. The inversion analysis illustrates the impedance log-trace overlying the impedance trace from the inversion itself. By looking at the different inversion analysis windows between the cable combination seismic as input and the single cable seismic as input we can identify differences within a time-section, differences in error from the original impedance log trace and the total error in acoustic impedance (shown as a number at the top of the illustration).

Despite the fact that this is called an inversion analysis window, the window only illustrates the difference between the traces in one trace location, the well location. All inversions consist of a time-window from 3852 ms to 4352 ms, and ranging a total of 700 different traces equal to the reservoir section. There is a large error at the end of the inversion in all volumes, which relates to the end effects of then inversion window. Since acoustic impedance in the original log is increasing dramatically at the end of the inversion window, the inversion suffers from end effects due to the slow change of the background model (low frequencies) and that the inversion only can deviate by a curtain degree outside this value (constrained inversion). The effect, when comparing the original log to the inverted trace, is that we have large error values at the end of every inversion done by the author. To compare the different inversions, it is important to keep that in mind, and not put too much weight on the end effects regarding the analysis of them.

The Inversion Analysis window for both cable combination seismic input and single cable seismic input can be observed in the figure on the next side (Figure 4-3). Since we have used 003_03 (see 1.3 Datasets) as reference volume for the correlation, we are comparing the single cable seismic input with the reference inversion, which has equal tide and vessel direction. The datasets compared are therefore 003_03 and 003_02 (see 1.3 Datasets).

By only looking at the error number at the top of Figure 4-3, the number indicates that the cable combination inversion is better resolved than the inversion with the single cable seismic as input. However, this error number is calculated by only adding the error number between the inversion trace and the original impedance log trace each 4 ms, which we can tell is both positive and negative. If we analyze the error between the two traces closer, we can tell that in some areas the single cable inversion is better resolved, and follows the original log trace better, e.g. in the area from about 4000ms – 4100ms. The single cable inversion in this area can follow the small changes in the original impedance trace, while the cable combination inversion has a smoother transition. Since the error is an added sum, the sum of errors in the single cable inversion would be larger (but more consistent) than the cable combination inversion.

There are also areas where the cable combination inversion is following the original log trace better than the single cable inversion. If we look in the area above 3900ms and from 4160ms – 4180ms, the cable combination inversion (b) is following the original impedance trace slightly better than in (a). It can seem that there is a small time shift error between the single cable inversion and the original log trace in these areas.

Since the error number here is an added number, we will look more closely at the absolute error for each time sample in the inversion time window (3852-4352 ms).

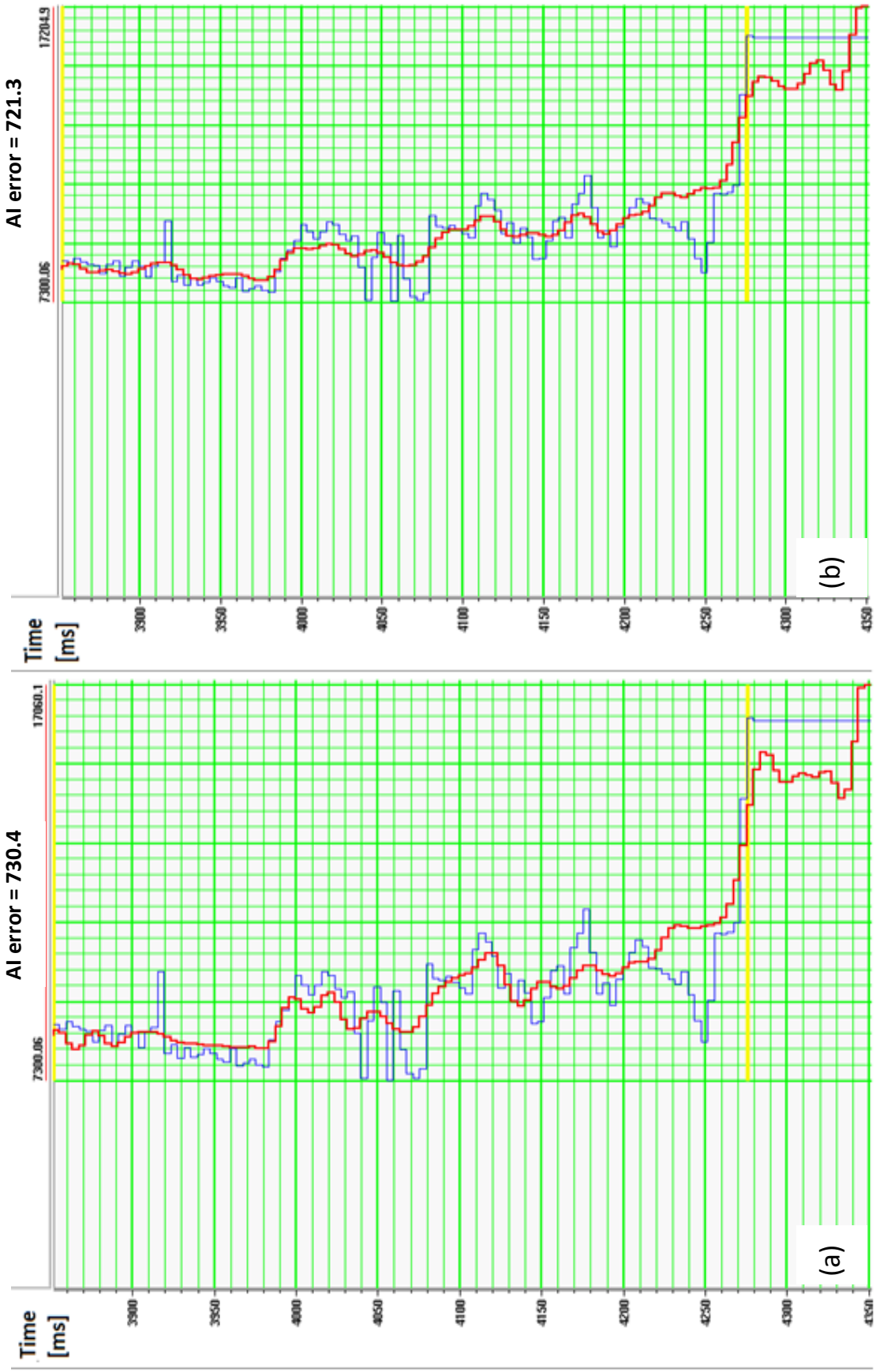

Figure 4 - 3: *Inversion analysis for both a single cable seismic input (a) and a cable combination seismic input (b).*

4.1.2 Crossplot absolute impedance error versus time

Because of the implications described in the previous subchapter (see 4.1.1 Inversion analysis), the need for a crossplot of the absolute error versus time were necessary. Then we could better analyze the error from the original log impedance trace with time. The error here is in absolute value to highlight the changes.

By analyzing the changes, we would like to see either a smaller change in one of the windows or a more consistent change through the time interval. Note that the inversion here is only one trace as for the inversion analysis window, so even if the error is better for one of the inversions, the uncertainty of what the result is for the other 699 traces is still present (700 traces in total). On the x-axis of the crossplot we have the time interval of the inversion (3852-4352 ms) with a sampling rate of 4 ms. The y-axis denotes the error in acoustic impedance and the color bar is also in the size of the error in acoustic impedance.

Since we already know that the end effects are significant for all inversions, the analyzed part is basically beneath this end effect. The changes that the discussion and results are based on are also beneath these larger values at the end.

The cross plots of the error versus time for both the cable combination inversion and single cable inversion can be seen in Figure 4-4.

4.1.3 Histogram count versus absolute impedance error

For closer evaluation of the error for that trace, a histogram of the count (error) versus acoustic impedance is also included in the paper. As for the crossplot, we want to see a consistent change for the count, respectively to lower values or to a narrower width of the distribution of the error. The histograms for both inversions previously mentioned are outlined in figure 4-5.

To make an analysis of the inversion and the differences, all these cross plots, inversion analysis and histograms must be compared to each other to fully see the effect of the different acquisition methods. This will be more discussed in Chapter 5.

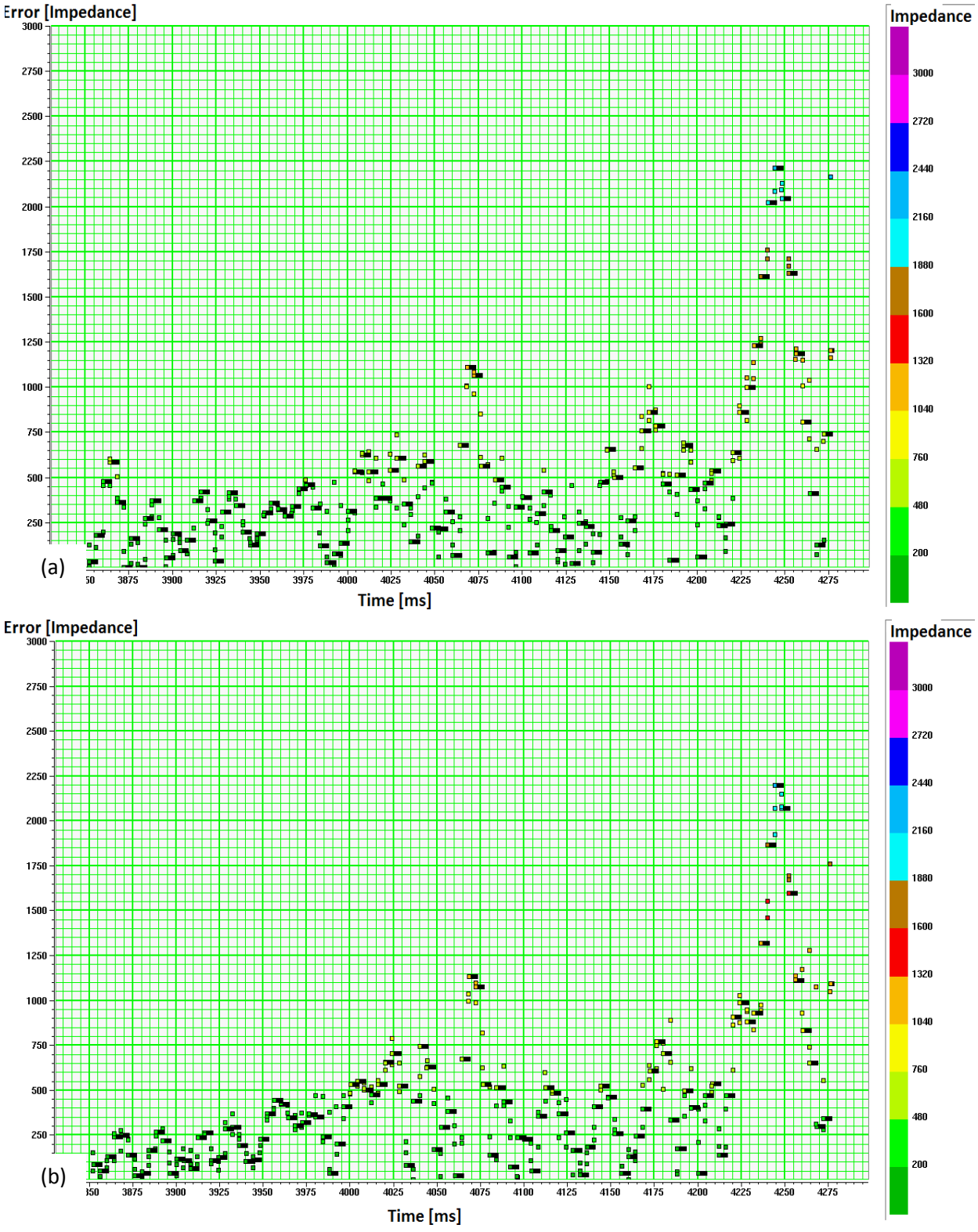

Figure 4 - 4: Cross-plots of error versus time. Figure (a) uses single cable inversion as input, while figure (b) uses cable combination inversion as input.

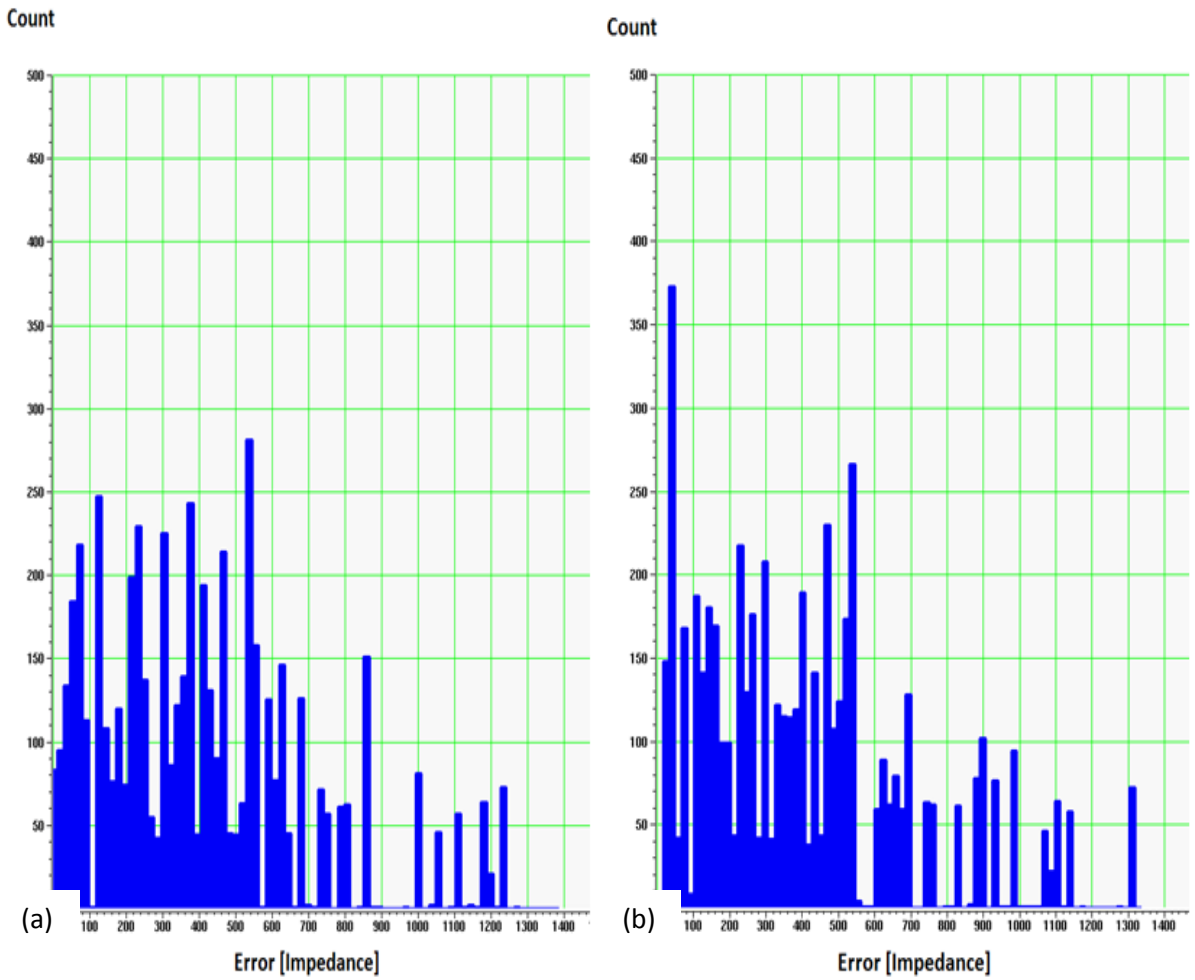

Figure 4 - 5: *Histograms of count versus error. Figure (a) uses single cable inversion as input, while Figure (b) uses cable combination inversion as input.*

4.1.4 Wavelets and vertical resolution

Since we are comparing the seismic from 2 different acquisition methods, we need to analyze the differences between the statistical wavelets to each seismic. Both seismic images are equal both in acquisition direction and tide, and are only separated by the acquisition method, respectively over/under cable combination and single cable.

Since vertical resolution plays a significant role in the seismic imaging, both for detecting the true geology (including thin layers) and inversion, analyzes of the vertical resolution due to the seismic wavelet in the reservoir section was important. Hereunder we will first illustrate the difference between the two wavelets;

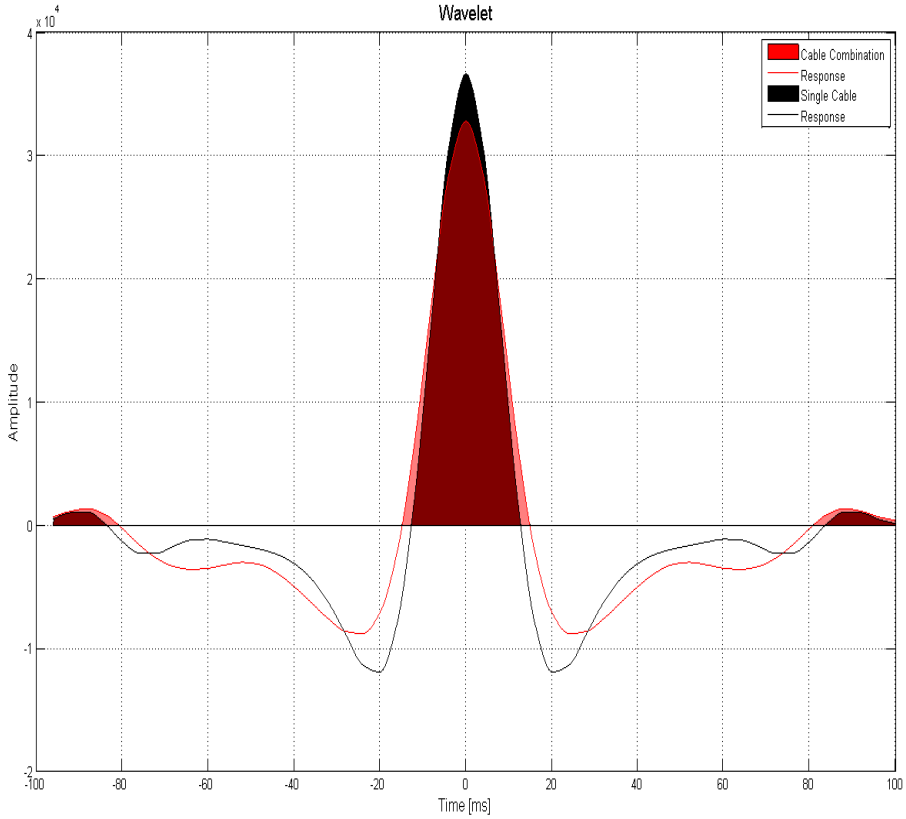

Figure 4 - 6: *Two zero-phase wavelets from the cable combination and single cable seismic. Both wavelets are statistical wavelets and are extracted in a time window equivalent to the reservoir section (3852 – 4352 ms).*

Both wavelets are zero-phase wavelets (see 3.2 Seismic wavelet). The difference in time response between the two is of a measurable size and creates different time response to depth for their respective seismic lines. The difference can be measured by several methods, e.g. from Fourier transforms, dominating frequency of the time window analyzed and response of a 'pinch-out' (Berkhout, 1984). In this thesis we have chosen to use the analysis of a 'pinch-out'.

By creating a reflection-coefficient matrix, we can determine at which point we want reflections from the wavelet. Creating a horizontal layer with reflection coefficients of 1, and a dipping layer also with reflection coefficients equal to 1 along the line, we can create the effect of a pinch out. Besides these reflection coefficients chosen by the user, the remaining points of the matrix are set to have the value 0.

After creating the reflection-coefficient matrix with a given wedge, we are convolving the matrix with the given wavelet, creating the time response a seismic line (without noise) would give in a similar case. By analyzing the reflections along the pinch-out plane we can observe at which point the time response along the line are not separable anymore, but has the response of a single wavelet. At this time interval between them, we can observe the seismic resolution given by the used wavelet.

Figure 4-7 to 4-9 are illustrating the response with the two different wavelets to a pinch-out, given the method explained above. The time response is programmed in Matlab and the code is given in the Appendix.

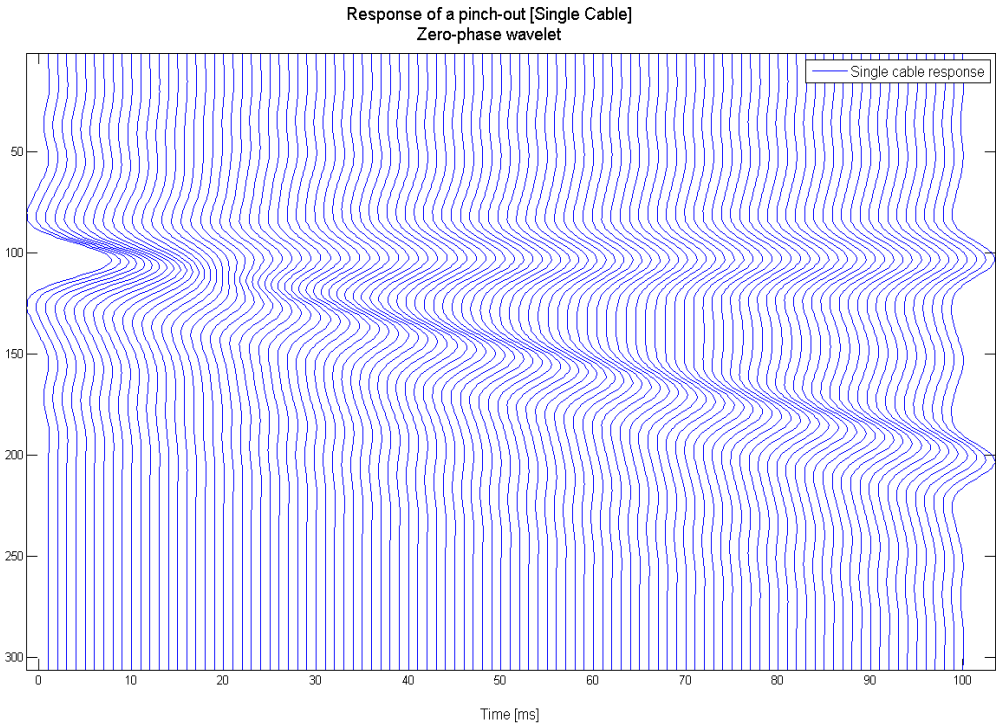

Figure 4 - 7: *Time response of a pinch-out with a zero-offset statistical wavelet extracted from single cable seismic in a time window equivalent to the reservoir section of the Kristin Field. The vertical resolution is given where we cannot separate the two responses, and is observed as 17 ms in this reflection configuration.*

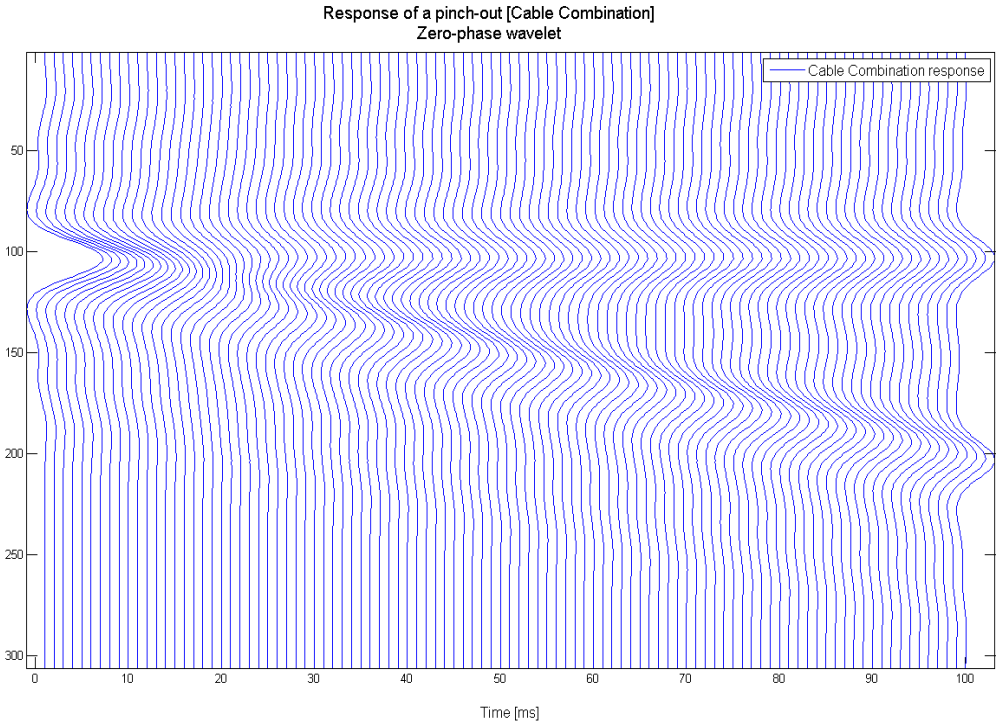

Figure 4 - 8: *Time response of a pinch-out with a zero-offset statistical wavelet extracted from cable combination seismic in a time window equivalent to the reservoir section of the Kristin Field. The vertical resolution is given where we cannot separate the two responses, and is observed as 20 ms in this reflection configuration.*

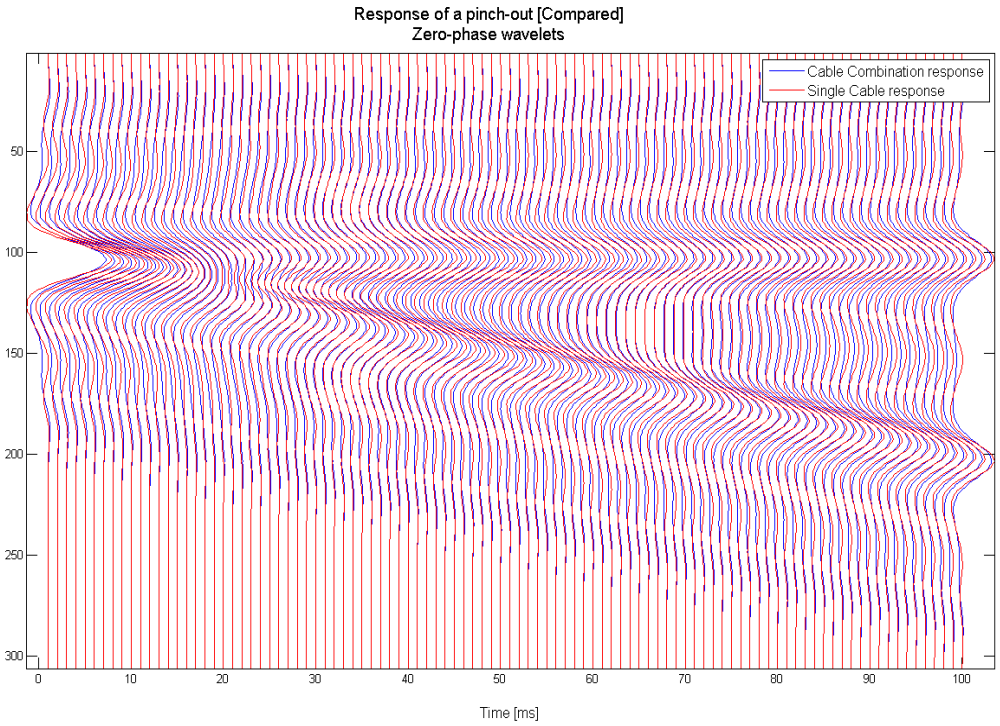

Figure 4 - 9: *The two time responses of a pinch-out given by Figure 4-7 and 4-8. The differences can easily be observed close to the pinch-out, where the single cable has observable better vertical resolution than the cable combination.*

As illustrated by figures 4-7 to 4-9, the single cable seismic has better resolution than the cable combination seismic, respectively 17 ms and 20 ms in a reflection configuration given the reflection matrix of the experiment. The difference between them is hence 3 ms. This is the result for that particular experiment, but identifies the relative difference in vertical resolution favoring the single cable method. We can here calculate the improvement, which is **17.6%** in favor of the single cable method. Note also that after the responses cannot be separated from each other towards the pinch-out, we have tuning effects in the figures.

Since the change of the vertical resolution, the reflection in the single cable seismic would detect narrower transitions than the cable combination seismic, resulting in detection of thinner layers than the cable combination seismic.

4.1.5 Differences in seismic and inversion volumes

We are comparing volumes with two different input seismic files in this subchapter, respectively 003_03 and 003_02 (see 1.3 Datasets). They are equal both in vessel direction (296 degrees) and tide (high tide), while the acquisition method is different. Suffix 02 denotes single cable, while 03 denotes cable combination.

Based on figures 4-7 to 4-9 the difference in vertical resolution between the two different acquisition methods is favoring the single cable method. The change is consistent when comparing the other datasets as well.

Because of the wavelet differences, we would theoretically see differences in the seismic images. In Figure 4-10 we can observe a difference-image, where the single cable seismic is subtracted from the cable combination seismic. The difference image will give us a clue where we have differences in the two seismic images (the two seismic inputs can be seen in Appendix). The differences might be a result of the wavelet, different signal-to-noise ratio and different multiple attenuation in the processing.

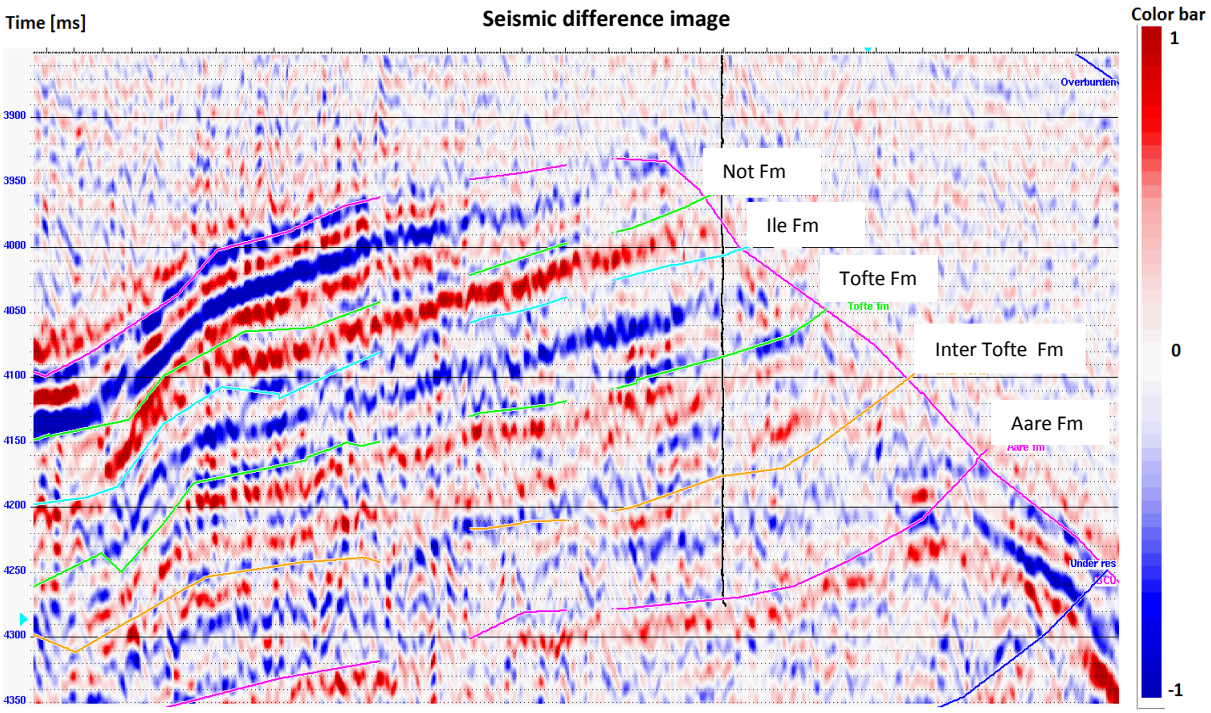

Figure 4 - 10: *Difference image between the cable combination seismic and the single cable seismic. The time window is from 3852 ms to 4352 ms (the Kristin reservoir section). The color bar has the unit* $[(\frac{m}{s}) * (\frac{g}{cm^3})]$.

The interpreted horizons are from the original seismic, which is common for all the seismic images. The reservoir section has the extent from the BCU (purple top layer) to the Aare Formation (purple layer at the bottom). The interval between BCU and the first green horizon (Not Formation) is called Garn Formation. We can easily see that the largest changes are on the western flank of the reservoir in this layer. Because the well does not cover the Garn Formation, the differences in this layer will not be weighted.

It is also important to mention that were the slope of the layer changes on the western flank (changing from a steep to a flat slope), there is a fault (see Figure 2-6).

The figure above illustrates however that there is changes between the seismic inputs in the Ile Formation. This change is horizontally consistent throughout the layer. Consistent changes throughout the layers is important to look for in difference images concerning seismic input, because

these changes can be layers which are not covered by one of the seismic lines. Random changes which are not consistent often turn out to be just noise. We can also observe another horizontally consistent change which starts in the Aare Formation and crossing over to the Inter Tofte Formation in the more eastern part of the seismic.

Based on the differences in the seismic images, we want to investigate if we could see equal changes in the inversion image, hence Figure 4-11 illustrates the difference image between the cable combination inversion and single cable inversion. If the process of inversion has been optimized using the cable combination acquisition method, we could identify similar changes in the inversions also.

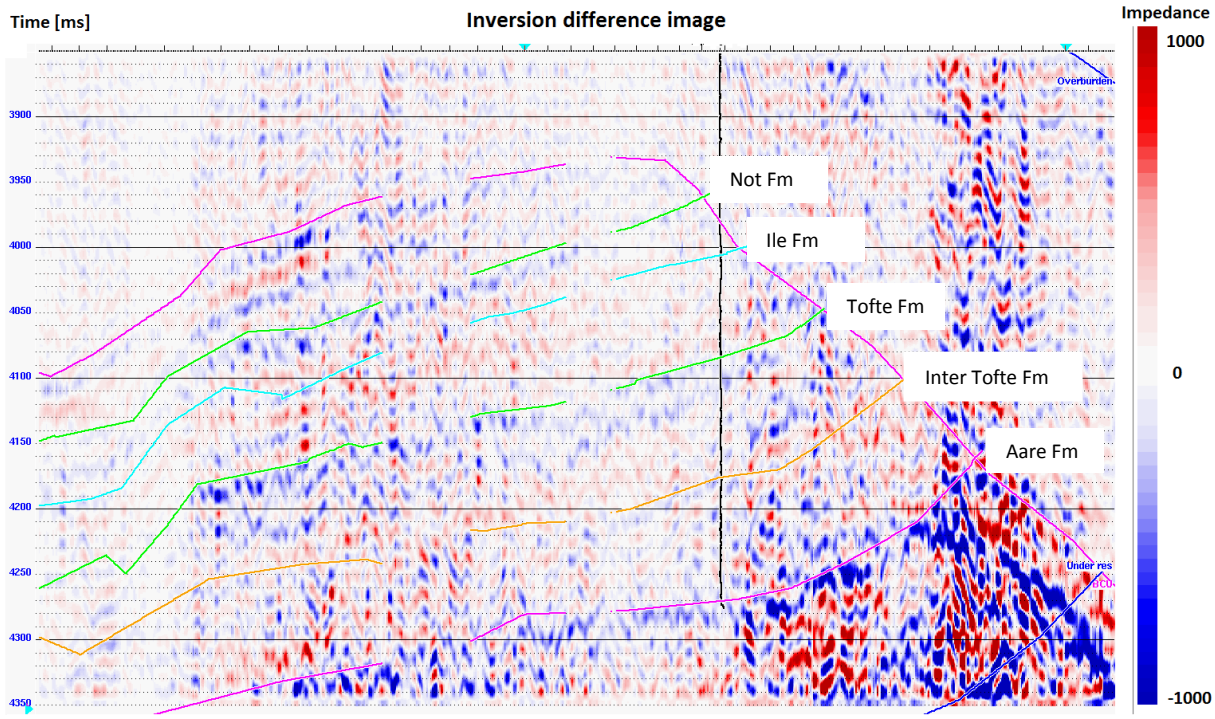

Figure 4 - 11: *Difference image between the cable combination inversion and the single cable inversion. The image covers exactly the same area as figure 4-10. The color bar has the unit* $[\left(\frac{m}{s}\right) * \left(\frac{g}{cm^3}\right)]$.

The inversions of both datasets are illustrated in figure 4-12 and figure 4-13. If we compare these volumes with the result in figure 4-11, we can tell that the deviations are basically changes in size of impedance within the layer. This is also confirmed by the extent of the color bar in figure 4-11, which ranges from -1000 $[\left(\frac{\mathbf{m}}{\mathbf{s}}\right) * \left(\frac{\mathbf{g}}{\mathrm{cm}^3}\right)]$ to 1000 $[\left(\frac{\mathbf{m}}{\mathbf{s}}\right) * \left(\frac{\mathbf{g}}{\mathrm{cm}^3}\right)]$, indicating changes within a layer and not a difference in number of layers (since the color bar from the inversion ranges from 7000 to 11500$[\left(\frac{\mathbf{m}}{\mathbf{s}}\right) * \left(\frac{\mathbf{g}}{\mathrm{cm}^3}\right)]$).

Yet, the difference between the between the two images is still valid, and will be discussed in Chapter 5. Larger images of the inversion volumes can be seen in the Appendix.

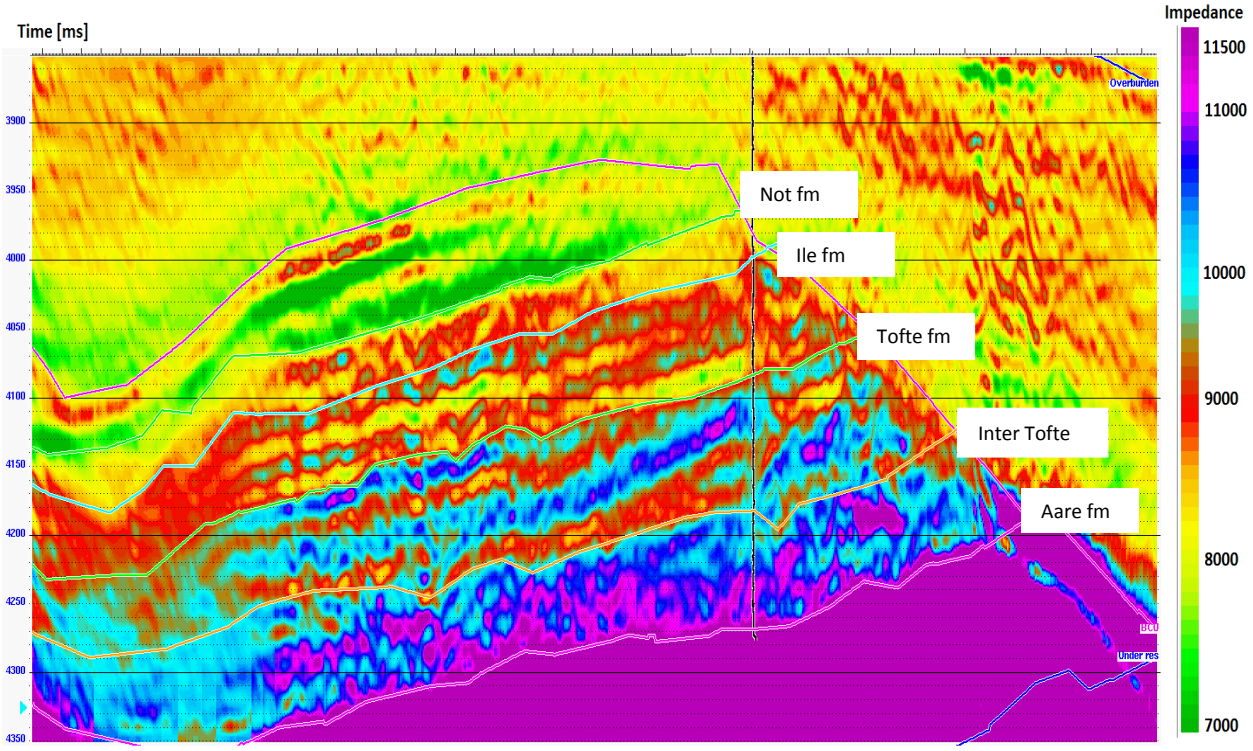

Figure 4 - 12: *Inversion volume with the single cable seismic as input (003_02). Values are in acoustic impedance.*

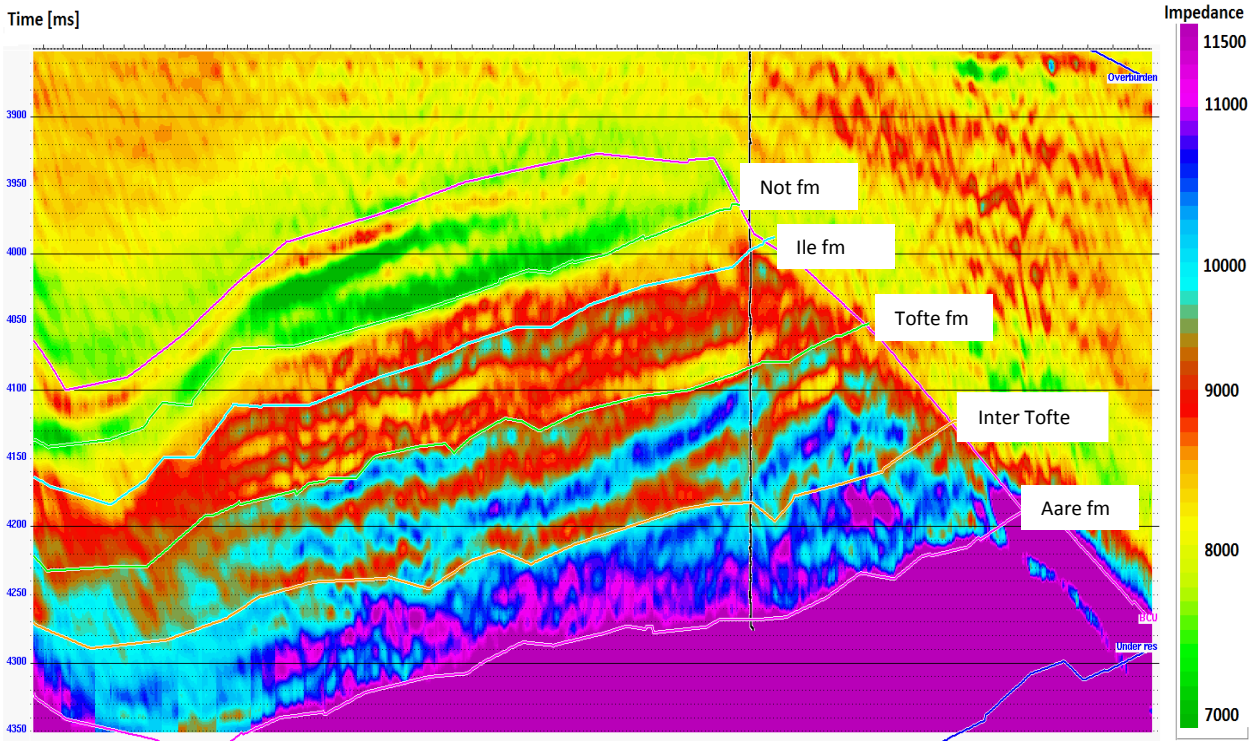

Figure 4 - 13: *Inversion volume with the cable combination seismic as input (003_03). Values are in acoustic impedance.*

4.2 Correlation with synthetic traces

Before the process of inversion can take place, we are correlating the well to the synthetic trace based on the different seismic lines and their respective wavelets. The correlation is the basis that we build the background model on. Since we in this paper have one common background model, the stretch applied to the well log is equal for all the seismic lines, and the correlation between them would therefore be based on how much they correlate with the reference volume and its respective wavelet (and might also suffer from it).

Still, we want this correlation to be as good as possible, without stretching the original too much. By stretching the log, we then are tweaking the a-priori information to best fit the data. The stretching must be done carefully to prevent the a-priori information to be destroyed. The reference volume is therefore the volume that has the best correlation with the well log with the least amount of stretch to the log.

Since the synthetic data is made by their respective wavelets, the correlation between the respective seismic lines would be best between the seismic with similar wavelets, hence the best correlation between the seismic with equal acquisition method. This will be explained more in Chapter 5.

A correlation table could be necessary to analyze which volumes has the best correlation, and in comparison with other parameters see what has the most influence on the correlation and also on the inversion. In figure 4-11 we are illustrating the different correlation in a histogram, where the reference volume is 003_03 (see 1.3 Datasets). We are here comparing both equal direction and equal tide, and also the changes from single cable to cable combination. The changes in the seismic wavelet must also be taken into account, see figure 4-6. The synthetic and the well trace are 1 trace in the middle to eastern part of the reservoir and describe the time response for that trace. The only part we with absolute certainty can conclude with is hence this trace. We will describe this in the next chapter (see Chapter 5).

There are different trends that are valid in the correlation histogram of figure 4-14. First of all, the cable combination correlations are all larger than the single cable combination, except the correlation where the seismic is acquired in high tide and vessel direction of 116 degrees. For the cable combination, the correlation is best with equal direction (correlation with the synthetic is best for the volumes with equal direction).

4.2.1 Correlation with single cable outlier as reference

The single cable correlations are all fairly similar, except one outlier, which is “116 degrees, low tide”. For comparison reasons, we then wanted to do the correlation with the different lines of the single cable seismic with this outlier as a reference. The different correlation can be seen in a histogram in figure 4-15.

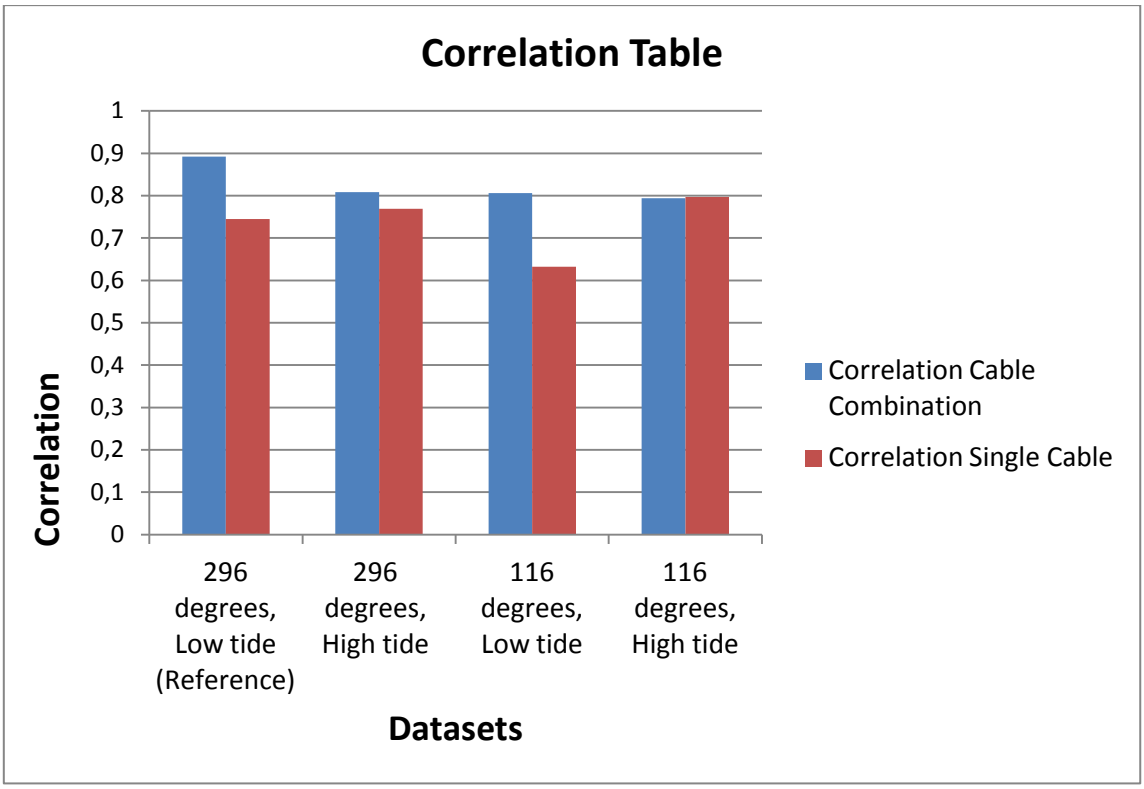

Figure 4 - 14: *Size of the different correlations between the seismic and the synthetic traces at the well location. The correlation size is sorted in cable combination and single cable with equal tide and direction.*

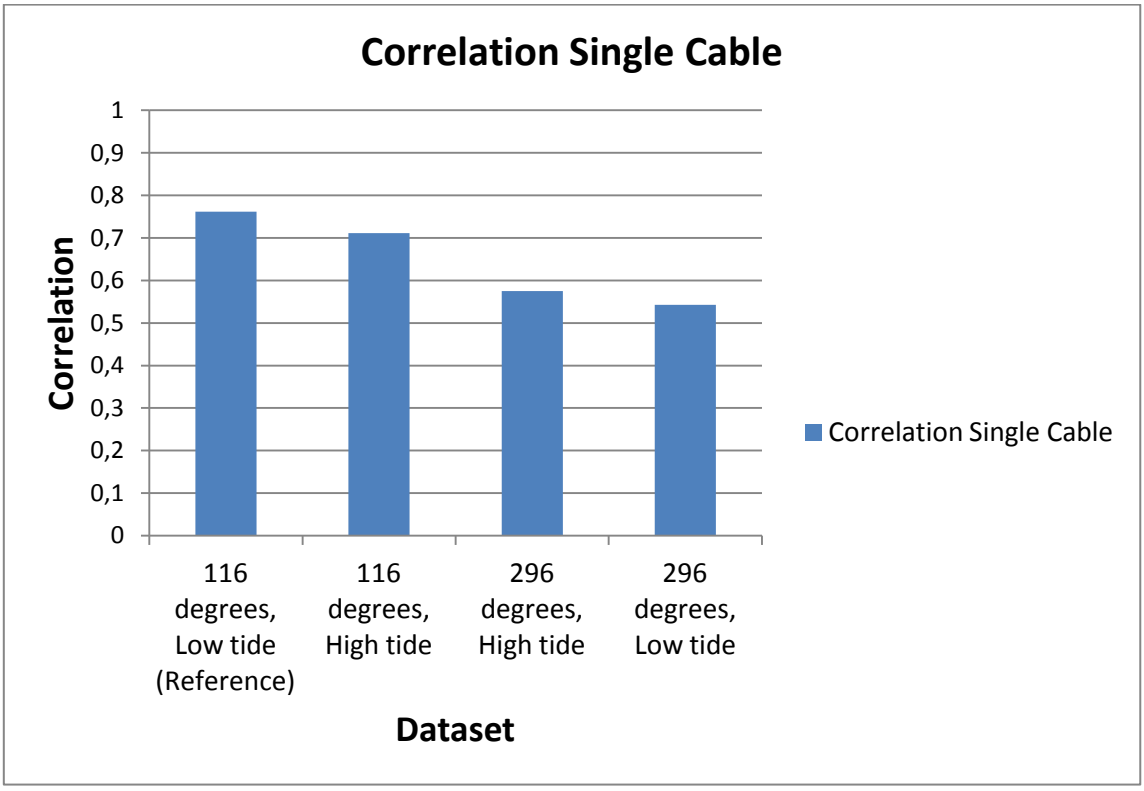

Figure 4 - 15: *Size of the different correlation between the seismic and the synthetic traces at the well location. The correlation size is sorted based on the size of the different correlations.*

From figure 4-15 we can observe that the reference volume has the best correlation (which is natural, since the stretch for the correlation is now optimized for this volume). A trend in the histogram is that the best correlations are based on equal tide. The correlations of the seismic with vessel direction 116 degrees are significant larger than the seismic with opposite vessel direction. These are also fairly similar in size, as is for the opposite direction.

If we compare the result in the figures 4-14 and 4-15, we can tell that by using the outlier in figure 4-14 as a reference for figure 4-15, the change in correlation is a positive change with the size of 0.13, or an increase of 20.6%. The correlation here is done with as little stretch as possible to the original log, and the reference`s respective wavelet. The change for the correlations of the other single cable seismic lines is a negative change, which was expected, since the reference now was an outlier of the previous correlation and was the one that had the largest deviation compared to the other correlations.

4.2.2 Comparison with the error in inversion analysis

The correlations are based on the correlation with the synthetic trace in the well location, we can therefore compare the results in the correlation result, with the error in the inversion analysis, to analyze if some of the same trends can be observed after the inversion. The inversion in the inversion analysis window is one inverted trace at the well location.

In figure 4-16 we can observe the size of the sum of the error between the inverted trace and the original log impedance trace. In the figure we can observe that for the error with cable combination seismic as input is of smaller size than the single cable seismic as input for low tide, while the opposite is the case for the high tide case. The smallest error is with the reference volume as input, and this is also the case for the single cable seismic with equal tide and direction. This trend is not consistent with the observed trend in the correlation tables.

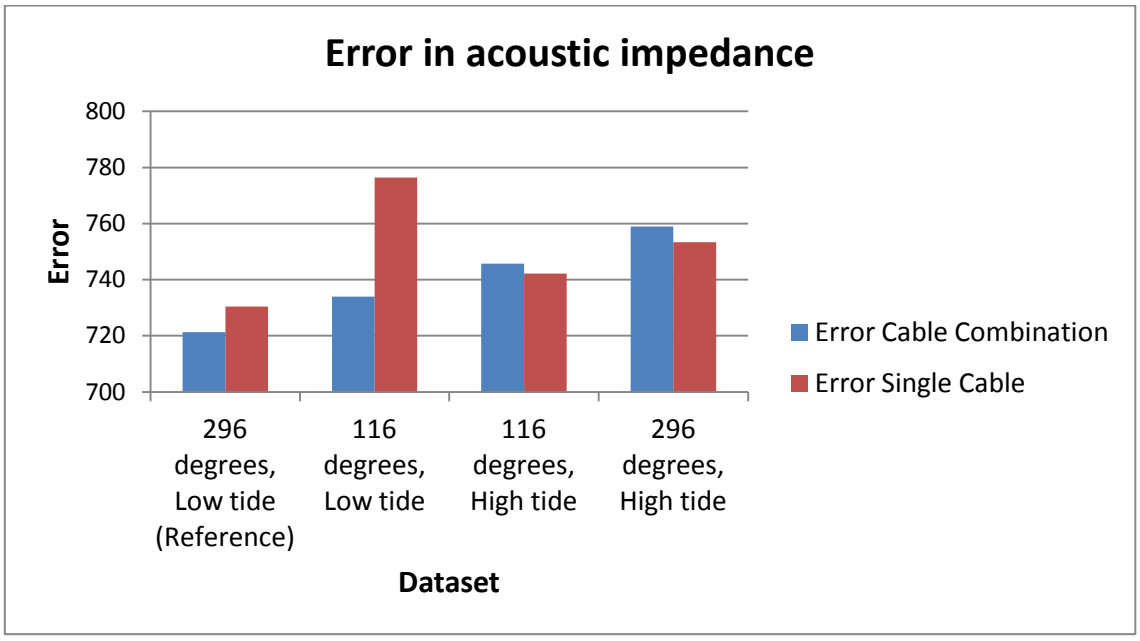

Figure 4 - 16: *Size of the error between the inverted trace and the original log impedance trace at the well location.*

4.3 Comparison of the inversion volumes with an average

Acquisition was done in 4 different stages, all resulting in 2 different datasets for each stage and a total of 8 different datasets. They all cover the same line, the differences between them are high and low tide and 2 opposite directions within each tide. To see if there were any improvements comparing all 4 datasets within the same acquisition method, respectively cable combination and single cable seismic, we wanted to compare them to an average volume.

Since the lines are covering equal areas, we can take the average of the 4 different volumes (for each acquisition method) and compare them to each of the lines. We are doing this for the inversion of both acquisition methods, to analyze if we have any improvements between them. For the best overview of the comparison, we are cross-plotting the inversion of each line to the average of the 4 lines. If we have a perfect fit between them, we would have a straight line, were each impedance volume in the line has the exact same value of impedance in the volume we are comparing it to.

For each inversion comparison, we are making a linear regression with the best fit between them, which are plotted on top of the crossplot. The theory behind minimizing the sum of squares can be evaluated in chapter 3.5 Inversion and Probability. Then the line would take the form of;

$$y = ax + b \tag{4-2}$$

where a is the slope and b is the intercept. Analyzing the data also requires that we take into account the uncertainty for the best fit. A method that can easily be calculated from the datasets is statistical mean and standard deviation between these, hence we have plotted a line above and below the linear regression line. These two lines are representing the uncertainty, and can be calculated through;

$$\begin{aligned} y &= ax + b + SD(x_1 - x_2) \\ y &= ax + b - SD(x_1 - x_2) \end{aligned} \tag{4-3}$$

where x_1 is the inversion, x_2 is the average of all the inversions and SD is the standard deviation. These lines now illustrate the uncertainty graphically, and can be easily interpreted by their size and also in comparison with the datasets. However, since standard deviations for all plots is of a relative small size compared to the size of the acoustic impedance, the values added and subtracted to create the comparison lines in the crossplot have been multiplied with 4. Statistical mean should be analyzed graphically to see how good the data fit with each other with increasing trace number. The mean is then illustrated as a number for each trace and then cross plotted with increasing trace number. We want this line to be as close to 0 as possible, or have a mean which is close to 0.

The cross-plots for inversion of the different datasets versus the average of them can be seen in two different figures on the next page. These are for the two different acquisition methods, to analyze if we can observe some improvements when moving from the single cable acquisition method to the cable combination method. Note that the scales are covering equal impedance values and the reference in each of the figures is an average of the inversions represented in the figure. The uncertainty and the plotting are programmed in MatLab (see 2.4 MatLab). The code can be seen in the Appendix.

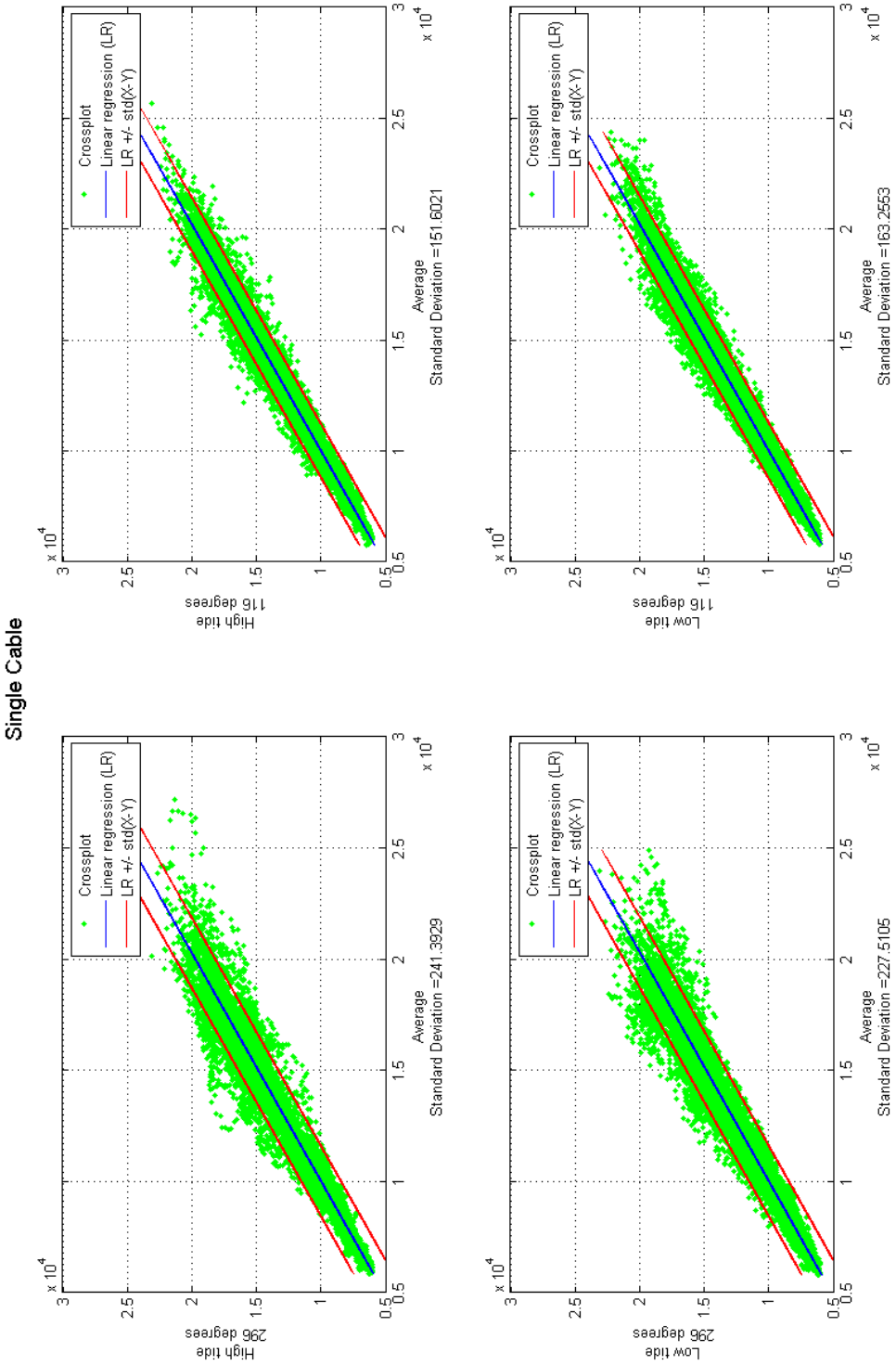

Figure 4 - 17: *Crossplot of 4 different inversion volumes versus the average of the 4. In this case the inversion volumes are the 4 different inversions with the single cable seismic as input.*

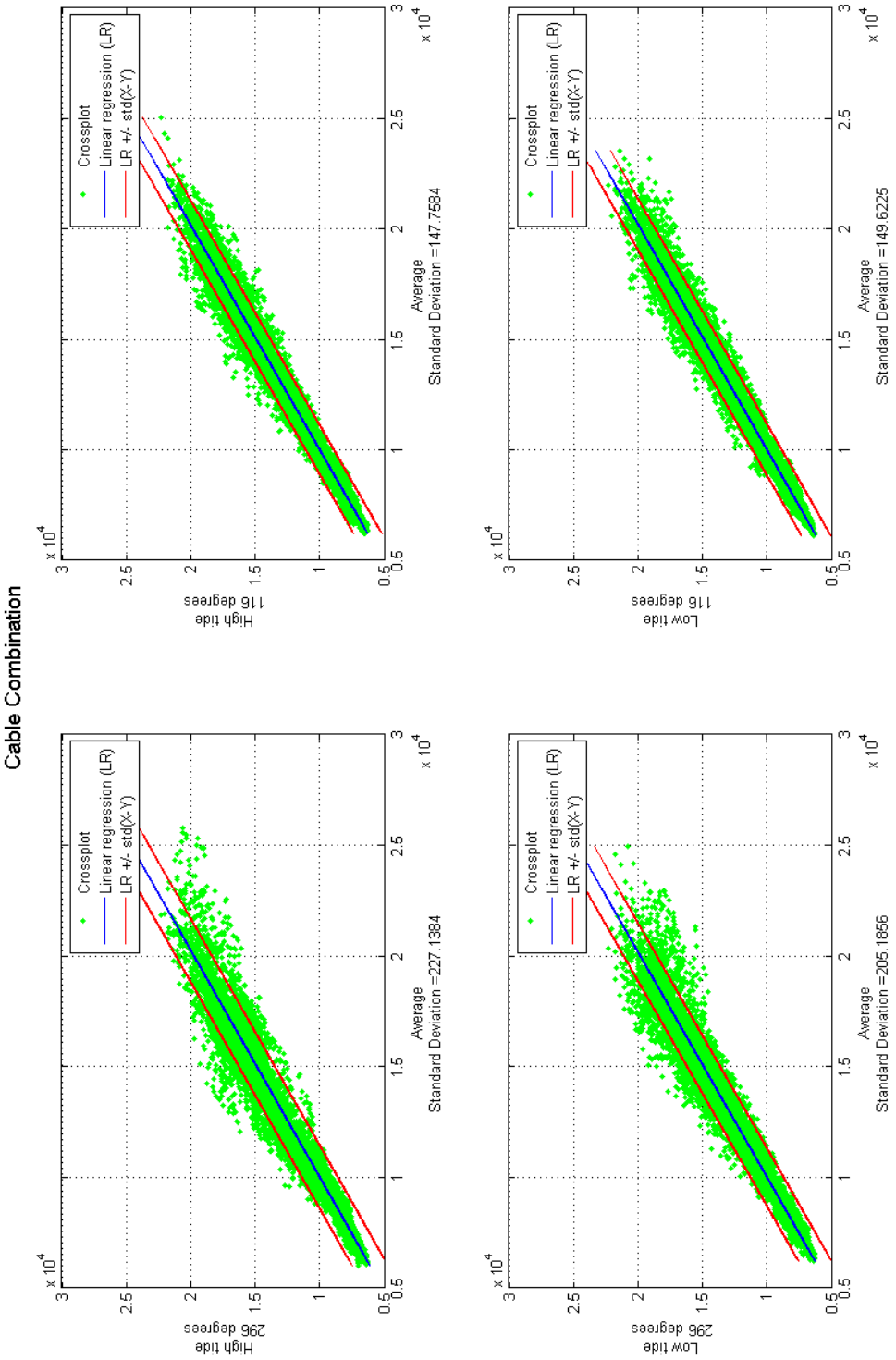

Figure 4 - 18: *Crossplot of 4 different inversion volumes versus the average of the 4. In this case the inversion volumes are the 4 different inversions with the cable combination seismic as input.*

If we compare figure 4-17 and figure 4-18, we can observe that the plots have many similarities. Both have the largest spread in the inversion versus the average with input seismic acquired in vessel direction of 296 degrees. Also, both have significant smaller spread when comparing those results to the inversion versus the average with input seismic acquired in vessel direction of 116 degrees. This can also be confirmed by the standard deviation, which has its value printed under the x-axis of every plot.

Comparing the difference in standard deviation, we observe that for similar cross-plots with different acquisition method, this value is decreasing when moving from the single cable to the cable combination crossplot. However, this difference is less significant than when we compare the different cross-plots based on opposite vessel direction.

4.3.1 Statistical mean with increasing trace number

For equal datasets as in the two previous figures, we can observe their respective statistical mean versus trace number. Since we know that we have large end effects in the east of the reservoir, due to the fault which cuts off the lower east corner, the statistical mean at higher trace number would deviate more than the mean at lower trace numbers.

As we can observe from the difference in figures 4-19 and 4-20, the mean tends to have the opposite trend as to what was observed for the standard deviation. The means tend to be of a lower value when we are moving from the inversion with cable combination versus their average to the inversion with single cable versus their average as input.

The general trend for the mean is that the single cable has lower values than the cable combination, and also seems to deviate less from graph to graph.

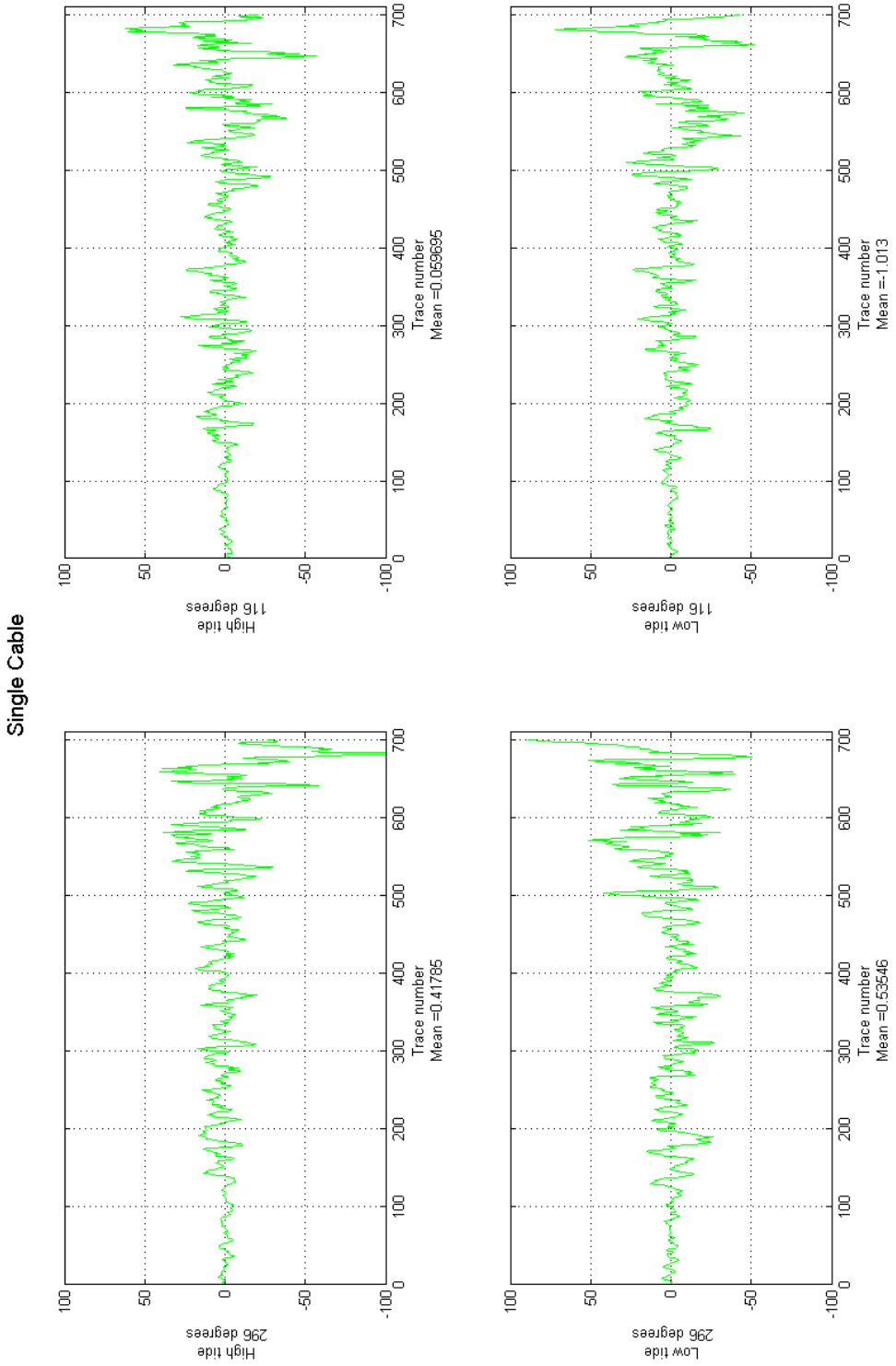

Figure 4 - 19: *Statistical mean for each dataset with increasing trace number. Each graph is the mean between the inversion with their respective dataset as input versus the average of all the 4 different inversions based on the single cable seismic as input.*

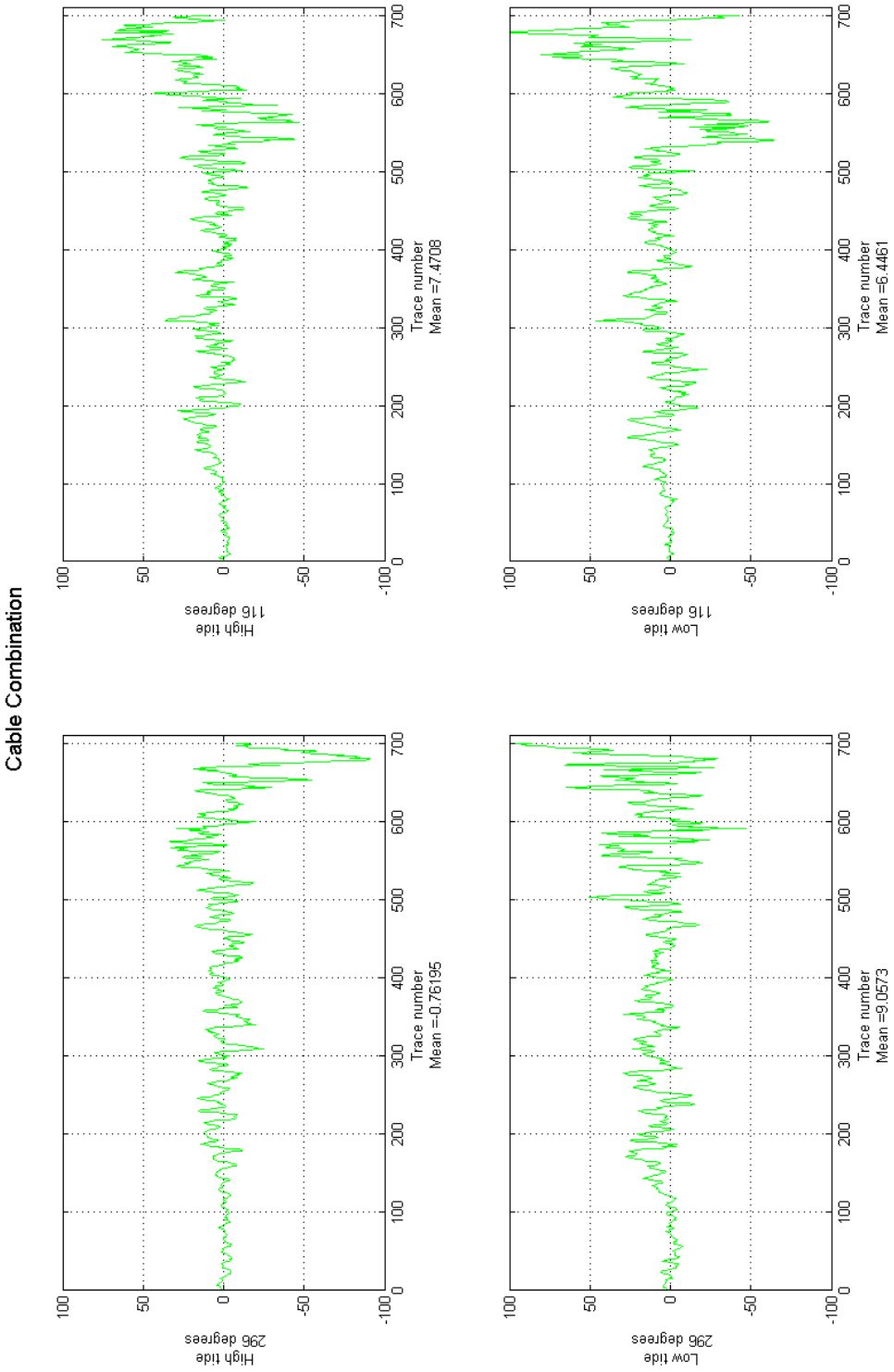

Figure 4 - 20: *Statistical mean for each dataset with increasing trace number. Each graph is the mean between the inversion with their respective dataset as input versus the average of all the 4 different inversions based on the cable combination seismic as input.*

4.4 Comparing the inversion volumes to the reference inversion volume

As previous mentioned all the inversions in the paper are based on a common background model (see figure 4-2). This background model uses the stretch done in the well correlation for one reference volume, dataset 003_03, to build the low frequency model. Dataset 003_03 is the seismic acquired with the over/under cable combination receiver and is acquired with vessel direction of 296 degrees and in low tide. Since we then have a model based on a reference volume, we want to compare the different inversions to this the inversion based on the input 003_03 seismic. From now on this will be referred to as *the reference inversion volume.*

The most important parameters we are analyzing are the differences between the inversions with single cable seismic input to the inversions with cable combination seismic input. For the cable combination acquisition method to have a significant impact on the inversion process, the differences between the inversions should be of a significant measure. As for all crossplot comparisons, we are also here using the standard deviation as a measure for the uncertainty for each crossplot. The comparison cross plots can be seen in figures 4-21 and 4-22.

From figure 4-21 we have different trends and results. The standard deviation, which is given beneath the x-axis of every plot, tells us that we have the best correlation with the reference in the cross plots where the input seismic is acquired in low tide with vessel direction of 296 degrees. This inversion is acquired in equal setting as the reference inversion volume. The other 3 volumes has a significant larger spread, and hence a significant larger standard deviation. For comparison reasons, we can see the different standard deviations for each dataset in table 4-1, where the table is organized by the input seismic.

Acquisition method	Tide	Direction	Standard Deviation
Single Cable	High tide	296 degrees	356.2
Single Cable	High tide	116 degrees	303.5
Single Cable	Low tide	296 degrees	179.8
Single Cable	Low tide	116 degrees	326.4
Cable Combination	High tide	296 degrees	350.1
Cable Combination	High tide	116 degrees	299.9
Cable Combination	Low tide	296 degrees	0.0
Cable Combination	Low tide	116 degrees	308.3

Table 4 - 1: *The different standard deviations in the cross plots of figure 4-21 and 4-22. The table is sorted by the cross plots` input seismic.*

Comparing the results in figure 4-21, figure 4-22 and table 4-1, there are one standard deviation which has the value of 0.0. This is because this inversion volume refers to the reference inversion volume. Comparing different acquisition methods with equal tide and vessel direction, the table and figures tell us that we have small improvement between each crossplot, with similar vessel direction and tide for the input seismic, in favor of the cable combination inversion. Analyzing the cross plots by visualization, we observe that these similar cross-plots contain approximately equal form and spread, this is also confirmed by the table (see table 4-1).

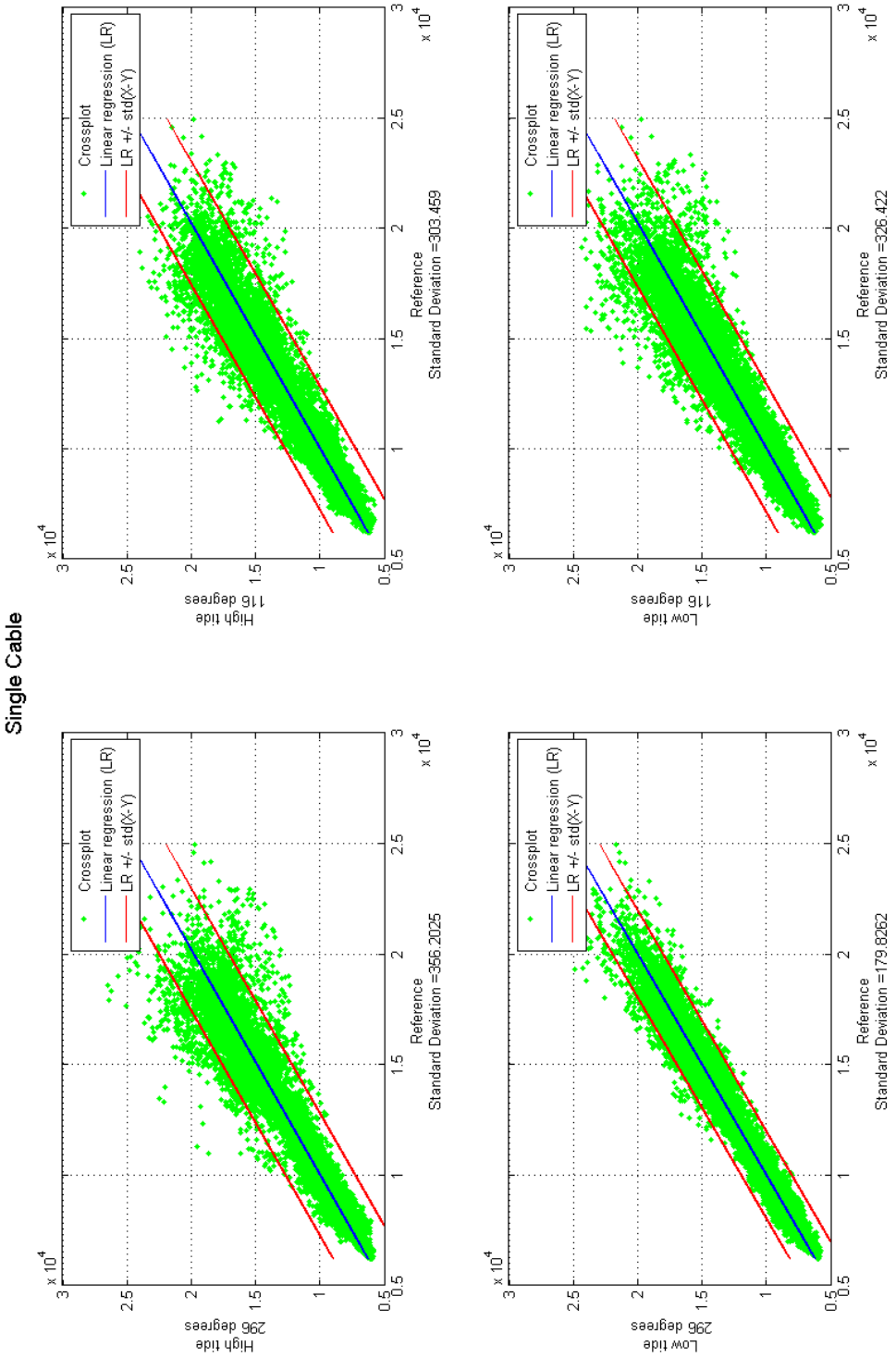

Figure 4 - 21: *Cross-plots of inversions, with single cable seismic as input, versus the reference inversion volume.*

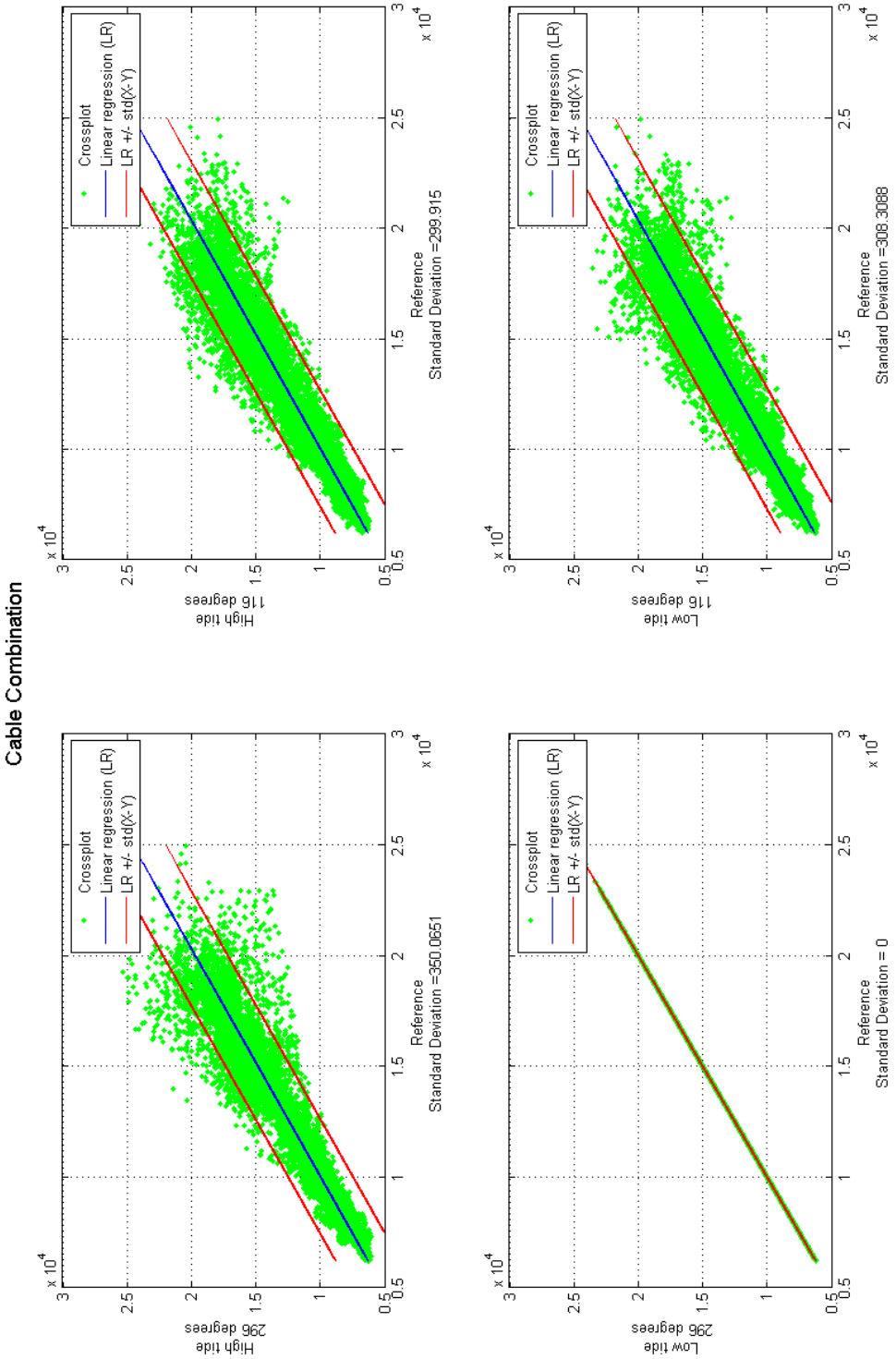

Figure 4 - 22: *Cross-plots of inversions, with cable combination seismic as input, versus the reference inversion volume.*

4.4.1 Reference inversion volume and average inversion volume

Since we now have the result from both the comparison with the reference volume and comparison with an average volume, we can compare the results. By comparing each crossplot, interesting trends and similarities can be analyzed for better understanding of which important parameters has the largest impact of the inversion process.

We are both comparing the different cross-plots, their standard deviation, cross-plots with equal input acquisition method, cross-plots with equal input acquisition direction and tide and where we have the largest difference between these plots. Table 4-2 is the table of the standard deviations within these cross-plots both for comparison with average and comparison with the reference inversion volume.

Acquisition method	**Acquisition tide**	**Acquisition direction**	**Standard deviation (reference)**	**Standard deviation (average)**
Single Cable	High tide	296 degrees	356.2	241.4
Single Cable	High tide	116 degrees	303.5	151.6
Single Cable	Low tide	296 degrees	179.8	227.5
Single Cable	Low tide	116 degrees	326.4	163.3
Cable Combination	High tide	296 degrees	350.1	227.1
Cable Combination	High tide	116 degrees	299.9	147.6
Cable Combination	Low tide	296 degrees	0.0	205.2
Cable Combination	Low tide	116 degrees	308.3	149.6
Average			**265.5**	**189.1**

Table 4 - 2: *An overview of the standard deviations for each crossplot in figure 4-17, figure 4-18, figure 4-21 and figure 4-22.*

There are 5 values that are significantly lower than the rest in this table (if we don't include the crossplot where we have reference versus reference, resulting in a standard deviation with a value of 0). 4 of them are within the cross plots compared with an average volume, and all of them are with input seismic acquired in the direction of 116 degrees, regardless of tide. The 5th value is within the cross plots compared with a reference inversion volume. The specific crossplot is where we are comparing the inversion with input seismic equal to the reference but different acquisition method.

At the end of the table, the author has also included an average value. This is the average of all the standard deviation, based on what they are compared to, respectively a reference inversion volume and an average inversion volume. Even though the comparison with the reference volume include a value of 0.0 (explained earlier), the average of the comparison with an average inversion volume still has the lowest average value. This is also the case for the single cable and cable combination alone.

4.5 Differences with respect to acquisition direction

In the last subchapter, we had some results indicating improvements in the inversion comparison where the input seismic was acquired in a specific direction, respectively 116 degrees. Hence we wanted to analyze the inversions based on the vessel direction of the acquisition.

The next plots are ordered into the direction of the acquisition of the input seismic, and also which acquisition method that was used. There are therefore 4 different plots that are highlighted, where all are acoustic impedance values from the inverted volumes which are ordered by their respective input seismic. Under is a list of the 4 volumes based on the input seismic;

1. Single cable seismic acquired in 296 degrees, high tide versus low tide
2. Cable combination seismic acquired in 296 degrees, high tide versus low tide
3. Single cable seismic acquired in 116 degrees, high tide versus low tide
4. Cable combination seismic acquired in 116 degrees, high tide versus low tide

Figure 4-23 consists of (1.) and (2.), while figure 4-24 consists of (3.) and (4.). By analyzing the inversion crossplot based on acquisition direction, we can see if there are differences between the cable combination and single cable inversion based on direction, which direction has the best correlation and why, and which measures that are significant.

Note that there originally were some differences in time due to the tide when comparing high tide and low tide, but these are corrected for in the processing of the seismic (Langridge, 2010). The impedance values with depth and two-way-travel-time are therefore fully comparable.

As we can observe from the cross plots in the figures, there are many differences between figures 4-23 and 4-24, while within each figure, the cross-plots are fairly similar. Both cross-plots of figure 4-23 have a large spread, hence also a large standard deviation. Comparing this to the result in figure 4-24, we can tell that the cross plots here have significantly smaller spread and standard deviation. The results for the standard deviation are summarized in table 4-3.

Acquisition direction	Acquisition method	Standard deviation
296 degrees	Single cable	377.6
296 degrees	Cable combination	350.3
116 degrees	Single cable	153.3
116 degrees	Cable combination	152.5

Table 4 - 3: *Results of the standard deviations from figure 4-23 and figure 4-24.*

Table 4-3 is a good illustration of the overall trend in the figures. We have improvements when moving from single cable to cable combination acquisition method, however this is not significant when comparing the result to the cross-plots with opposite direction. We could easily observe that the cross-plots comparing the acoustic impedance values based on the acquisition direction of 116 degrees has a significantly better correlation than the cross plots with direction of 296 degrees.

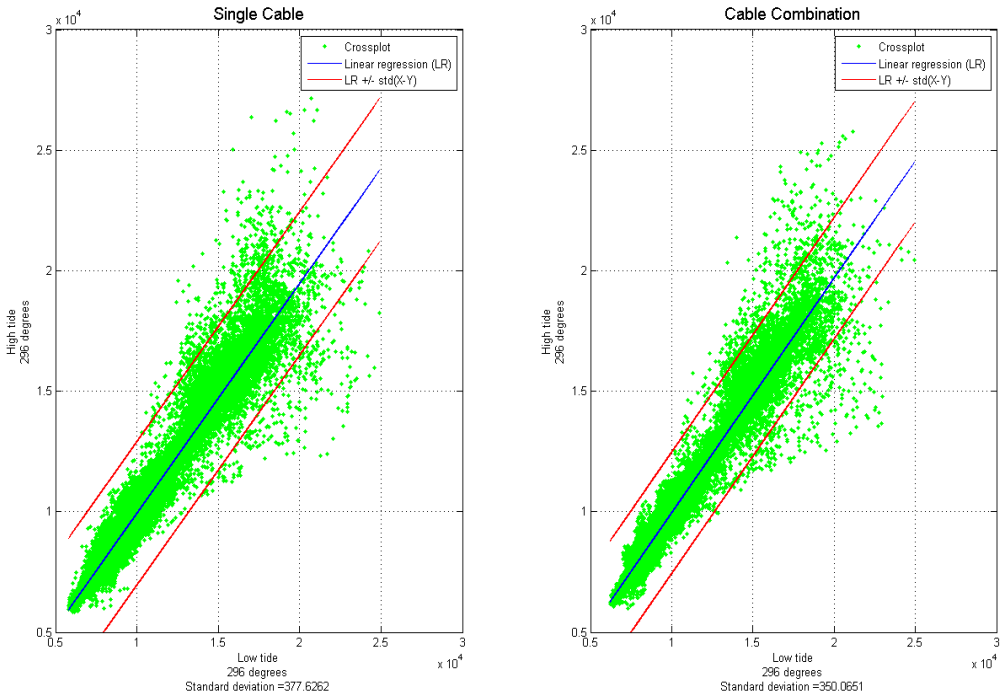

Figure 4 - 23: *Cross-plots of acoustic impedance values with 2 different acquisition methods. The direction of the acquisition of the input seismic is 296 degrees, and each crossplot are comparing high and low tide within that direction.*

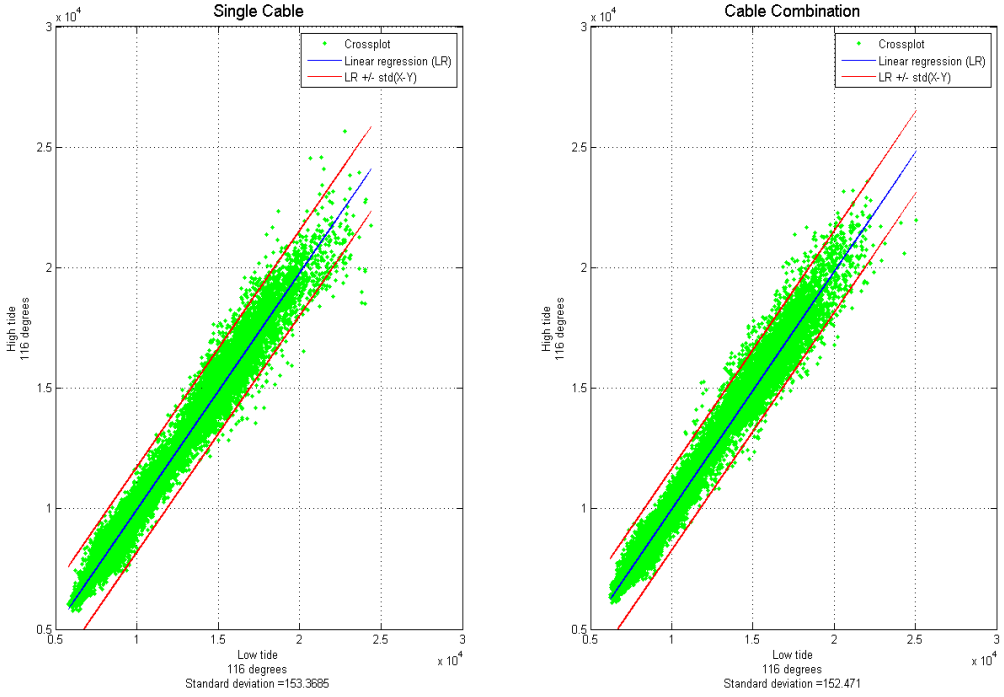

Figure 4 - 24: *Cross-plots of acoustic impedance values with 2 different acquisition methods. The direction of the acquisition of the input seismic is 116 degrees, and each crossplot are comparing high and low tide within that direction.*

The comparison of the inversions based on equal acquisition direction should in theory have more or less equal spread and standard deviation, since we are comparing low and high tide within equal direction (if we neglect different signal to noise ratio). However, the fact that the figures are very different made it important that this effect needed to be further investigated.

4.5.1 Signal to noise ratio

The figures 4-23 and 4-24 acknowledged that there is a difference in the inversion based on the acquisition direction of the seismic. Since we have a larger spread comparing the crossplot with acquisition direction of 296 degrees than with acquisition direction of 116 degrees, this raised the question if there could have been differences in the weather noise at the different acquisitions. This question was also discussed with Mr. Mark Thompson, which could conclude that the weather was quite stable during the whole extent of the acquisition. However, the signal to noise ratio could still vary between the acquisition directions and needed to be further evaluated.

The reason for the higher frequencies in figure 4-25 to 4-28 is because the spectra are extracted before migration, so they contain higher frequencies than in the post stack seismic that is used as input to the inversion process. However, the signal to noise ratio illustrated in figure 4-25 to figure 4-28 is still a god indication of the ratio after migration as well.

Comparing the results for the signal to noise ratio, there are small improvements in the ratio in favor of the cable combination for each acquisition, except for the spectra extracted from the acquisition in high tide and vessel direction of 116 degrees (sequence 002) were the ratios are equal. Comparing the result from the last section with the results for the signal to noise ratio, we can summarize them by table 4-4;

Acquisition direction	Acquisition method	Standard Deviation	S/N High tide	S/N Low tide
296 degrees	Single cable	377.6	3.1	2.9
296 degrees	Cable Comb	350.1	3.3	3.2
116 degrees	Single cable	153.3	3.1	3.1
116 degrees	Cable Comb	152.5	3.1	3.3

Table 4 - 4: *Results from table 4-3 and the result from the signal to noise ratio from figure 4-25 to figure 4-28.*

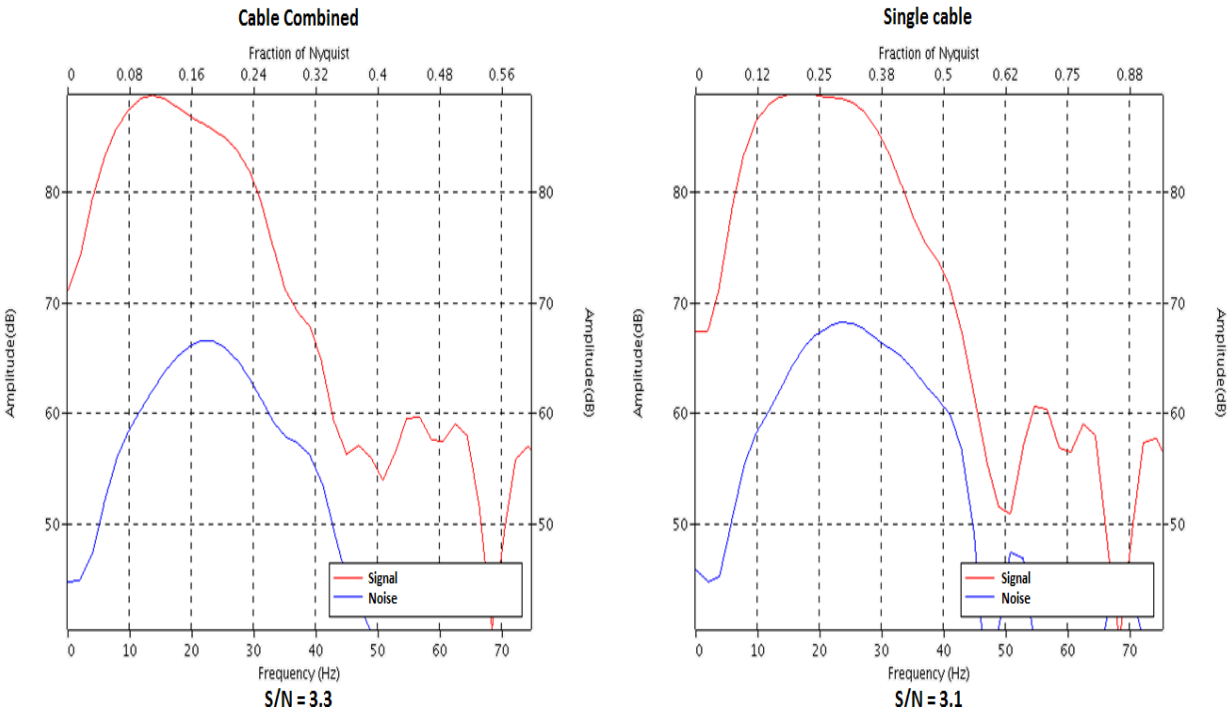

Figure 4 - 25: *Overlying spectra of the signal response and noise response in the time window 3852 to 4602 ms, which covers the reservoir section plus about 150 ms below. The spectra are extracted from the acquisition in high tide and vessel direction of 296 degrees. The average signal to noise ratio is given below the x-axis.*

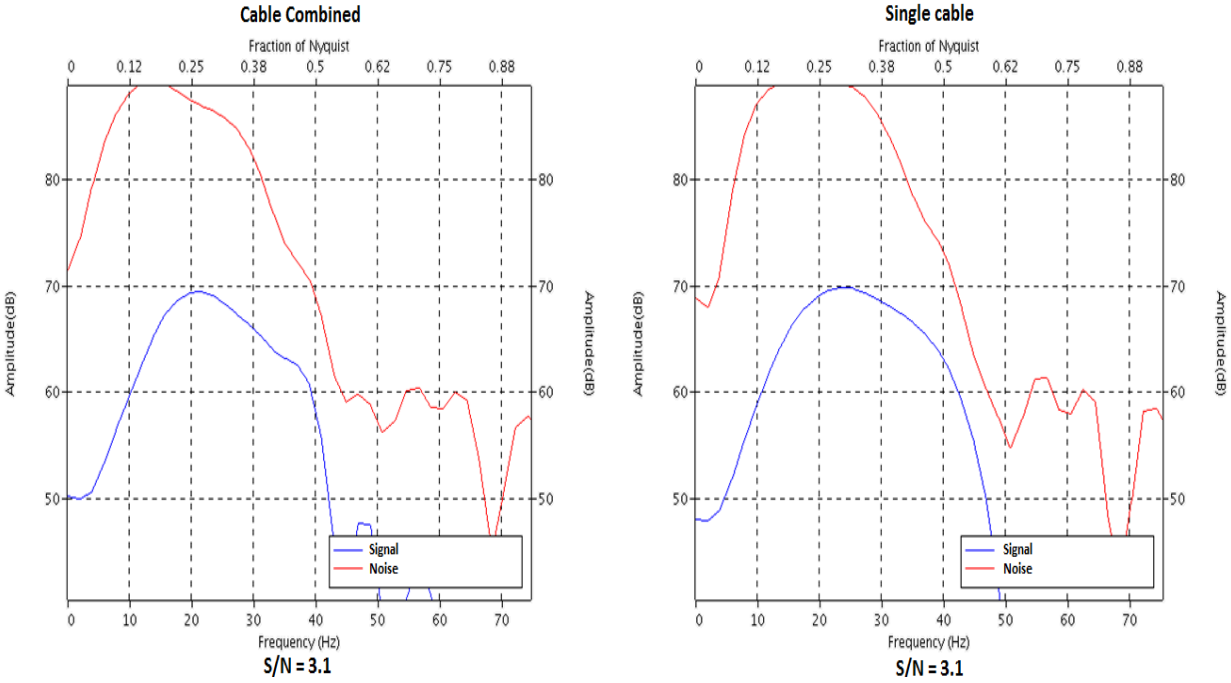

Figure 4 - 26: *Overlying spectra of the signal response and noise response in the time window 3852 to 4602 ms, which covers the reservoir section plus about 150 ms below. The spectra are extracted from the acquisition in high tide and vessel direction of 116 degrees. The average signal to noise ratio is given below the x-axis.*

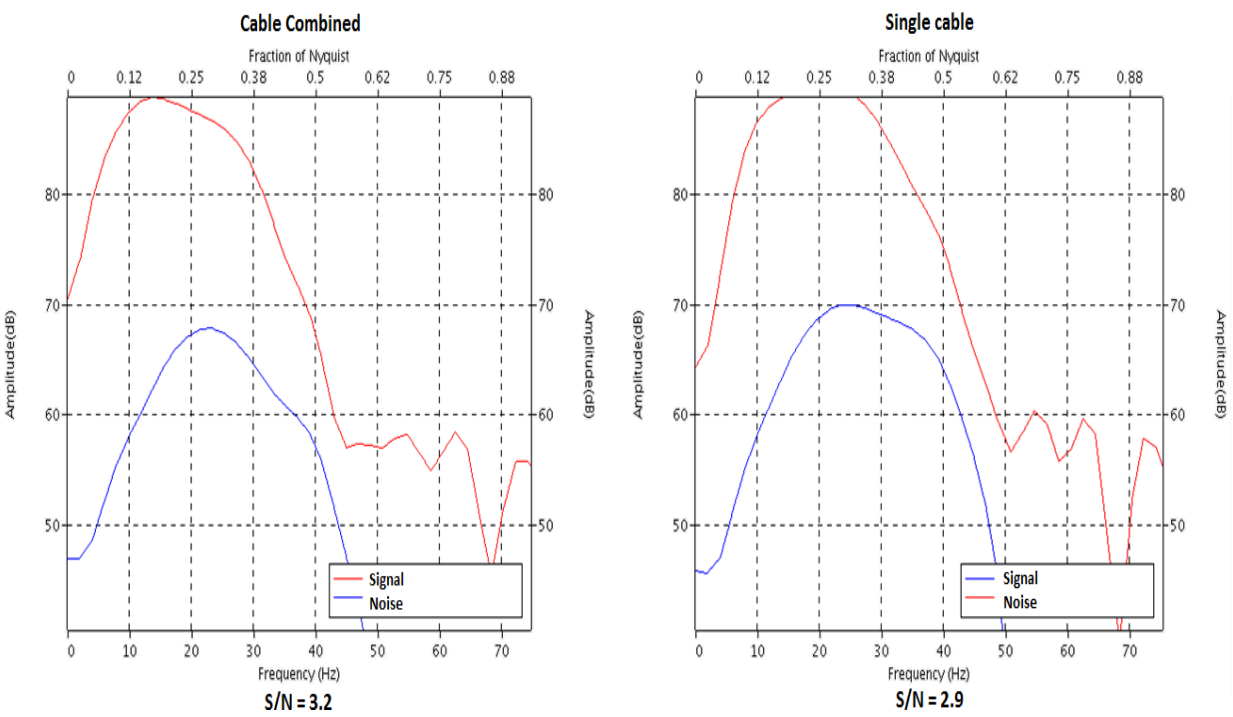

Figure 4 - 27: *Overlying spectra of the signal response and noise response in the time window 3852 to 4602 ms, which covers the reservoir section plus about 150 ms below. The spectra are extracted from the acquisition in low tide and vessel direction of 296 degrees. The average signal to noise ratio is given below the x-axis.*

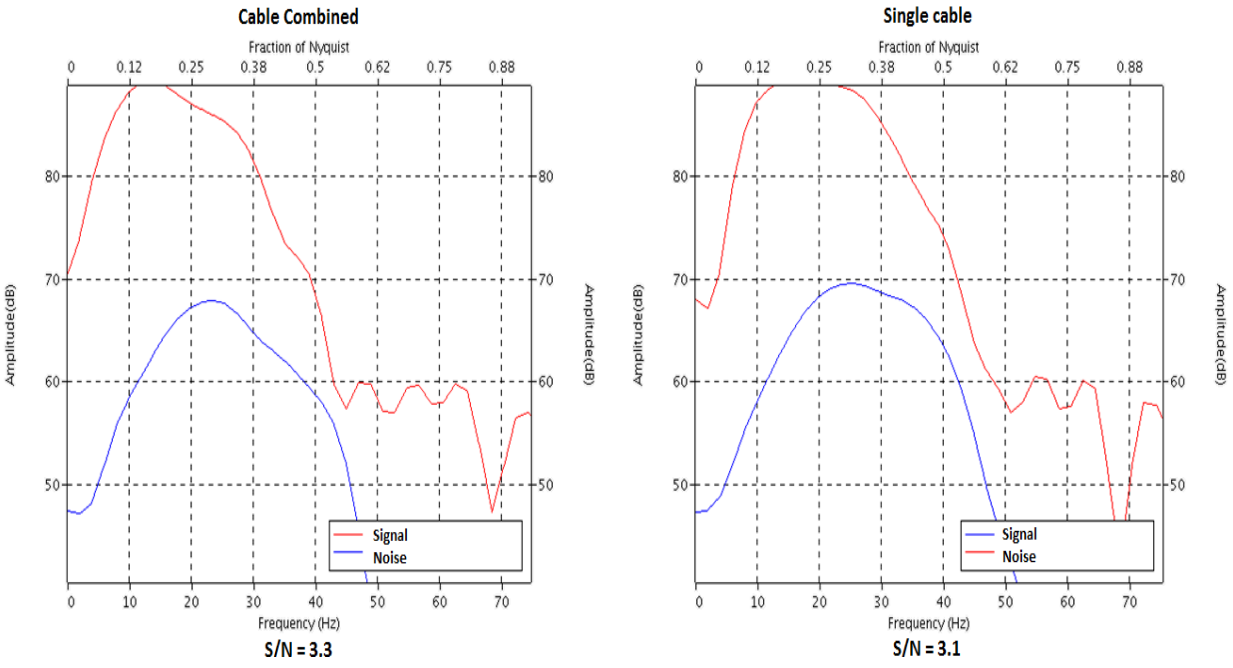

Figure 4 - 28: *Overlying spectra of the signal response and noise response in the time window 3852 to 4602 ms, which covers the reservoir section plus about 150 ms below. The spectra are extracted from the acquisition in low tide and vessel direction of 116 degrees. The average signal to noise ratio is given below the x-axis.*

For the noise to have an impact on the inversion, and explain the differences between the inversions for the acquisition direction of 296 degrees to acquisition direction of 116 degrees, there would be a significant larger noise response or a significantly lower signal response, when comparing S/N spectra of those directions. By analyzing the overlaying spectra of the figures above, we can tell that neither the signal nor the noise response changes by a significant size, but is rather similar to each other, both for the cable combination and the single cable. Also table 4-4 has similar result. The signal to noise ratio difference between high tide and low tide in each acquisition direction doesn't have this consistent change which we can observe in the standard deviation.

The acquisitions seem quite stable in terms of noise and signal, which were expected since the weather was both stable and good throughout the whole survey.

4.5.2 Inversion difference due to feathering

By feathering of the seismic streamers we mean the deviation of the streamer cables from a straight line astern of the seismic vessel. The seismic survey was done in both high tide and low tide, and the different tidal currents caused the receiver cable to deviate from a straight line astern of the seismic vessel.

Feathering of each cable during the whole survey was monitored and plotted into a coordinate grid. Feathering is varying for each session, and this has an impact on the area covered in the seismic. The source to detector separation differs from where there is no streamer feathering. Feathering causes some deviations in the seismic images, hence also has an impact on the inversions.

Because of the effect illustrated in figure 4-24, where the inversions seem to have similarities in equal acquisition direction, we wanted to analyze feathering due to equal acquisition direction. Figures 4-29 and 4-30 is the monitored coordinate plots of the shot and receiver points from the full survey.

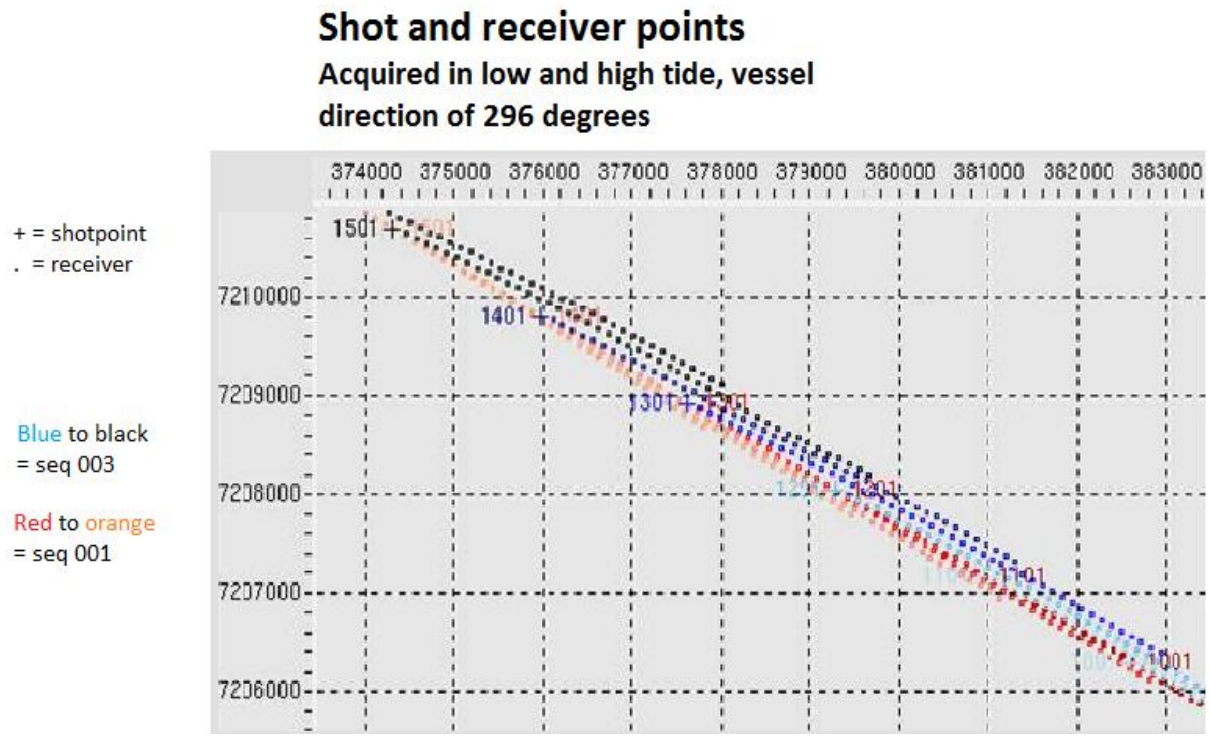

Figure 4 - 29: *Monitored shot and receiver points, plotted in a coordinate grid. There are two sequences; sequence 003 is acquired in low tide, while sequence 001 is acquired in high tide. Both are acquired with vessel direction of 296 degrees.*

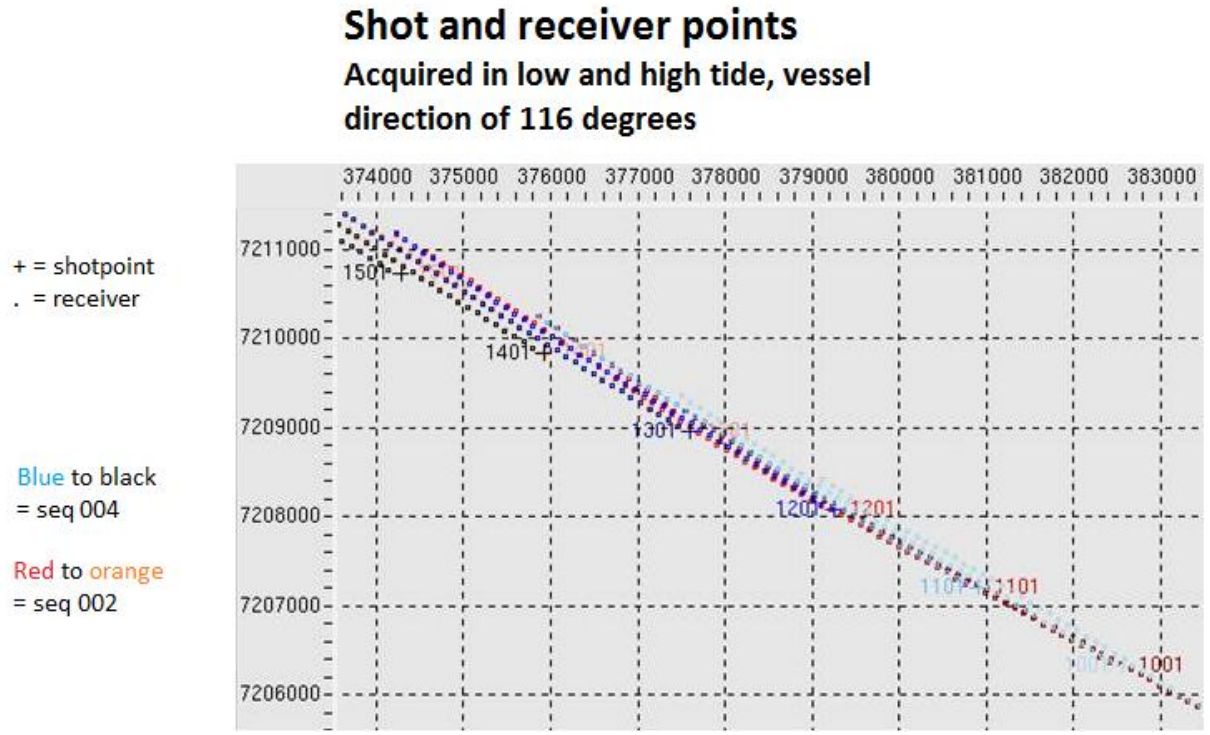

Figure 4 - 30: *Monitored shot and receiver points, plotted in a coordinate grid. There are two sequences; sequence 004 is acquired in low tide, while sequence 002 is acquired in high tide. Both are acquired with vessel direction of 116 degrees.*

From figure 4-29 we can observe that sequence 003 has relatively more feathering than sequence 001. And the receiver points from each sequence lie in an angel to each other. Sequence 001 is the sequence where we have least feathering of all the different sequences.

From figure 4-30 we can observe that both sequences have more or less the same amount of feathering of the receiver streamers. Another interesting effect is that both sequences have feathering that is aligning with each other, which results in equal area covered by the acquisition. The sequences that have alignment of feathering are the same sequences that after inversion have the best correlation compared to each other (see figure 4-24). This is consistent regardless of the acquisition method.

The opposite effect happens for sequence 001 and 003 (high and low tide, 296 degrees). After inversions of the respective seismic as inputs, the crossplot between them have larger spread and a higher standard deviation than compared to the inversion crossplot of the other 2 sequences.

Differences from the inversion cross plots due to acquisition direction are in agreement with the results from the feathering plots of the figures 4-29 and 4-30. The differences of the standard deviations from the inversion crossplot due to acquisition direction are also of a significant value, and the feathering seems to have a large impact on the inversion volumes.

Good alignment in one of the directions of the survey also explains the crossplot where we are comparing the different inversions with an average inversion volume based on acquisition method (see 4.3 Comparison of the inversion volumes with an average). Since two of the volumes have significant better correlation than the other, these will then have larger weight on the average. As a result, the average will tend to be more similar in comparison with the inversion volume with acquisition direction of 116 degrees than with the inversion volumes with acquisition direction of 296 degrees.

4.6 Differences with increasing weight factor

All the different inversion in this paper is consistently processed with 1% weight factor on the background model, regardless of the acquisition method. Since we have more of the lower frequencies in the cable combination seismic than in the single cable seismic, it was anticipated that the inversion process based on the cable combination seismic as input would be more stable with lower weight factor on the background model than for the inversion process based on the single cable seismic as input.

On that basis, the author has processed the inversion for both the single cable and cable combination seismic as input, with 80% and 1% weight factor on the background model. The outcome is 4 different inversion volumes;

1. Inversion (cable combination) with 80% weight factor on the background model (**80-INV-CC**)
2. Inversion (single cable) with 80% weight factor on the background model (**80-INV-SC**)
3. Inversion (cable combination) with 1% weight factor on the background model (**01-INV-CC**)
4. Inversion (single cable) with 1% weight factor on the background model (**01-INV-SC**)

Input seismic is from sequence 003 for both cable combination and single cable acquisition method, which is acquired in low tide and vessel direction of 296 degrees (see chapter 1.3 Datasets).

For comparison reasons, and to valuate if the cable combination is more stable with lower weight factor, we are comparing the inversions to each other in cross plots and analyzing both the correlation and the standard deviation. The cross plots we are analyzing are;

1. 80-INV-CC versus 01-INV-CC (figure 4-31)
2. 80-INV-SC versus 01-INV-SC (figure 4-31)
3. 80-INV-CC versus 80-INV-SC (figure 4-32)
4. 01-INV-CC versus 01-INV-SC (figure 4-32)

The results of the standard deviation from figure 4-31 and 4-32 are summarized in table 4-5;

Comparison plot	**Standard deviation**
01-INV-CC versus 01-INV-SC	186.0
80-INV-CC versus 80-INV-SC	128.7
80-INV-SC versus 01-INV-SC	131.2
80-INV-CC versus 01-INV-CC	131.4

Table 4 - 5: *Table illustrating results of the standard deviation from figure 4-31 and 4-32.*

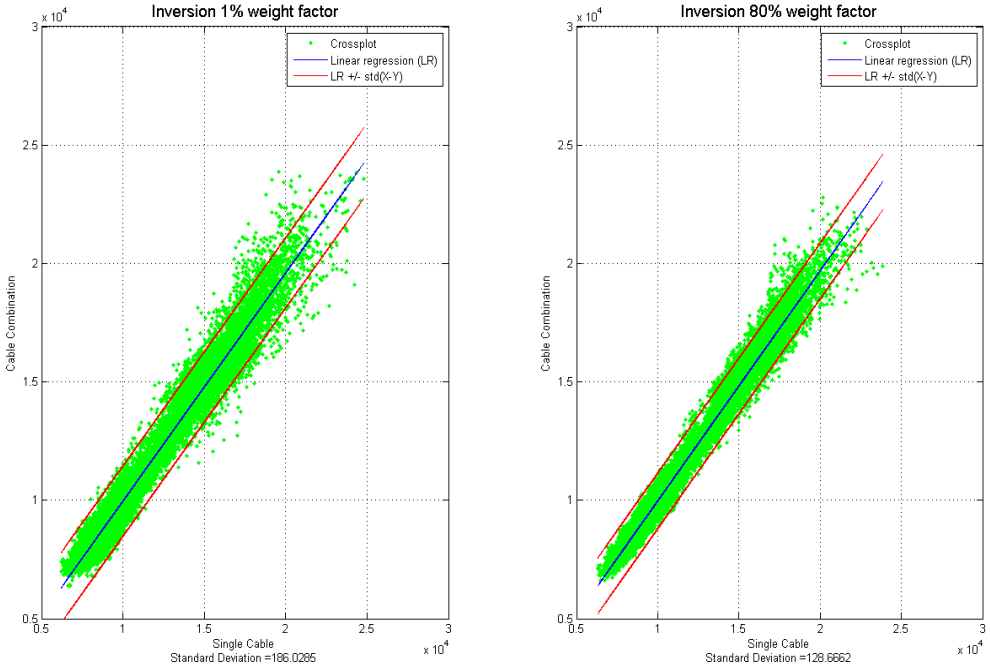

Figure 4 - 31: *Cross-plots comparing inversions with 1% weight factor and 80% weight factor. Both cross plots contain inversions based on both acquisition methods for the seismic input.*

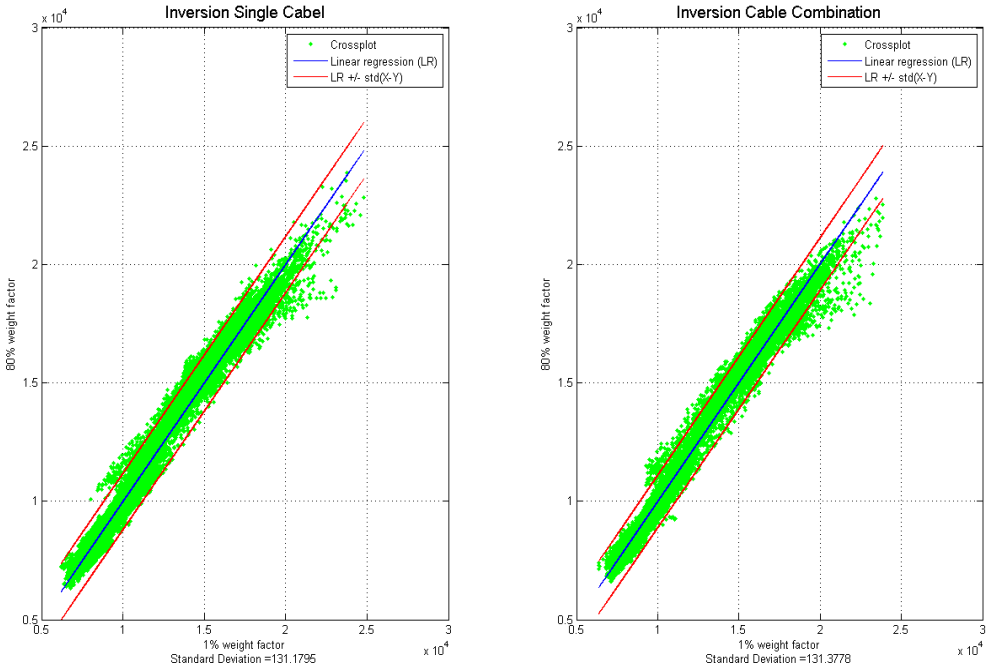

Figure 4 - 32: *Cross-plots comparing inversions based on the acquisition method for the seismic input. Both cross plots contain inversions with 1% and 80% weight factor on the background model.*

As we can observe from figure 4-31 and table 4-5, the 01-INV-CC versus 01-INV-SC crossplot have larger spread than the 80-INV-CC versus 80-INV-SC crossplot. This is also expected, since the background model is equal for all inversions, while the seismic vary from each acquisition direction, tide and method. The inversions based on 80% weight on the initial model are then moving towards a more similar solution. If the inversion were done with a weight factor close to 100% of the background model, the crossplot of the two inversions would be close to a straight line.

The effect of the differences in the seismic can be observed in the crossplot were the inversions are based on 1% weight factor on the background model. Even though the spread is not very large, it still is larger than the other crossplot in figure 4-31.

From the two cross plots of figure 4-32, we can observe that they contain more or less similar trends. Both cross-plots are comparisons of inversions with 1% and 80% weight factors. For the inversion to be more stable for the cable combination seismic as input, the trend would be that the 80-INV-CC versus 01-INV-CC crossplot would have a lower value for the standard deviation and that the crossplot would be more similar to a straight line than the 80-INV-SC versus 01-INV-SC crossplot. Results indicate that there is no such significant improvement, and the standard deviation for the single cable comparison has a slightly lower value than the cable combination comparison.

From observing figure 4-32, we can see that both have bending spread on the upper part of the crossplot, and also a similar deviation at the lower part of the cross-plots.

4.6.1 Statistical mean and standard deviation with increasing trace number

Results from the two figures above can also be analyzed closer, and further validate the explained effects by analyzing the mean and standard deviation from each crossplot with increasing trace number. As previous explained, the inversion ranges over 700 trace numbers, and for each trace we can extract the respective mean and trace number between the two datasets plotted in each crossplot.

For each horizontal pair of mean and standard deviation in figure 4-33, these have a corresponding crossplot in figure 4-31. Equal trend occurs for figure 4-33 and 4-32.

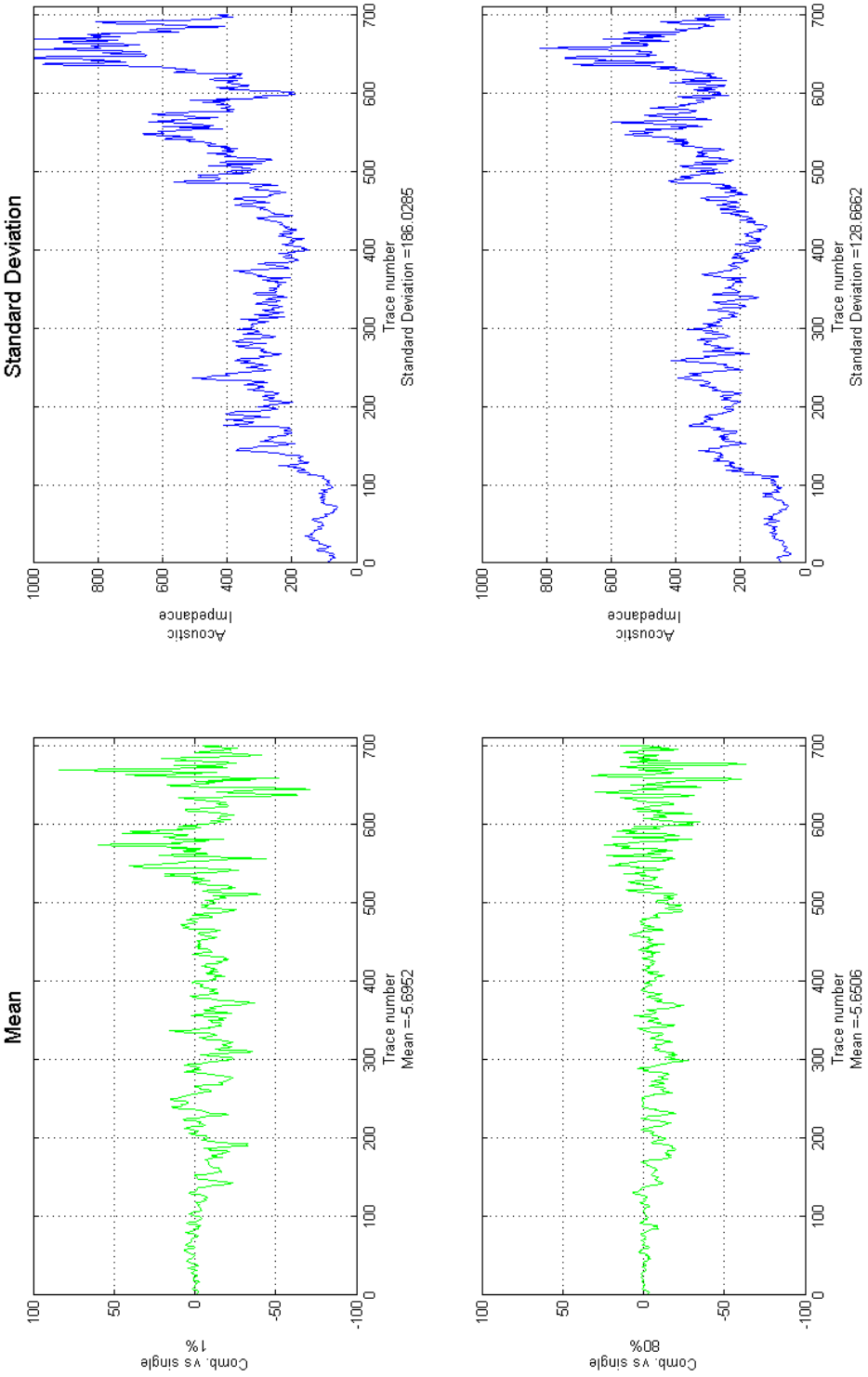

Figure 4 - 33: *Statistical mean and standard deviation with increasing trace number from the cross-plots of figure 4-31. Each horizontal pair corresponds to the crossplot explained by the y-axis of the mean.*

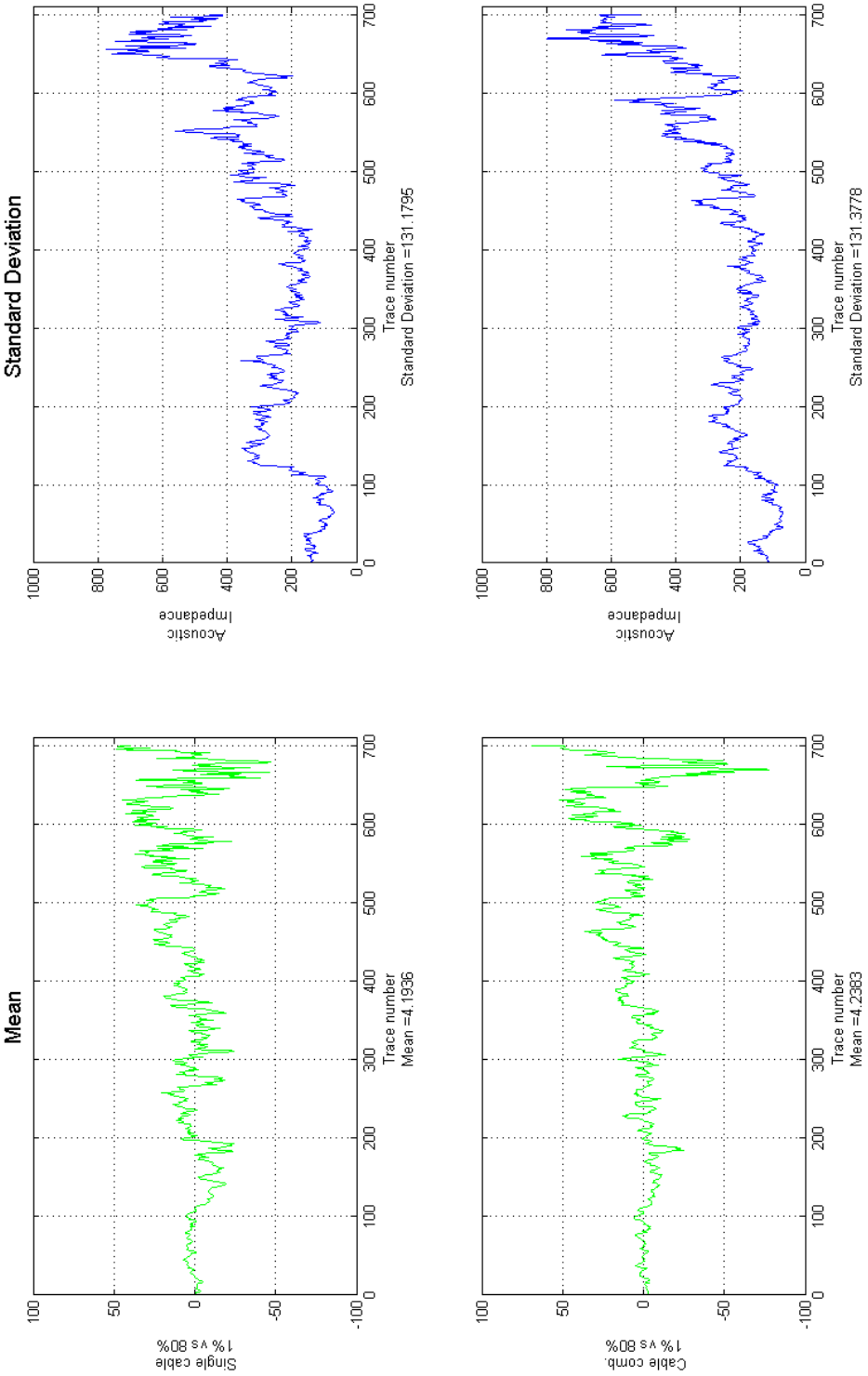

Figure 4 - 34: *Statistical mean and standard deviation with increasing trace number from the cross-plots of figure 4-32. Each horizontal pair corresponds to the crossplot explained by the y-axis of the mean.*

4.7 Frequency spectra

Broadening of the frequency spectra was one of the possibilities we had for the over/under cable combination seismic. The broadening could help the inversion to be more stabile, and to increase the amount of information from the seismic in the area. To analyze the two different amplitude spectra of the frequency, we are comparing both in figure 4-35.

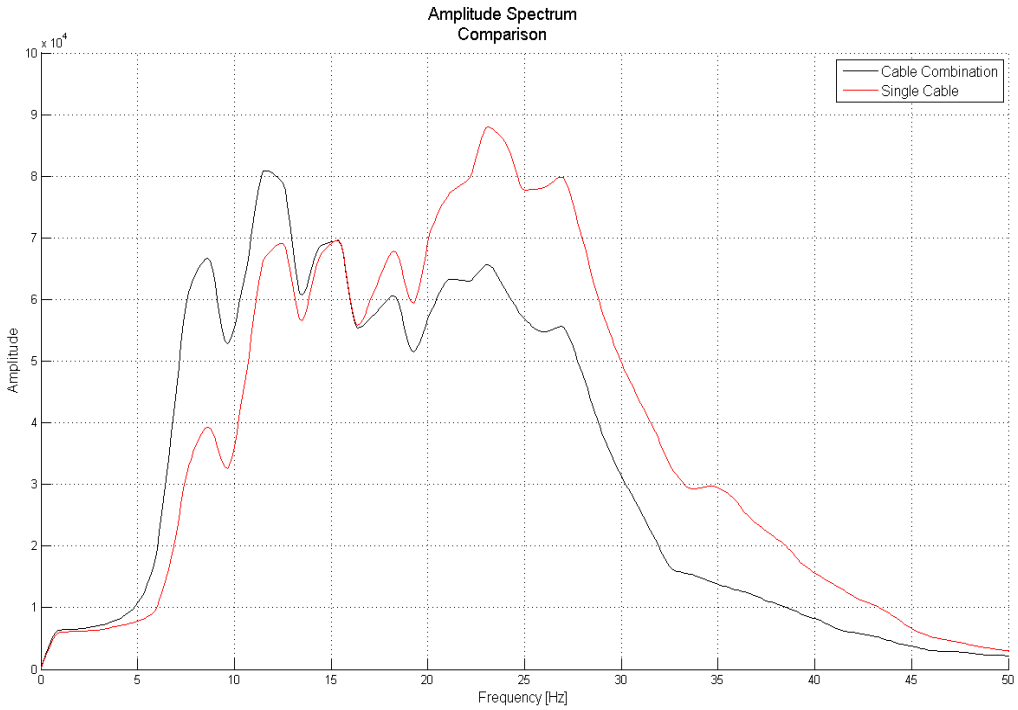

Figure 4 - 35: *Amplitude spectra for both the cable combination and single cable seismic. The spectra are extracted from a time window equivalent to the reservoir section of the Kristin Field (3852 – 4352 ms)*

The figure illustrate that we have an increase of the lower frequencies in the cable combination seismic in the reservoir part, but we also have a decrease in the higher frequency part compared to the single cable seismic. The two spectra overlay each other at approximately 16-18 Hz. Before this overlay, the amplitudes from the cable combination seismic are stronger, while the opposite happens after the overlay.

Comparing the results from the amplitude spectra above and the difference in seismic wavelet, the wavelet from the single cable seismic causes better resolution, while the wavelet from the cable combination seems to have more weight from the lower end of the spectra and the resolution decreases. Dominating frequency for the area is hence different for the two spectra and causes also differences in the inversion.

Chapter 5 Discussion

"*The scientist is not a person who gives the right answers, he`s one who asks the right questions"* – Claude Lèvi-Strauss.

The main reason for the survey, performed by Statoil, was to investigate the possibilities for the over/under cable combination receiver, and if there were any improvements compared to regular seismic surveys. Hereunder were the possibilities for improved multiple attenuation, improved signal to noise ratio, improved seismic imaging and a more stable and robust inversion.

This paper has the intention to get a better quantative understanding of the effects of the different acquisition technologies (the cable combination receiver and the single cable receiver) on the inversion results and if the improvements are significant. As indicated in the results, there are different inputs and parameters which affect the final inversion result.

This chapter will discuss the results from the inversion of the different datasets and identify the differences between the results from the two acquisition methods.

There will also be a short discussion of the split spread data at the end of the chapter. Even though split spread data is not covered in the results, the discussion of the output from the inversion process of split spread data is important to mention to make the quantification more robust.

5.1 Analytical methods in Hampson-Russell software

The Hampson-Russell STRATA software was used to do all the different inversions. The software is a user friendly software tool and has the objective of letting the user make inversions without doing the calculations himself. The process is straight forward, but suffers from the fact that the software performs more or less as a black box process, where the user is only allowed to make certain changes, and the calculations within the different stages is not illustrated to the user. Much of the quantification of the final inversion results in hence calculated in Matlab and other interpreting tools, which is fully controlled by the user.

However, the STRATA software holds the basis of the inversion process itself, and the results will be discussed further hereunder.

5.1.1 Background model

Since we are comparing inversions with inputs from two different acquisition methods, it is important that the basis of the inversion is comparable. In the well correlation the logs are stretched by a small amount to best fit the synthetic data, which changes the original log curves. All seismic volumes are different, and would have had different stretches to the original log if each of the correlations were to be optimized. This would also lead to different background models, and the comparison between them would suffer from different basis upon the inversion process. To keep the background model equal for all the different inversions, we based the stretch on a reference volume, which had the best correlation between the synthetic traces and the seismic traces from the well location. By doing this, the differences between the inversion images would be fully comparable.

The background model is build from the a-priori information of the reservoir (well logs) and is interpolated throughout the field with a reservoir geometry interpreted by the user (the horizons). We can change some input parameters of the background model, as high cut frequency, the use of the horizons for the background model to follow, and in which time domain the model is to be calculated in. The calculations in the process are automated and are not controlled by the user. Calculations of a good background model are important in an inversion process, since it is the initial guess which the inversion is to be calculated from. The process is therefore not known, and the user is expected to thrust the black box process. However, this is similar for all the inversions, since the model is the basis for all the processes with different input seismic. From the background model we can observe that there is one area where the calculations seem to have an error. The error is observed in the border between the Inter Tofte Formation and the BCU. The error is illustrated in figure 5.1, and it seems that the calculations are error prone in the border area.

The error is not observed in the inversions, but is still important to look into. Amplitude difference between the layers outside the reservoir and the Inter Tofte Formation is quite high, and the transition area could be too narrow for the calculation method of the program. The inversion results should hence be evaluated with that error in mind.

In addition to this, the Garn Formation, which is between the BCU and Ile Formation, is not covered by the original log. The background model values for this area is therefore less certain, and should be taken into account when evaluating the final inversion results.

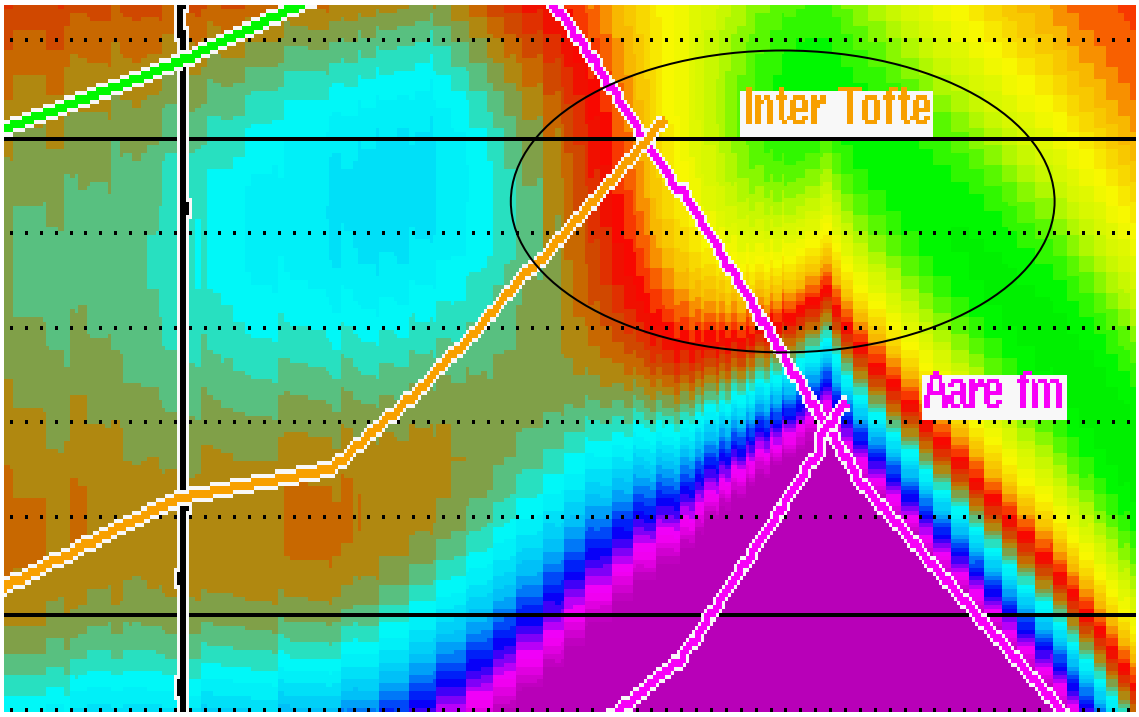

Figure 5 - 1: *Figure illustrating the background model error at the border between Inter Tofte Formation and the BCU (capped by the oval). The background model can be observed in figure 4-2.*

5.1.2 Error in acoustic impedance versus time

By analyzing the error in acoustic impedance versus time, we are plotting the error between the original log impedance trace and the inverted impedance trace from the well location. Here we would like to observe either a lower error throughout the plot, or a more consistent error (flatter plot) in the comparison between the two plots. In either of these cases, the correlation between the original log and the inverted impedance trace were better. As we can observe in figure 4-4 there is some improvements in the first part of the crossplot, when comparing the single cable to the cable combination. However, after 3950 ms, it is difficult to separate the two different plots. Comparing these results to the histogram of the impedance error versus count and the inversion analysis window from Hampson-Russell can give us a better picture of the trends.

The difference between the inversion analysis windows can be observed in figure 5-2. As illustrated by the figure, the top box indicates that the inversion based on the cable combination seismic is better resolved, while the lower box indicates that the inversion based on the single cable seismic is better resolved. As we can see by the figure below, the changes between them are not significant of any measure, which is also indicated by the crossplot of error versus time.

However, the comparison between the inversion trace and the original log trace is only based on one single trace in the reservoir, which is from the well location. The trends seen in these figures might differ from the results throughout the reservoir and cannot be the basis of an interpretation for the whole reservoir section.

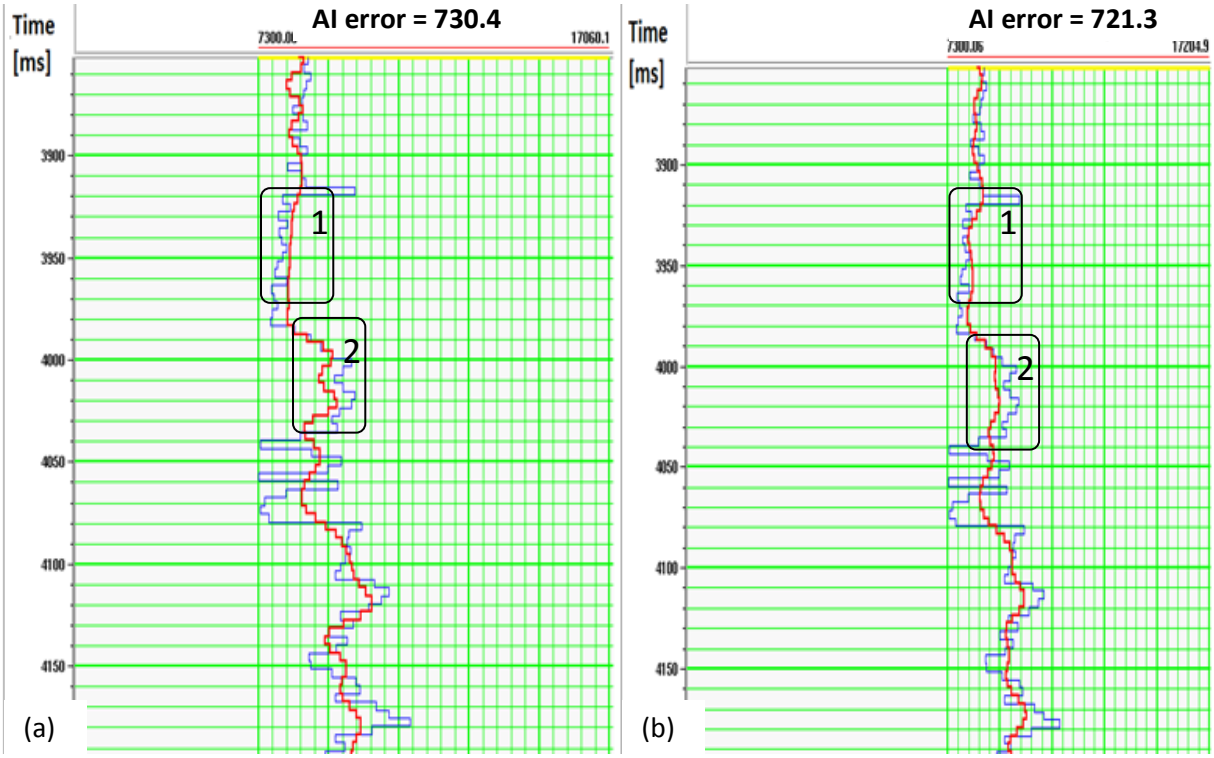

Figure 5 - 2: *The figure illustrates the Inversion Analysis with both single cable seismic input (a) and cable combination seismic input (b). The two boxes in each picture illustrates important differences between (a) and (b).*

Comparing the bottom box in the figure above, we can also see another trend which is continuous throughout the inversion analysis window; the inversion based on the cable combination seems to be based on a weight prone to lower frequencies compared to the inversion based on the single cable. The inverted trace is more smoothed over the time interval, which also affects the correlation between the traces. Even though the single cable inversion might be better resolved, the cable combination has a lower summed error through the time interval. The comparison with the error in acoustic impedance versus time crossplot and visual analyzes of the two were important.

5.2 Difference in wavelet and vertical resolution

Since one of the objects of performing the survey was to achieve a broadened frequency spectrum, we wanted to illustrate the two true spectra of the reservoir interval for both cable combination seismic and single cable seismic. As illustrated in the results, the two different spectra were in fact different, but not broadened as first anticipated. In figure 5-3 we are observing the two spectra and their difference areas.

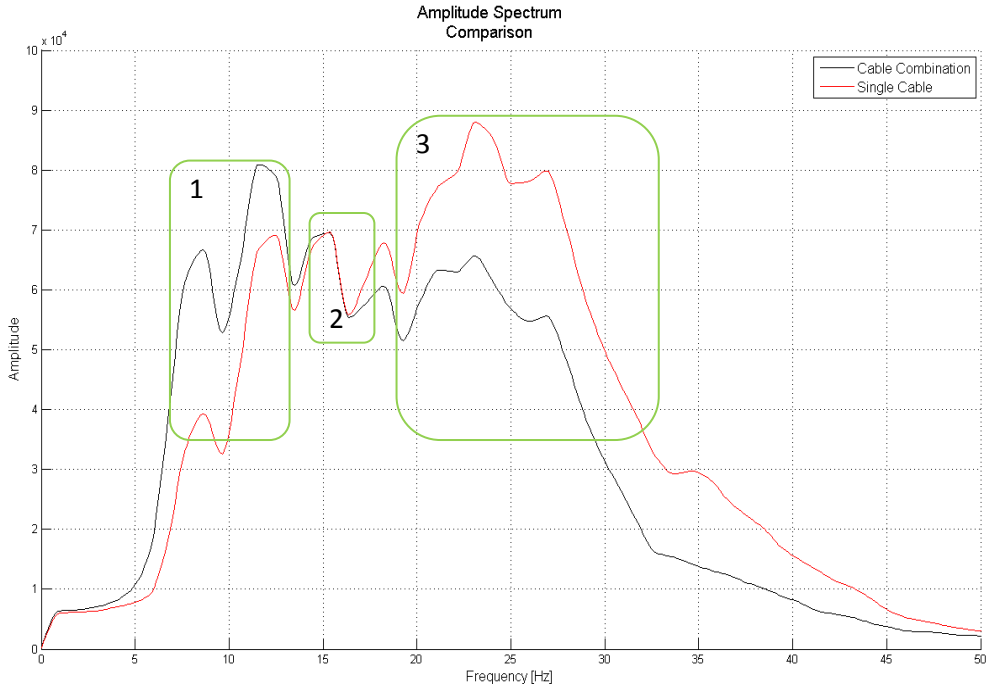

Figure 5 - 3: *Frequency spectra for both cable combination seismic and single cable seismic in the reservoir area [3852-4352 ms]. The three boxes illustrate important areas of the comparison between the two spectra.*

Figure 5-3 illustrates that there are differences both in the lower part and the higher part of the spectra. In box 1 we can observe that the cable combination seismic has more of the low frequencies, and also higher amplitudes in this area, while box 3 illustrates the opposite. Box 2 shows where the spectra overlay each other. As we can observe, we don't have a broadening of the spectrum, in fact, the spectrum is narrower, but has more of the low frequency part, which is important for the inversion to follow the correct absolute trend with depth. However, this part doesn't give enough impact on the inversion to be significant, which we will discuss later in the thesis.

By an interview with Andrew Langrigde in April 2012 (Langridge, 2012), we concluded that these spectra might be improved. When comparing the spectra of the cable combined and single cable, we have to remember that the single cable is the upgoing plus the downgoing, and so there is a factor of [20*log(1/2) =] 6 db lower amplitude on the cable combined data (upgoing only). This will affect the correct normalization of the spectra (Langridge, 2012). This is not corrected for in the processing of the seismic data, and might change the results. However, this is theoretically and is yet not corrected for in the processing.

The difference in the spectra of the two can also affect the wavelet. The wavelet based on the cable combination seismic is slightly broader than the wavelet based on the single cable seismic. These differences affect the vertical resolution, which was illustrated in figure 4-7 to 4-9. The difference between the two difference wavelet and the difference in vertical resolution can be observed in figure 5-3.

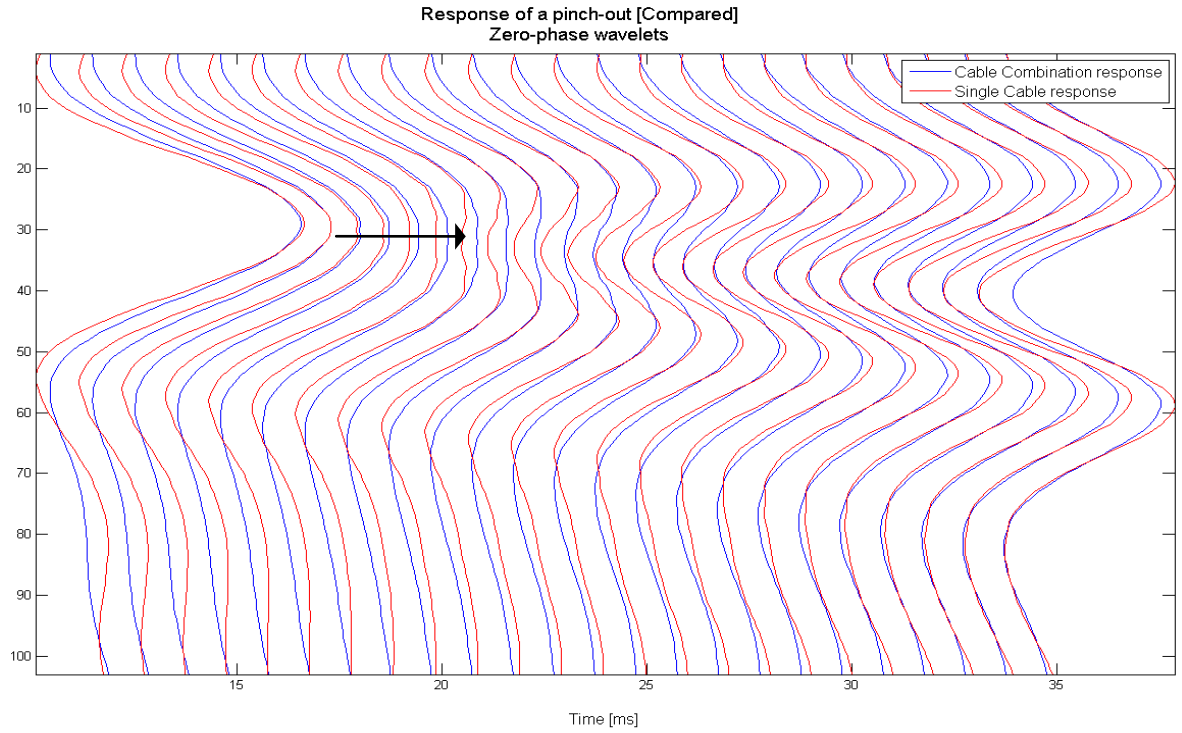

Figure 5 - 4: *Difference in vertical resolution between the cable combination seismic and the single cable seismic in the reservoir section of the Kristin field [3852-4352 ms]. The arrow points out where the two wavelets differ when convolved with the reflectivity of a wedge-model.*

As the figure illustrates, the difference in vertical resolution between cable combination and single cable seismic is quite clear. The difference in vertical resolution favors the single cable method, and by the configuration of the reflection matrix used in figure 5-4 the difference in resolution is about 3 ms. The difference is **17.6%** favoring the single cable seismic. By inversion we remove the wavelet by applying its inverse (deconvolution). Even though we remove the wavelet in inversion and find the acoustic impedance volume that would have a response of the input seismic, the vertical resolution differences would still affect the inversion volume. If we have a seismic volume which has very good vertical resolution and one that has poor resolution, the latter would not detect as thin layers as the first, hence we would have an initial difference in the two seismic volumes. The seismic with poor resolution would have no information of the layers that it couldn't detect, and hence the inversion would suffer from it. The vertical resolution in the seismic and the vertical resolution in the inversion are hence connected to each other to a certain degree.

In inversion we need both high and low frequencies. Higher frequencies are needed for vertical resolution, while lower frequencies are needed for deeper penetration and correct absolute vertical trend. Even though the cable combination seismic has increased frequency content (reservoir time interval) in the lower part of the spectrum, the advantages of that part seem to be smaller due to a narrower bandwidth than the single cable seismic.

5.3 Differences in the inversion volumes compared to the seismic

The differences in the wavelet also created differences in the seismic volumes. Since we already have illustrated the differences in the frequency spectra and the wavelet, we also want to discuss the changes in both the seismic and the inversion volumes.

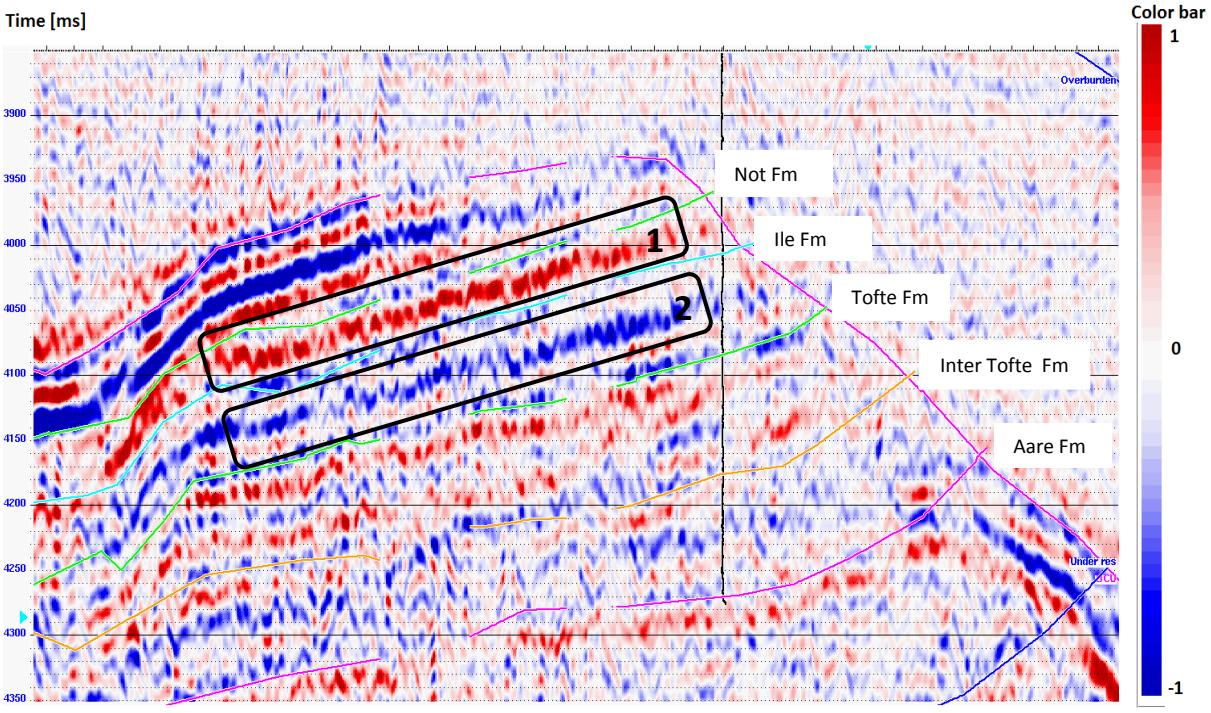

Figure 5 - 5: *Difference between the cable combination and single cable seismic. The two numbered boxes illustrate interesting differences between them where we have large variations in amplitude between the two compared volumes.*

The difference image illustrates that we have consistent amplitude changes within the Not Formation and within the Ile Formation. Since Garn Formation isn't covered by the well log, we don't take the variations in this layer into account on the basis that the background model would be error prone in the layer (Garn Formation is the layer between Not Formation and BCU).

By analyzing the amplitude difference in the figure, it is important to look for consistent changes, since these might be layers which are not covered by one of the seismic lines. By identifying these horizontally consistent amplitude differences we would investigate if similar changes can be observed in the difference image between the inversion volumes. From figure 5-6 we can observe that the changes seen in the seismic difference figure cannot be found to the same extent here. We have small changes between -1000 and 1000 $[\left(\frac{m}{s}\right) * \left(\frac{g}{cm^3}\right)]$, which indicates that the changes are within a layer, and not a new layer.

Since the changes are within a layer in the difference inversion volume, the difference in amplitude is most likely to be variations of the two different wavelets (which can be illustrated from figure 5-4). We can observe from figure 5-4 that there are also deviations in the side-lobes which cause an effect in the difference between the images. The reflection point might also be slightly different and can cause a mismatch in time between the events. There are also small deviations in the signal to noise ratio between the cable combination and single cable seismic, meaning that one of the volumes

contain more noise than the other which may also add to the difference between the images. By also analyzing the two different seismic volumes visually, we can see that the images are quite similar and that the number of layers reflected by the seismic is equal. The change in wavelet, signal to noise ratio, and time difference is hence more likely than an added layer in one of the volumes.

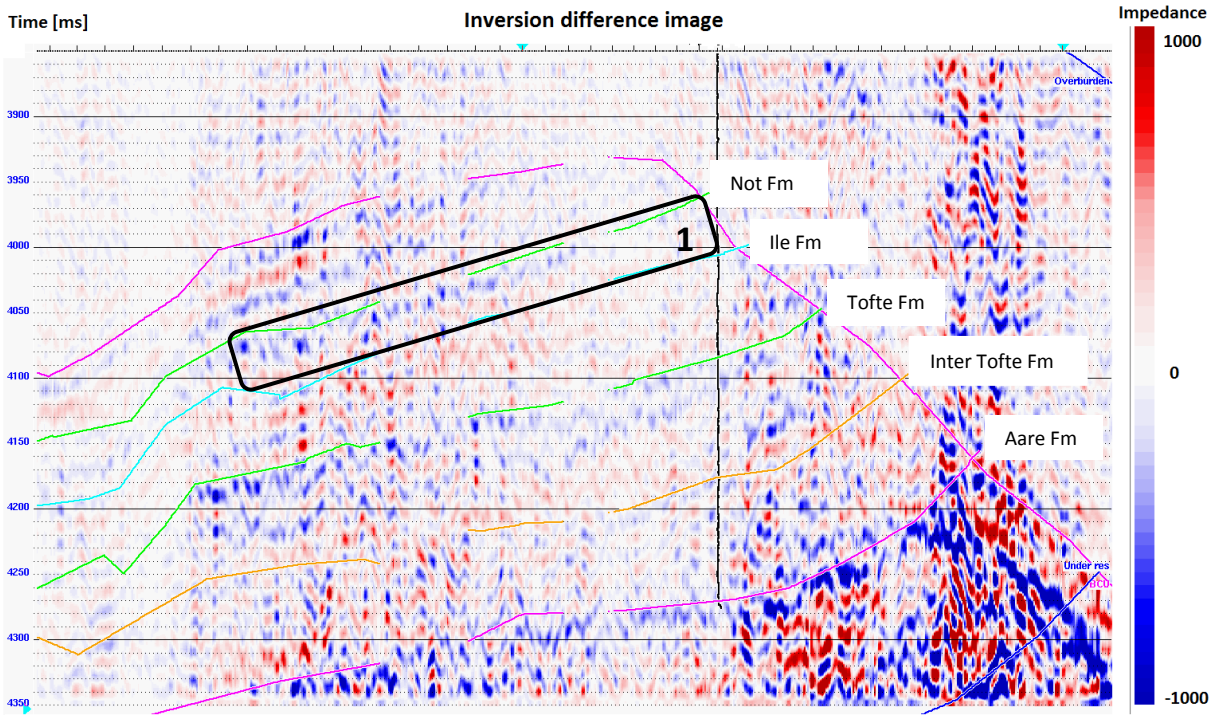

Figure 5 - 6: *Inversion difference between cable combination and single cable seismic as input. The numbered box illustrates the best observed feature which can be compared with the difference in figure 5-5.*

The changes in the inversions are not consistent or as significant as the changes in the seismic difference image. However, there are measurable changes between the two inversions and in the following subchapters we will discuss which parameters that have the most influence on the final inversion result.

5.4 Comparing the inversion volumes to their respective average

When comparing the inversion volumes to their respective average, we wanted to see significant changes from the single cable to the cable combination. Investigation of the similarities between the inversion volumes for each acquisition method would illustrate if the standard deviation would decrease when comparing the cable combination to the single cable inversion volumes. The results for the comparison were different than expected, where the most significant change were when comparing the direction to each other and not the acquisition method.

For each inversion comparison, the variation of the standard deviation and the correlation with the average is most significant when comparing the two different inversion volumes based on the vessel direction. As illustrated in figures 5-7 and 5-8 the standard deviation is comparable between the figures for each vessel direction, while there is no significant difference from the single cable to the cable combination.

The figures indicate that we have the best correlation with vessel direction of 116 degrees. Since the comparison is with an average inversion volume, this trend indicates that the inversion volumes based on vessel direction of 116 degrees is more similar to each other than the other direction. We have an average that tends to be more similar to the inversion with a specific vessel direction.

The weather effect on the inversion between the two different directions could be a reason why we have this trend, but as discussed with the survey managers, the weather throughout the whole survey was quite stable and also very good. Signal-to-noise ratio (S/N ratio)could also be an important factor, but as illustrated in the results, the changes between the single cable S/N ratio and the cable combination S/N ratio has no significant changes between the vessel directions and also no significant changes from the single cable to the cable combination.

Processing of the seismic was performed by a third part and not by the author, so the risk that the processing between the seismic volumes, based on vessel direction could be different, was valid. This was discussed with Andrew Langridge that could confirm that the processing were equal for all volumes based on equal acquisition method. The difference between the processing from the cable combination to the single cable seismic was mostly of combining the two seismic volumes to one in the cable combination seismic. Differences were therefore mostly likely to be between the directions in the survey, regardless of acquisition method. Feathering was an option here.

However, before discussing the feathering effect to the inversion, the comparison with the reference inversion volume, or the inversion volume based on the reference seismic, will be evaluated to see if there are any significant trends which have been overlooked.

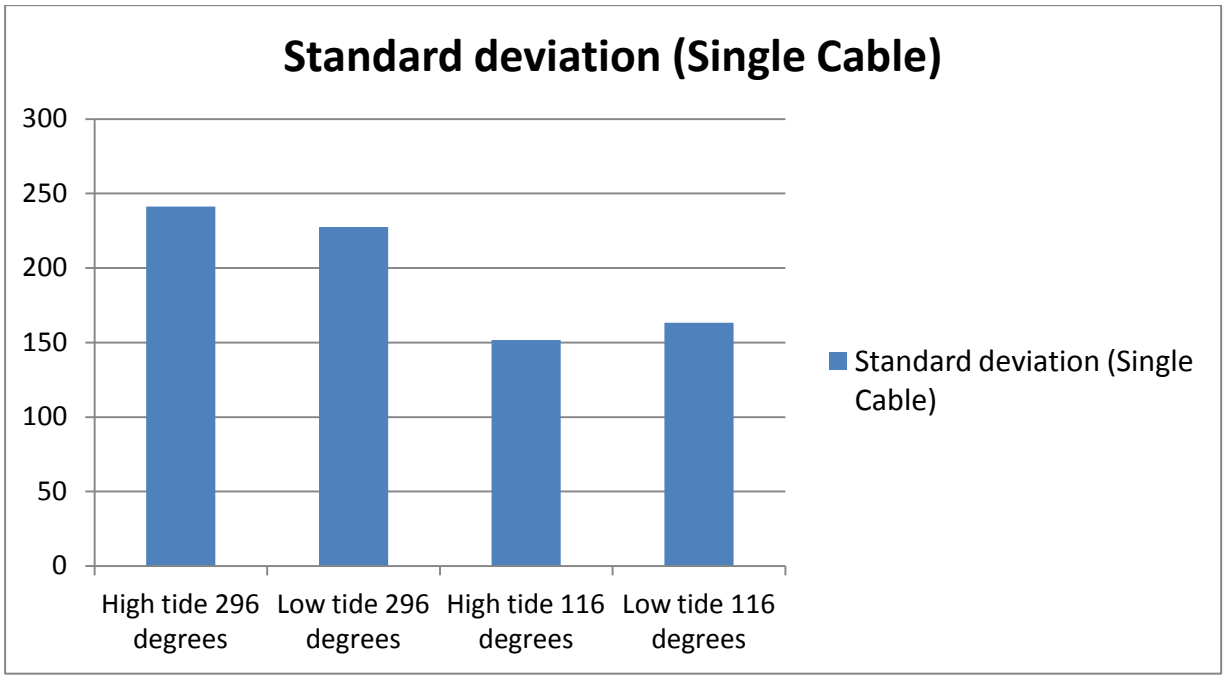

Figure 5 - 7: *Standard deviations comparing the single cable inversions with their average single cable inversion volume. The crossplot the figure is based on can be observed in figure 4-17.*

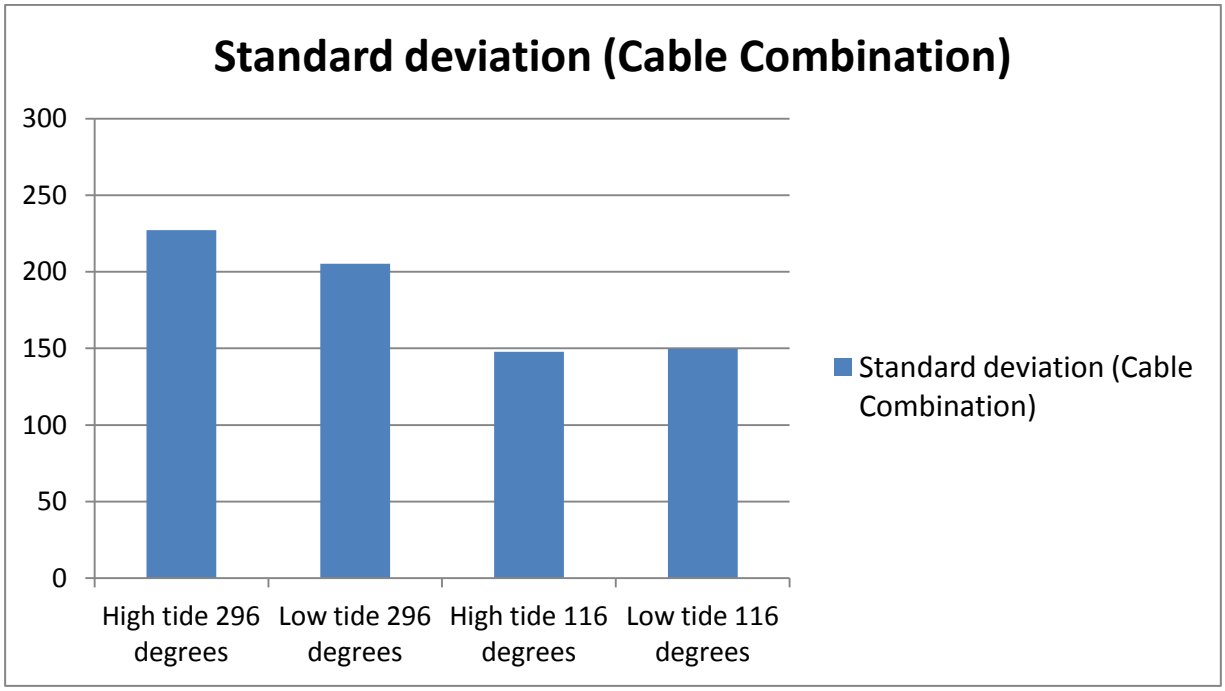

Figure 5 - 8: *Standard deviations comparing the cable combination inversions with their average cable combination inversion volume. The crossplot the figure is based on can be observed in figure 4-18.*

5.4.1 Reference inversion volume compared to all inversions

The background model used for all the inversions is based upon the P-wave velocity and density with a time to depth curve made with stretch regarding to one reference volume, as previously mentioned. Hence we wanted to compare the other inversions to the reference volume inversion, to illustrate the differences between the inversions and acquisition methods, and to investigate if any trends could be observed in the comparison.

Figures 5-9 and 5-10 illustrate the standard deviations shown in figures 4-21 and 4-22. If we compare the inversions from single cable to cable combination based on equal tide and vessel direction, we can see that there are improvements. The plots have narrower spread and the standard deviation is of a lower value. From the crossplot figures we can also see that even though we have these improvements, each comparison from cable combination to single cable inversion follows an equal trend. With that we mean that the spread of the compared cross-plots has equal recognizable trends but the width of the distribution is narrower for the cable combination crossplot.

As previously mentioned, the correlation with the reference volume can suffer from the fact that the reference is indeed a cable combination volume, and that the removed wavelet with its inverse might cause the differences between cable combination and the single cable inversion volumes. However, these changes are small compared to the variations based upon the comparison between the inversions comparison with the average, and is not significant.

Here we also have included the correlation between the reference volume and the respective inversion volumes. For the correlation, we can observe that one inversion volume has 1 in correlation, which indicate perfect hit between the inversion points. This effect is due to that this volume is the reference inversion volume used for the comparison. The same reason can be concluded in the figures for the standard deviation.

As indicated in figures 5-11 and 5-12, we have a significant better correlation between the reference inversion volume and the single cable inversion volume based on the same vessel direction and tide, than in any correlation with the other volumes. Since we have exactly the same reflection points with time in the input seismic in these two volumes, the correlation between them would indeed be significant better. Also in this plot an equal trend can be observed as from the figures covering the standard deviations. Equal trends for between the two figures can be observed, even though the cable combination inversion correlation has slightly better correlation than the single cable inversion correlation.

Comparing these to the comparison with their respective average, we can easily see that the variations found here are of less magnitude than for the average comparison, and they are not significant. The one interesting feature of figures 5-9 to 5-12 is that the correlation and standard deviation, when comparing equal vessel direction in input seismic, in the single cable inversion is significantly better than the rest. However, these are the two volumes that are being compared most in the thesis, and the variations between them are also quantified in the paper.

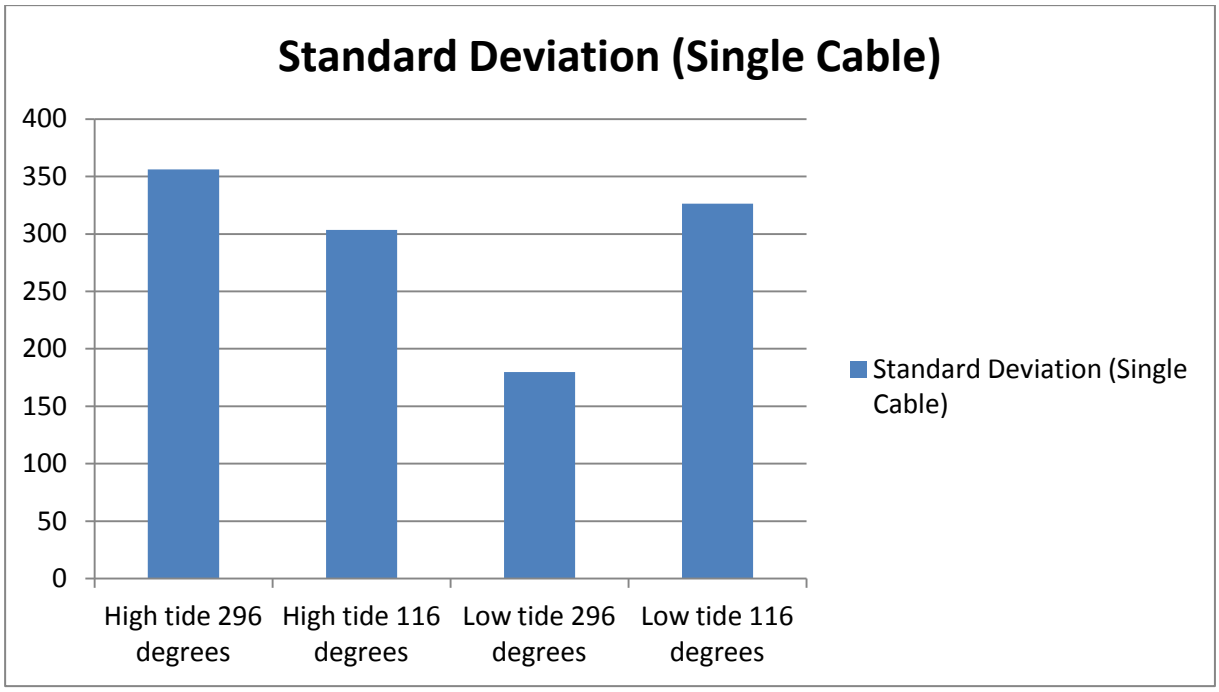

Figure 5 - 9: *Standard deviations comparing the single cable inversions with the reference inversion volume. The crossplot the figure is based on can be observed in figure 4-21.*

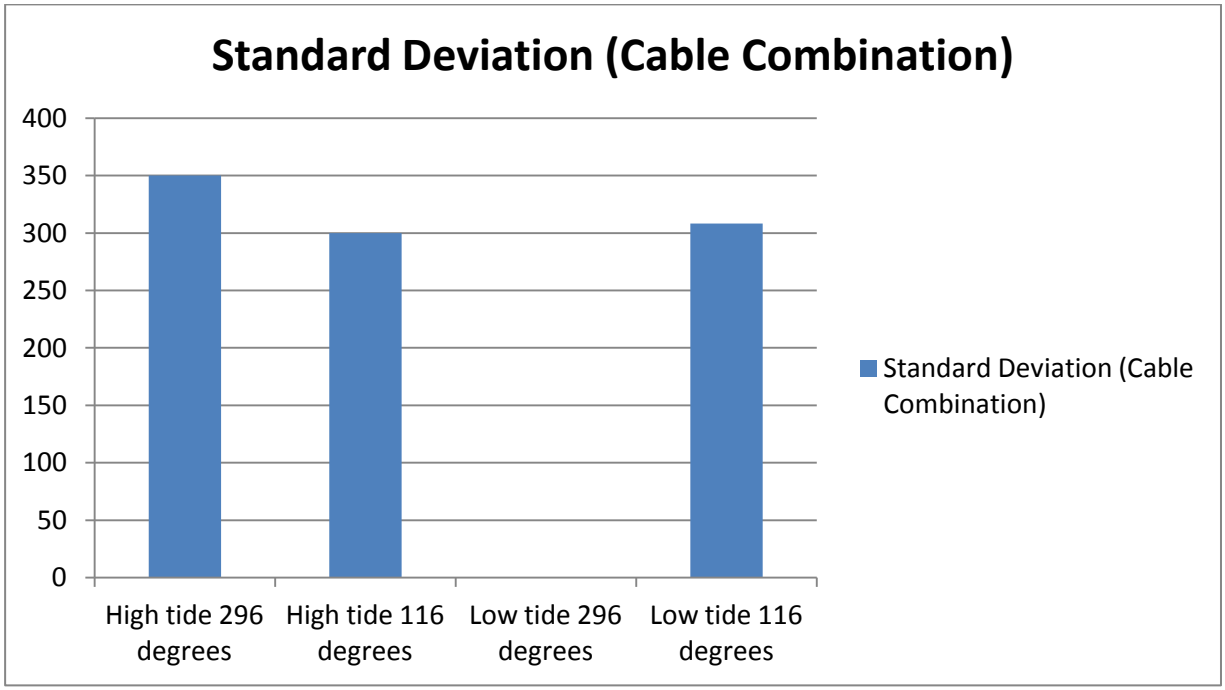

Figure 5 - 10: *Standard deviations comparing the cable combination inversions with the reference inversion volume. The crossplot the figure is based on can be observed in figure 4-22.*

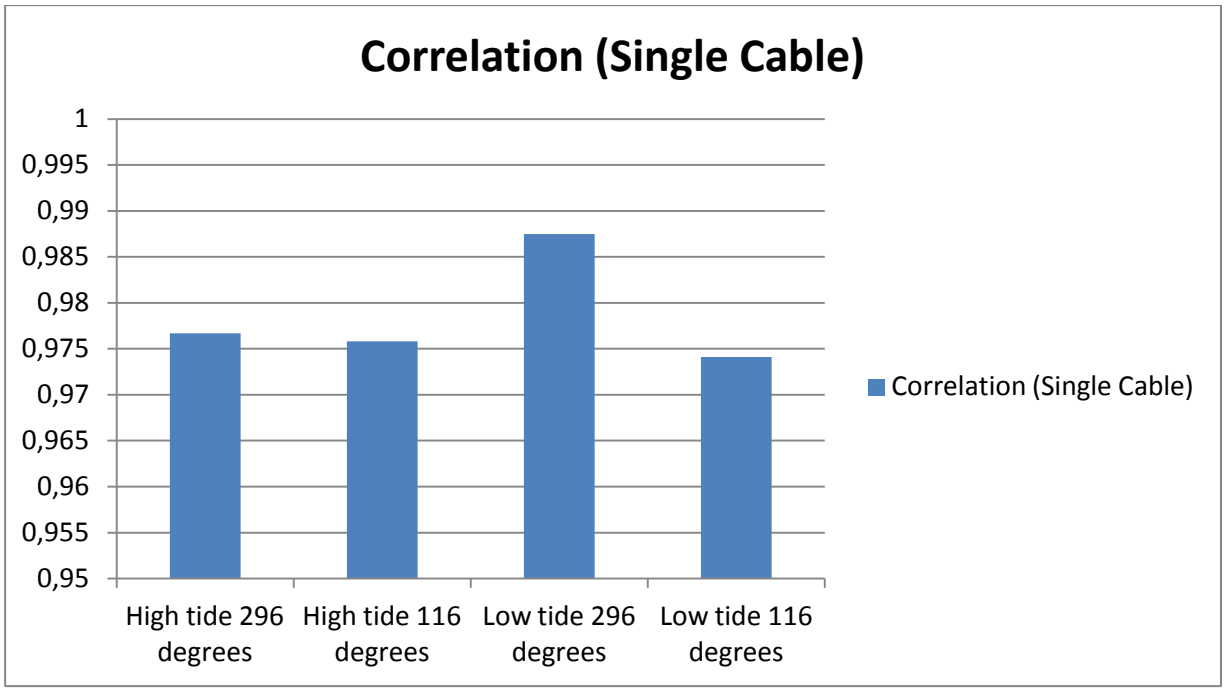

Figure 5 - 11: *Correlation between the single cable inversion volumes and the reference inversion volume. The crossplot the figure is based on can be observed in figure 4-21.*

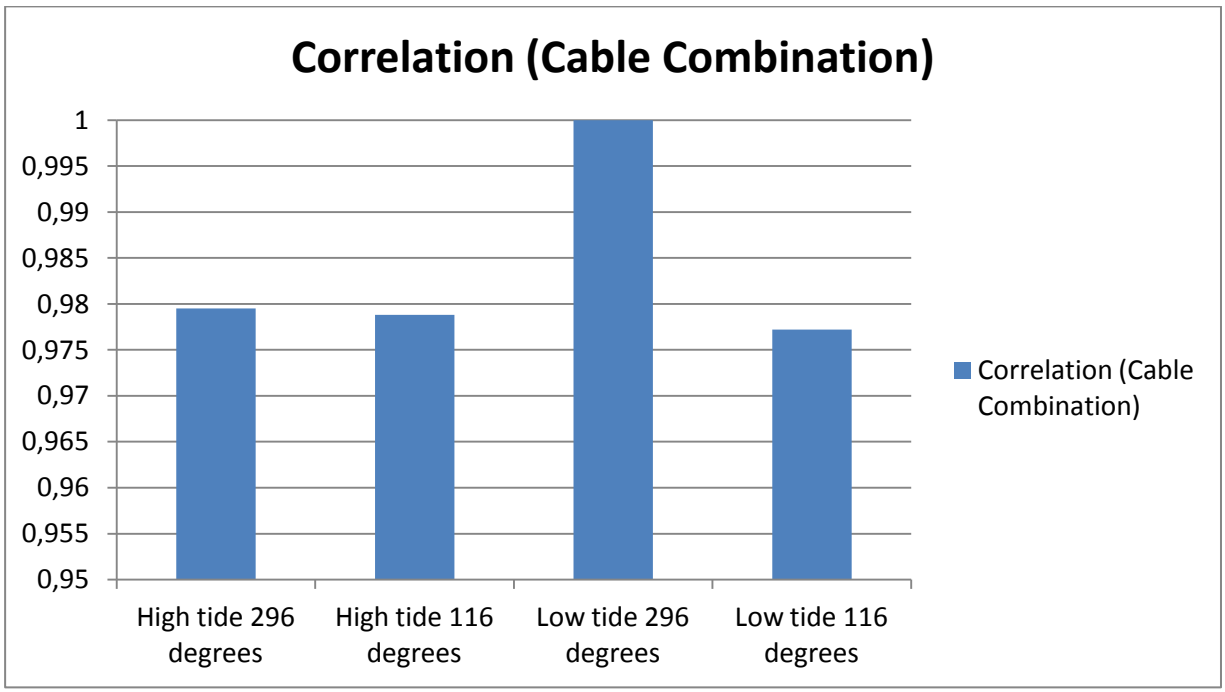

Figure 5 - 12: *Correlation between the cable combination inversion volumes and the reference inversion volume. The crossplot the figure is based on can be observed in figure 4-22.*

5.5 Acquisition direction and feathering

By comparing the inversion volumes based on the vessel direction to each other, we can verify if the results found in comparing the inversion volumes to an average is correct. In the results we can observe that the cross-plots where we are comparing the inversion volumes with input seismic acquired in vessel direction of 116 degrees has a significant better correlation than when comparing the other direction (296 degrees).

Since the change in the signal to noise in the input seismic to these inversion volumes did not indicate that there were significant variations between the different directions, we wanted to evaluate the feathering effect to the inversion.

As we can observe from figure 5-13, the standard deviation is of a significant lower value for the vessel direction of 116 degrees than the opposite. Also the correlation between them is significant better. The cross plots that these results are based on can be observed in figures 4-23 and 4-24.

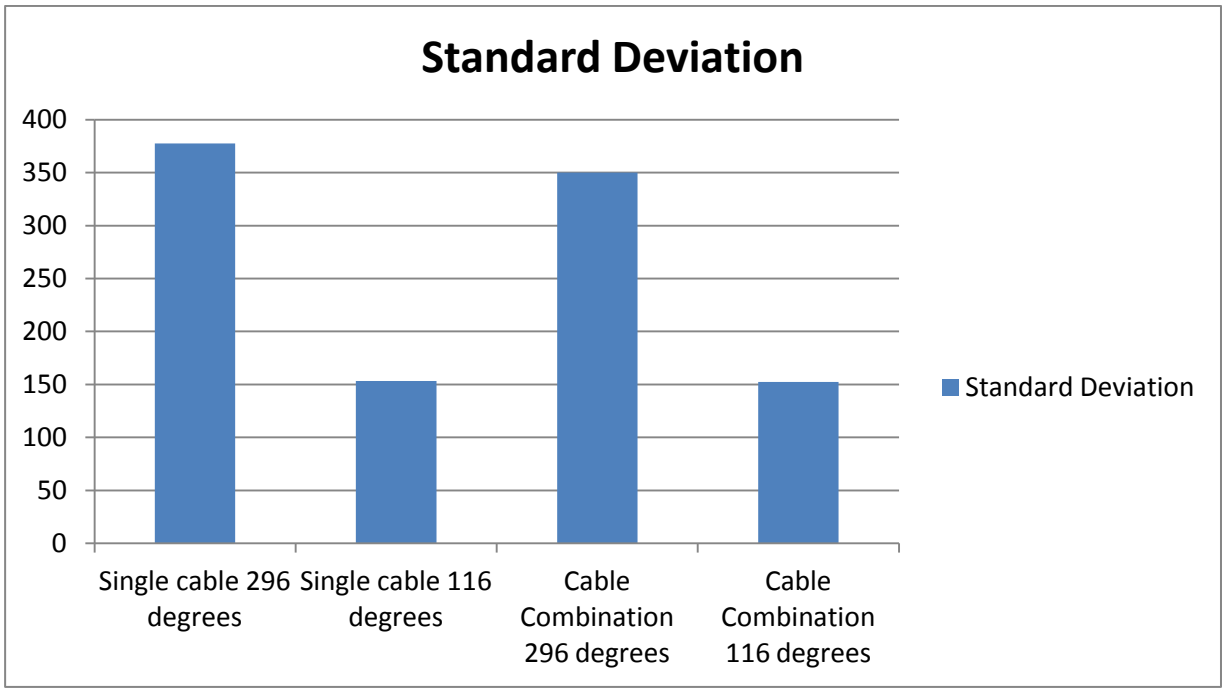

Figure 5 - 13: *Standard deviations when comparing the inversion volumes of each acquisition method based on the vessel direction. The standard deviations are results of the cross-plots in figure 4-23 and 4-24.*

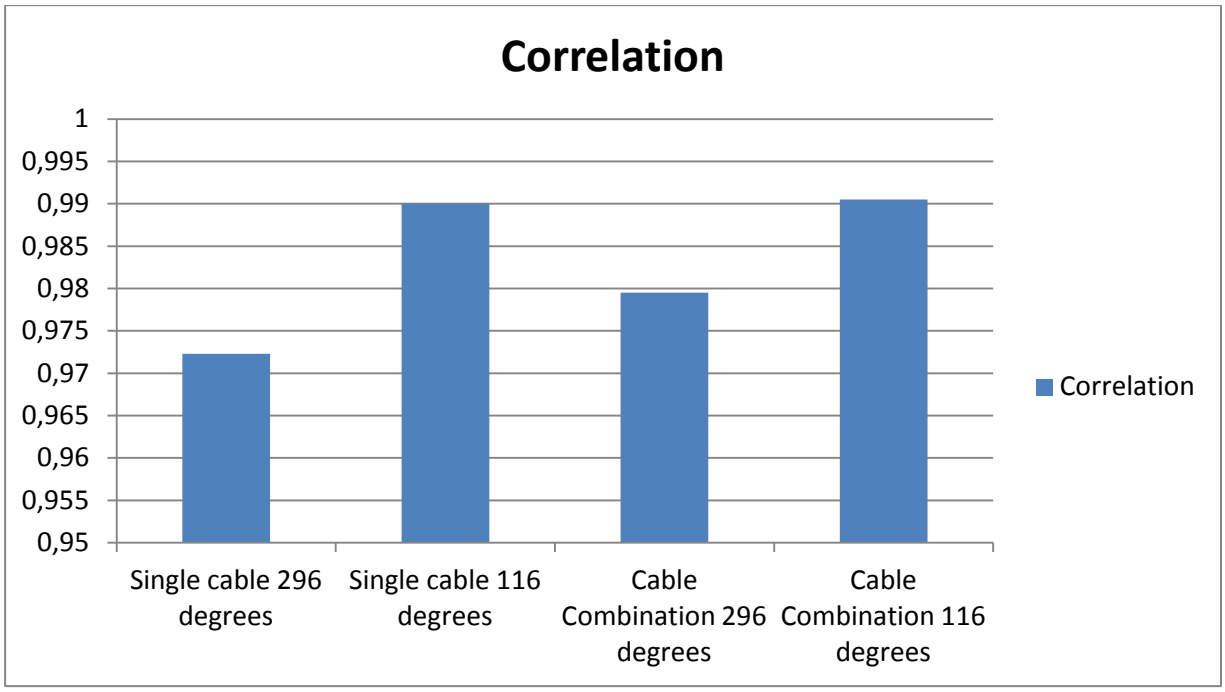

Figure 5 - 14: *Correlation between the inversion volumes of each acquisition method based on the vessel direction. The correlation is between the inversion values of the cross-plots in figure 4-23 and 4-24.*

From figure 5-13 we observe that there are variations between the single cable and the cable combination inversion, but that the significant change is between the different acquisition directions. Equal trend is observed in figure 5-14 where comparison between the inversions with acquisition direction of 116 degrees has a significant better correlation than the opposite. The correlation figure adds to the results seen in figure 5-13 and makes the conclusion, that the feathering has an impact on the inversion, only stronger.

5.5.1 Impact of feathering on the inversion volumes

Feathering occurred in some extent for every line throughout the survey, and causes effects both for the seismic and the inversion volumes. The fact that the feathering causes effects in the inversion volumes can be easily explained by the changes in the seismic. Since we have feathering in all the seismic lines, and the feathering is slightly varying for each line, the area covered by the seismic is also slightly different. Feathering causes the receivers behind the vessel to deviate from a straight line with each shot, and since the receivers is at slightly different locations for each acquisition, the reflections from the shot will be from a different location than if there were no feathering. The best solution would be if we had no feathering at all and the area covered by the seismic would be equal for all lines. However, this is not the case.

The feathering of the cables is most likely a result of the tidal currents, since the weather were good throughout the survey. During a period from low tide to high tide back to low tide, both the direction of the current and the velocity of the current changes. The direction is completely opposite when comparing the high tide (highest flood) and low tide (lowest ebb), while the velocity of the current

changes from highest flood to the slope and from the slope to lowest ebb. The direction change of the current is an abrupt change where the water level changes from higher than normal to normal water level and also similar for the opposite. The correlation between the flood and ebb and the current velocity can be observed in figure 5-15.

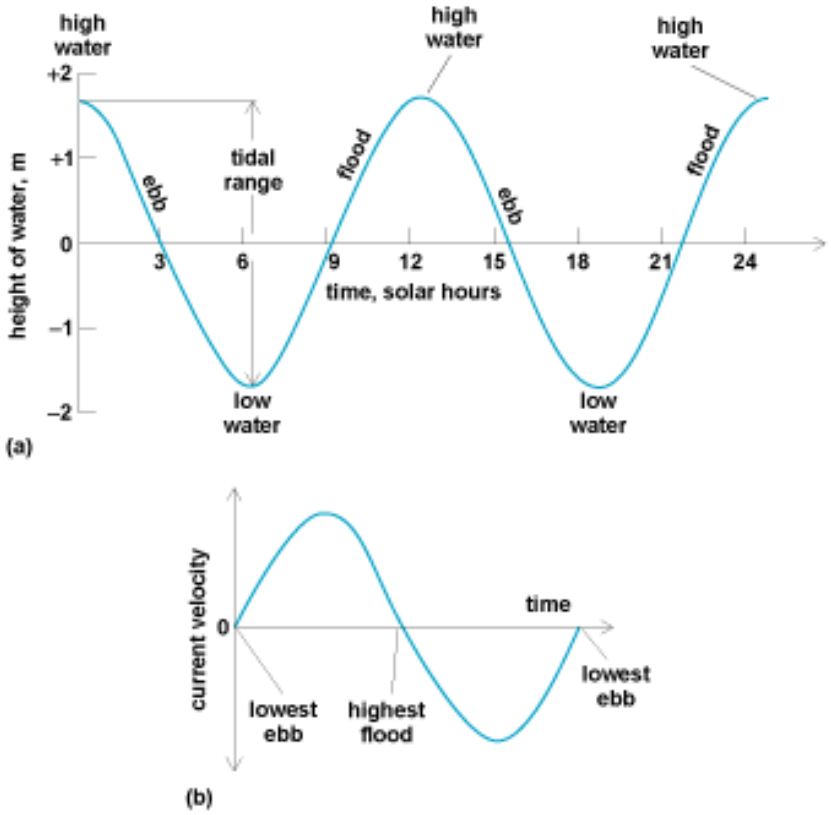

Figure 5 - 15: *Flood-ebb cycle. Figure (a) illustrates an idealized semidiurnal tidal cycle, while (b) is a time-current velocity curve. The figure is captured from* ***(Kvale, 2008)****.*

As illustrated in the figure, the highest current velocity is in the slope between highest flood and lowest ebb, while the lowest velocity is at lowest ebb and highest flood. The seismic is acquired in both high tide and low tide, and from the figure we can see that the velocity of the current changes throughout the period of one flood to ebb-cycle. Feathering will naturally happen in one survey since both the direction of the current and the velocity of the current changes.

As illustrated in the results, feathering happened at all acquisitions with different magnitude. The effect of the feathering in the seismic is therefore valid and causes all the seismic volumes to be slightly different. In alignment with the inversion comparison based on vessel direction and the inversion comparison with an average, the two inversions with the best alignment of the feathering causes the lowest error between them (highest correlation) and also the standard deviation value is lower due to this.

Comparing figures 4-29 and 4-30 we can easily observe these results which create a significant change in the inversion volumes when comparing them to each other. Figure 4-29 indicates poor alignment of the feathering, which can be compared with the wide spread in the cross-plot between the inversion volumes based on those acquisitions. The opposite effect happens in figure 4-30, where the feathering has very good alignment, and the correlation between the inversion volumes is high and the standard deviation is significantly lower than the first case.

By these comparisons we can illustrate that the feathering has a larger impact on the final inversion than observed from the cable combination method (when compared to the single cable method). This is due to the fact that the feathering actually changes the input seismic to the inversion. Since the inversion volume convolved with the used wavelet should be as similar to the input seismic as possible, the change in the seismic causes changes in the inversion volume.

5.6 Increasing weight factor in the inversion processes

From comparing the inversion volumes based on acquisition method and then processing the inversion based on 2 different weight factors on the input seismic, we can analyze the actual impact of the cable combination technology on the inversion volumes. We then have 4 different volumes as explained in Chapter 4.6. The most important crossplot from that chapter is the one where we are comparing the inversions based on different weight factor to each other, where each crossplot only constitute of inversions based on similar acquisition method. This crossplot can be observed in figure 5-16.

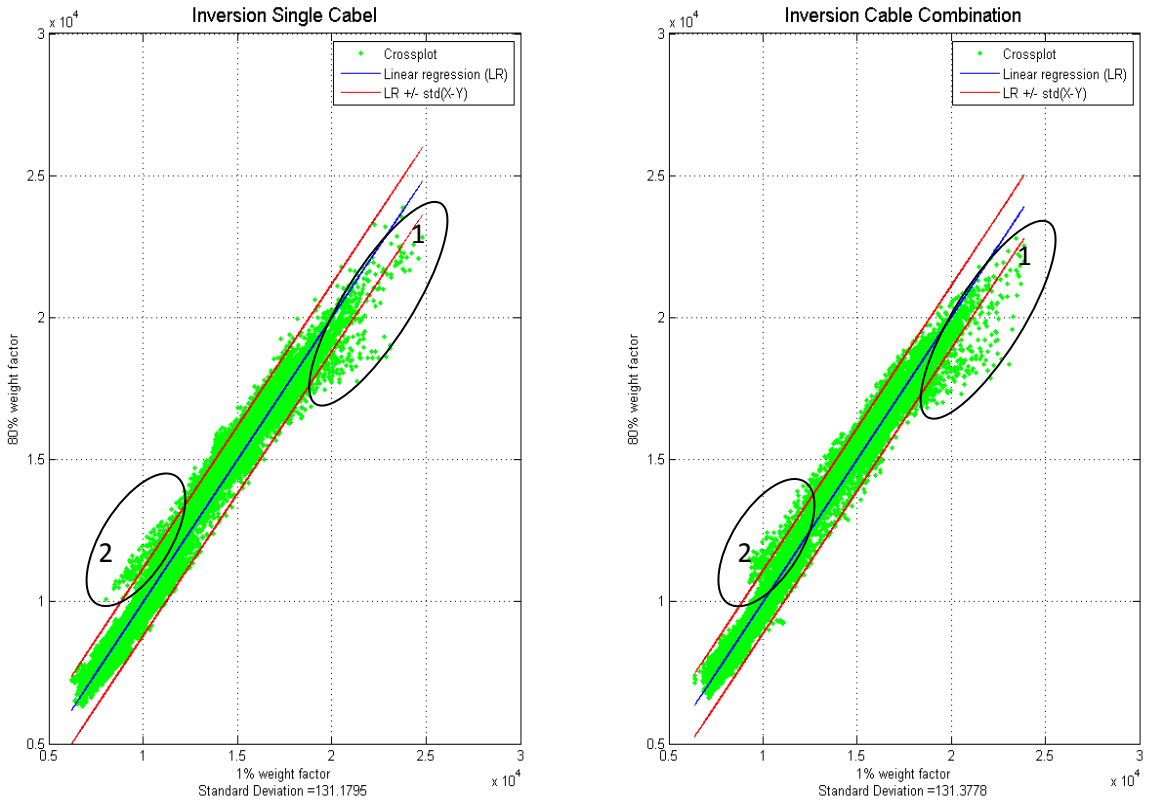

Figure 5 - 16: *Figure illustrating cross-plots where we are comparing inversions based on the acquisition method for the seismic input. Both cross-plots contain inversions with 1% and 80% weight factor on the background model. Ellipse number one and two, in both cross-plots, illustrates interesting features in the comparison between them.*

By comparing the two cross-plots from the figure below, we can see that both plots have the same outliers, capped by ellipse number one and two. Even though these are slightly different and the spread of the two is a bit different at the end, it seems that the calculation difference for the inversions are equal for both single cable inversion and cable combination inversion.

Another interesting part is that the standard deviation is a bit smaller for the single cable comparison than for the cable combination comparison. It was suggested that the cable combination seismic would lead to more stable inversion with lower weight factor on the background model than the single cable seismic could provide. However, the cross-plots from figure 5-8 tell another story. Since we don't have an improvement when lowering the weight factor (comparing the two cross-plots), it seems that the improvement in the lower part of the frequency spectra for the reservoir area is of a

so small amount that the loss in the higher part results in no significant improvements in the inversion volumes. This indication is also strengthened due to the results from the inversion comparison with an average and that the feathering has a more significant impact on the inversion volumes (and the alignment of it) than comparing the two acquisition methods.

Also keeping in mind that all the inversions were based on equal background model with a reference cable combination volume, many of the minor improvements from single cable to cable combination acquisition method could be caused by (or suffer from) this.

5.7 Split spread

Another setup for the acquisition was the split spread seismic, where we illuminate the sub-surface from 2 opposite sides. The split spread seismic volumes are in fact here done in processing of the seismic by adding the two different directions and merging them into one seismic volume. By increasing the fold of the acquisition we are removing much of the original noise by stacking the traces together. Removing noise improves the signal to noise ratio and also improves the inversion result.

Since the split spread seismic was of minor importance in this thesis, there is no notice of these results in Chapter 4. However, to illustrate the impact of the method to the inversion result compared to the difference between the single cable and cable combination method, we are discussing it to some extent here.

As introduced in Chapter 1.3, we have 4 different datasets of split spread volumes. These are for single cable, cable combination and for both high tide and low tide. To illustrate the improvements by increasing the fold, we have added the signal to noise ratio for the split spread data.

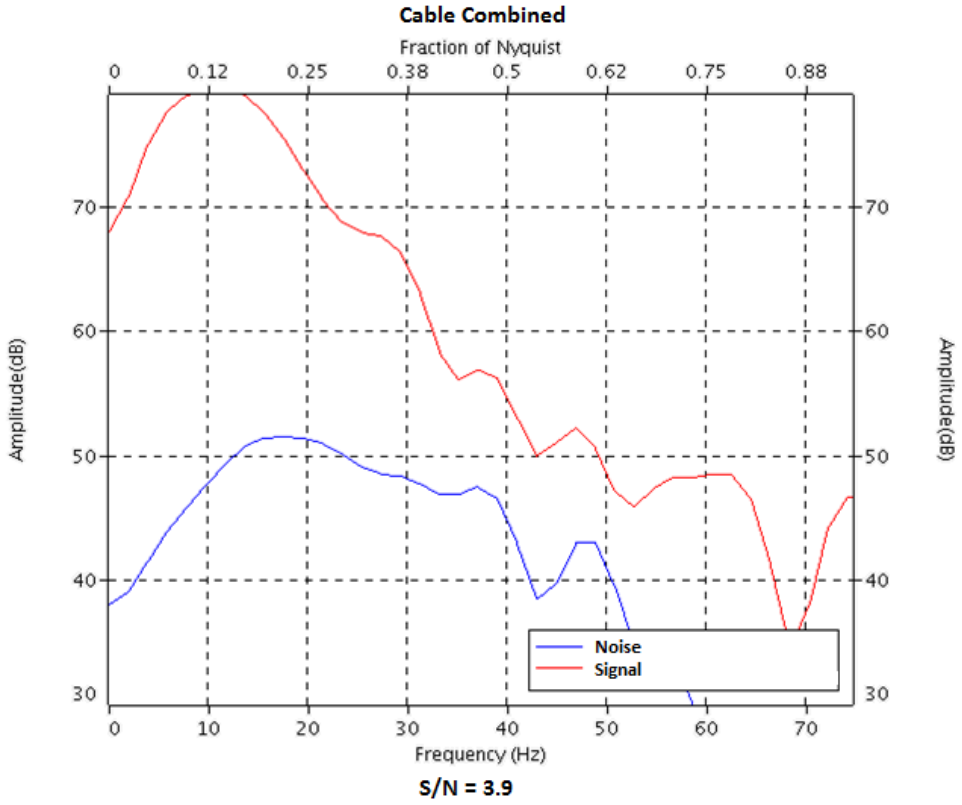

Figure 5 - 17: *Signal to noise ratio of the split spread cable combination seismic volume. The signal to noise ratio is 3.9.*

From the overlying spectrum of the figure above, we can observe that the ratio has improved significantly from the other signal to noise ratios previously described, where we had values ranging from 3.1 to 3.3 for the cable combination seismic volumes. This increase in the ratio is most likely to be a result of the stacking of the seismic traces, since the number of traces is increased by a factor close to 2.

This increase also affects the inversion results. The wavelet used is equal to the wavelet for the cable combination inversion volumes, since the split spread seismic volumes are merged from cable combination seismic volumes in opposite direction. However, since we have a better signal to noise ratio, the seismic volume is more likely to reflect the true geology of the area.

As we observe from the figure under, the inversion analysis illustrate that the inverted trace is closer to the log trace compared to the results given in Chapter 4. We have a lower error in acoustic impedance with time in the time interval equal to the reservoir area, but we also still have these large end effects which are common in all inversions. The inversion analysis indicate that the inversion is better resolved than the cable combination inversion, but it is still only one trace comparison and the rest of the reservoir also need to be investigated to see if the trend is valid also there.

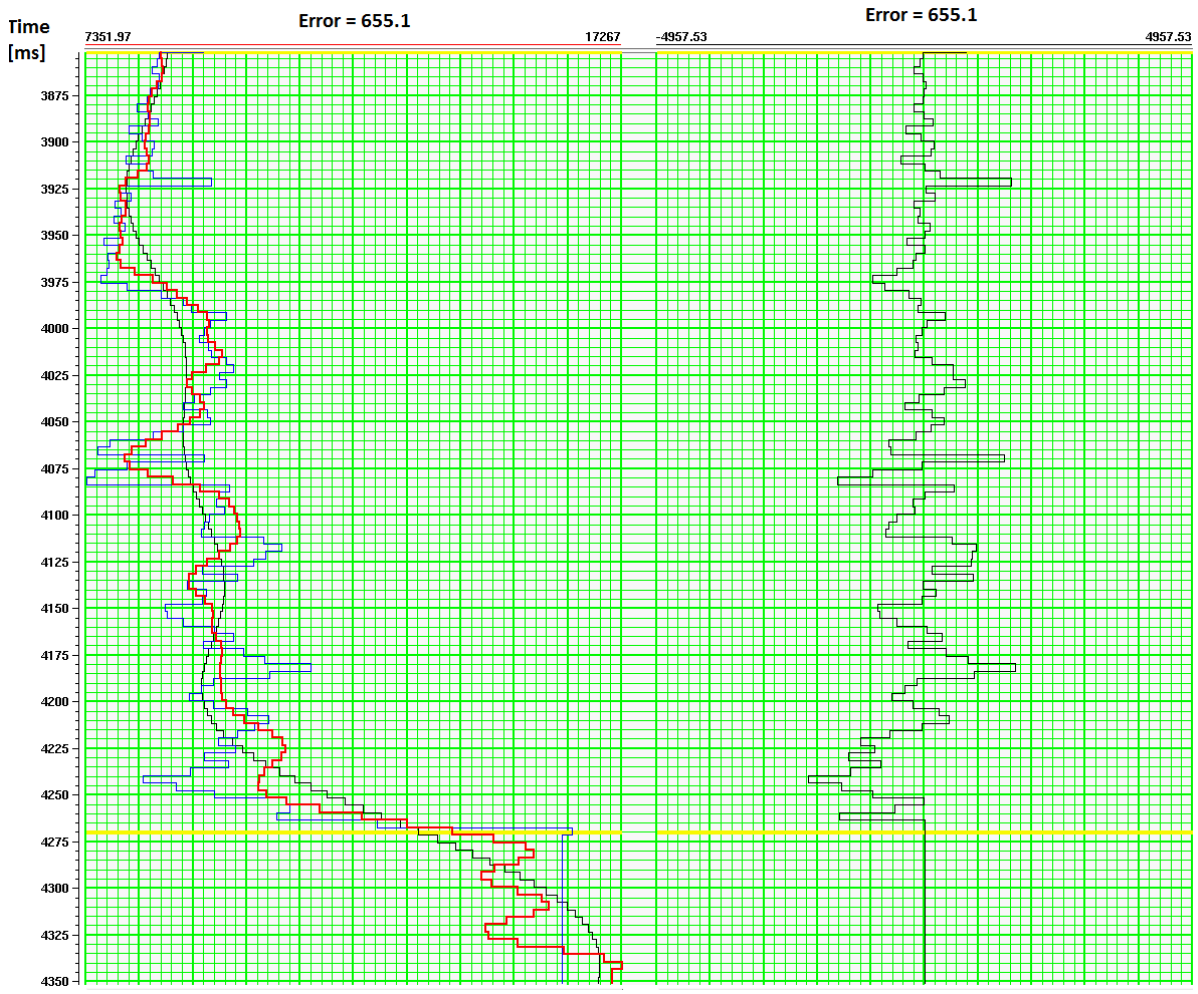

Figure 5 - 18: *Inversion analysis window for the split spread cable combination inversion of one trace in the well location. The blue trace is the original trace, the red trace is the inverted trace, while the black trace overlying these are the background model trace. The black trace to the right is the error trace of the error between the inverted and the log trace to the left.*

By observing the final inversion of the split spread inversion, we can identify various trends that is indicating that the inversion is more correct (more similar to the real geology of the area). As we see from the figure below, we can observe that the inversion volume is less cluttered than the results in

chapter 4. This indicates that there is less noise due to the increased signal to noise ratio. Layers are also more horizontally consistent, which are important due to the fact that the rocks don't overly each other, or interfere with each other, throughout the vertical extent of the layers. The changes are significant and important, since it seems that the split spread method has a larger impact on the inversion than the cable combination method.

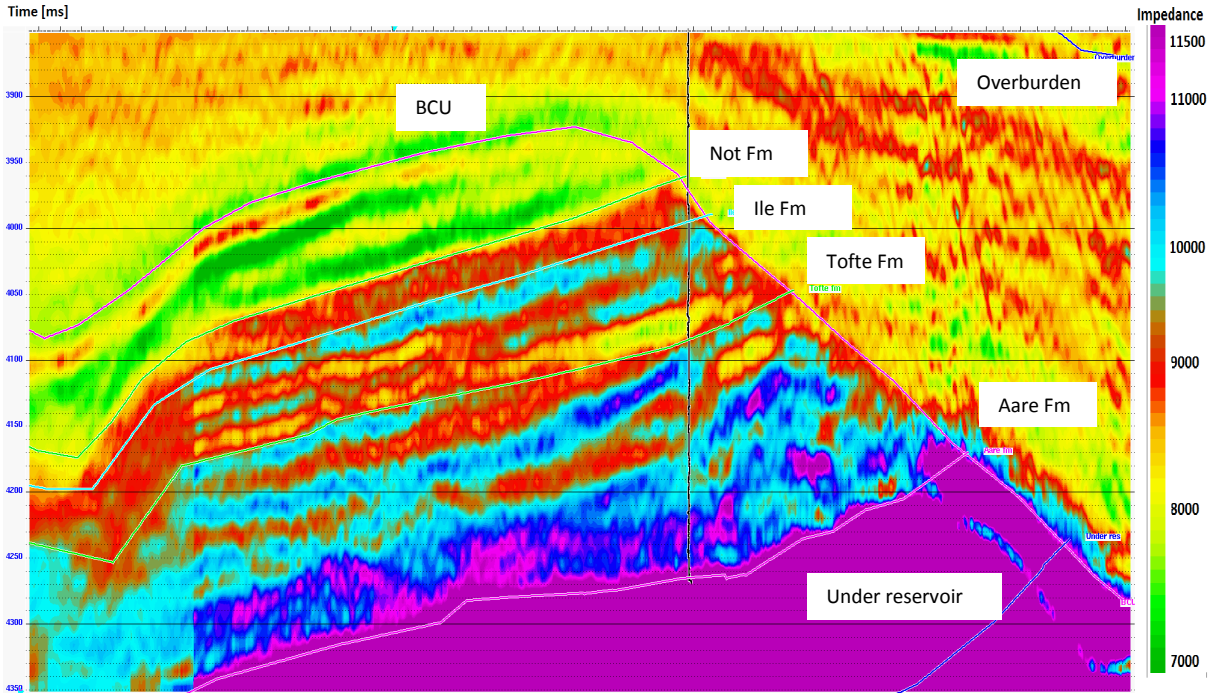

Figure 5 - 19: *Inversion result of the split spread cable combination inversion. The inversion window covers equal area as the other inversions [3852-4352 ms].*

By performing a split spread analysis, we can see that since we are illuminating the area from both sides, we are giving the area twice the information compared to the single side illumination from both the cable combination and the single cable seismic volumes. Inversion would also therefore be less error prone and contain less noise compared to signal as described earlier.

We also want to illustrate how the inversion volume changes from high tide to low tide using the split spread method. We have to keep in mind that the feathering effect is still valid, since the volumes used for the split spread is the original volumes from the cable combination seismic, only merged together. Still, the effect of the method can still be observed in the comparison, where we would like to see a close spread when cross-plotting the two volumes to each other. The crossplot can be observed in the figure below. Keeping in mind that the feathering caused large variations in the standard deviations between the two volumes, and that this effect could be observed in both the plotting of mean against trace number and standard deviation against trace number, we can see the improvements in figures 5-20 and 5-21.

Even though we have large end effects as illustrated in the standard deviation plot in figure 5-13, the standard deviation is quite low, and deviates around a difference in acoustic impedance of about 200. The large end-effects are due to the large change in acoustic impedance in the end of the reservoir are also increased by the feathering difference between these volumes. Base on that the feathering is not aligning in any of the inversion volumes used in the plot (only in direction, not

aligning in tide), the standard deviation is quite low and validates the similarities in the volumes when illuminated from both sides.

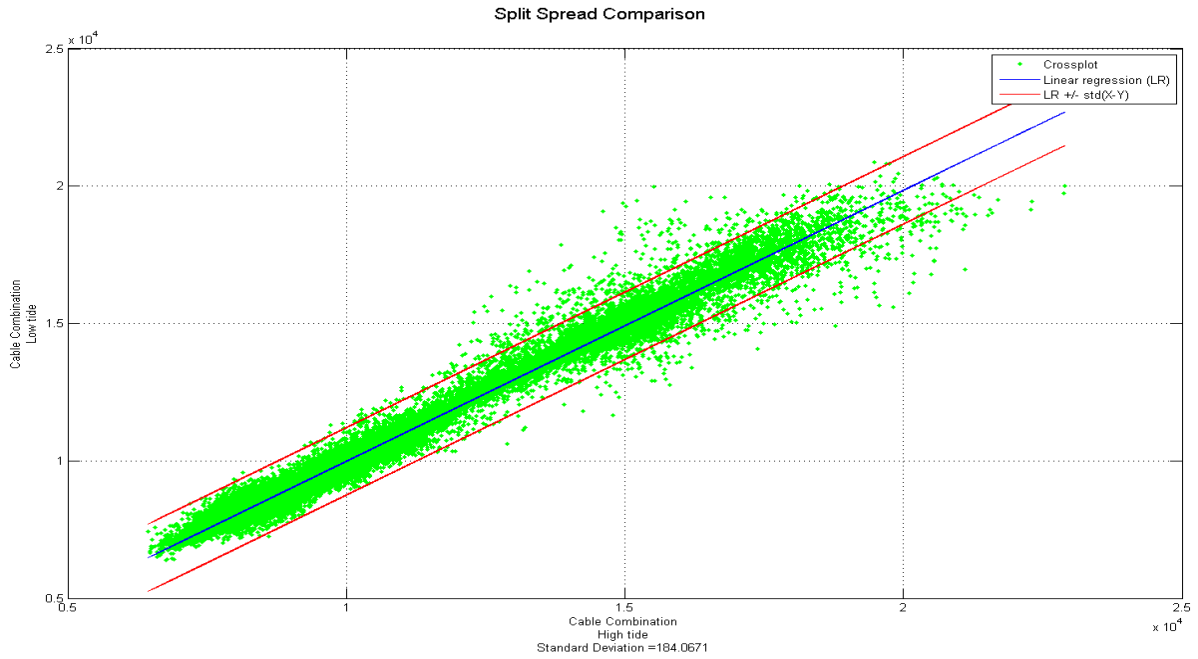

Figure 5 - 20: *Crossplot between the split spread cable combination inversion volumes of both high tide and low tide. Volumes are inversions from the time interval equivalent to the reservoir area [3852 – 4352 ms].*

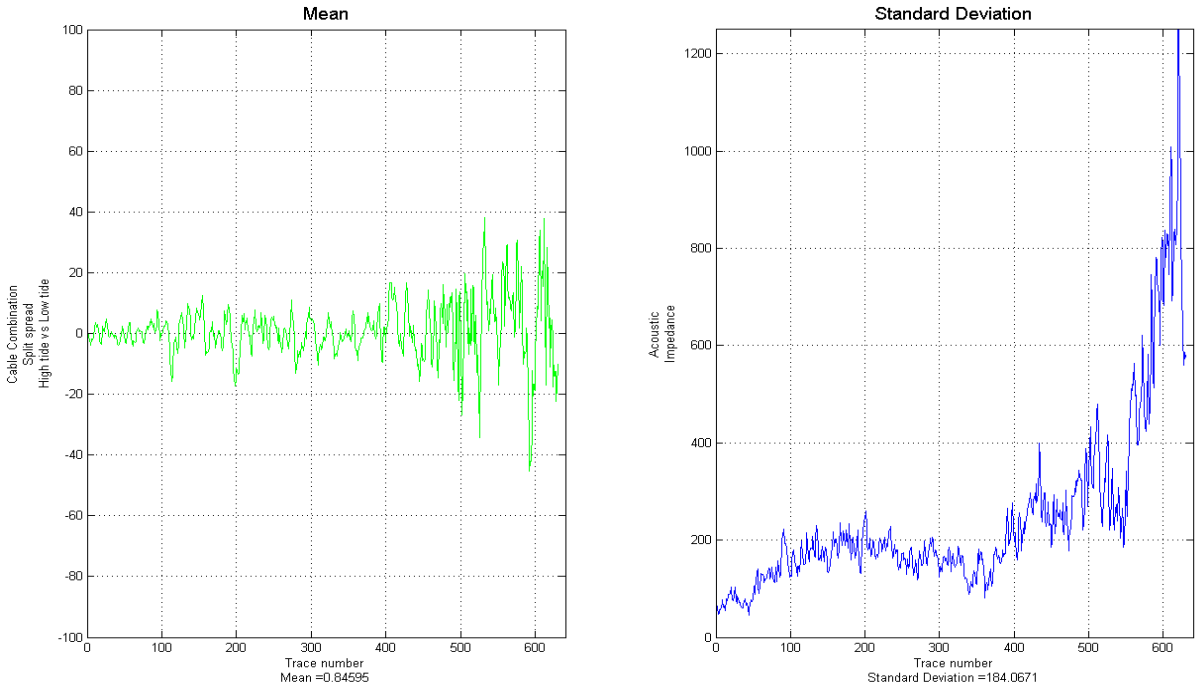

Figure 5 - 21: *Statistical mean with increasing trace number and the standard deviation with increasing trace number from the crossplot of the figure above. Both the standard deviation and the mean are included as a number beneath each plot.*

As illustrated in the figures above, the split spread method results in a better signal to noise ratio, better illumination of the area of interest, better resolving power in the inversion process and significant improvement of the correct geology of the area. These results are obtained both when comparing to the cable combination acquisition method and the single cable acquisition method.

The table below illustrates the improvements in the signal to noise ratio:

Acquisition method	**Tide**	**Vessel Direction**	**Signal to noise ratio**
Single cable	High	296 degrees	3.1
Single cable	High	116 degrees	3.1
Single cable	Low	296 degrees	2.9
Single cable	Low	116 degrees	3.1
Cable combination	High	296 degrees	3.3
Cable combination	High	116 degrees	3.1
Cable combination	Low	296 degrees	3.2
Cable combination	Low	116 degrees	3.3
Split spread	High	Both	3.9
Split spread	Low	Both	3.8

Table 5 - 1: *Signal to noise ratio for all the different datasets that were used in this work.*

Conclusion

The new streamer technology was developed in the 1980`s, but was shelved due to the lack of correct positioning of the cables during the survey. After the introduction of steerable streamers, using streamer birds, the technology could be used in this survey. The decomposition of the seismic wavefield into its upgoing and downgoing wavefields were possible and the possible improvements were to extend the seismic bandwidth both in the lower and higher end of the frequency spectra and to increase the signal to noise ratio to improve the seismic inversion process.

Results of the experiment on the Kristin Field are in contradiction to the improvements that were first anticipated for the survey. Results indicates that the frequency bandwidth from the time interval equivalent to the reservoir area (3852 – 4352 ms) contains more of the low frequencies for the cable combination seismic data, but suffers from the loss of the higher frequencies (see figure 5-3). The bandwidth is hence not broadened, but narrowed and shifted towards lower frequencies.

The narrowed and shifted frequency bandwidth of the cable combination seismic data results in a broader wavelet than the one for the single cable seismic data. From the results we have illustrated the differences between the two wavelets and the difference in vertical resolution due to the change in the shape of the wavelet. Extraction of statistical wavelet using the basis of single cable seismic data resulted in an improvement in the vertical resolution, when comparing with the statistical wavelet from cable combination seismic data. For the experiment using the configuration of the reflection matrix in figure 5-4, the relative difference is 3 ms favoring the single cable seismic. Based on the wavelet extracted from the reservoir time interval from seismic based on both the acquisition method, the change in vertical resolution is 17.6 % favoring the single cable method.

Signal to noise ratio was improved to some extent by using the cable combination technology, but is not significant when comparing to the result from the split spread seismic dataset. Figure 6-1 illustrates the change in signal to noise ratio comparing single cable, cable combination and split spread seismic data. The one significant change is when we are using split spread instead of single direction seismic.

Comparing the inversion volumes with inputs from both the single cable and cable combination seismic illustrates that there are significant changes when comparing the average volumes to one acquisition direction, which are 296 degrees. The change between inversions based on acquisition method was not significant and indicated that both direction and feathering of the cables has a larger impact on the final inversion volume than the change of acquisition method. Figure 6-2 illustrates results found for comparing inversion volumes with their average and with a reference volume, and display the difference between acquisition direction and acquisition method. As previously

mentioned we can see that the significant changes were to acquisition direction, which was observed to be an effect of the different feathering of the receiver cables due to tidal currents.

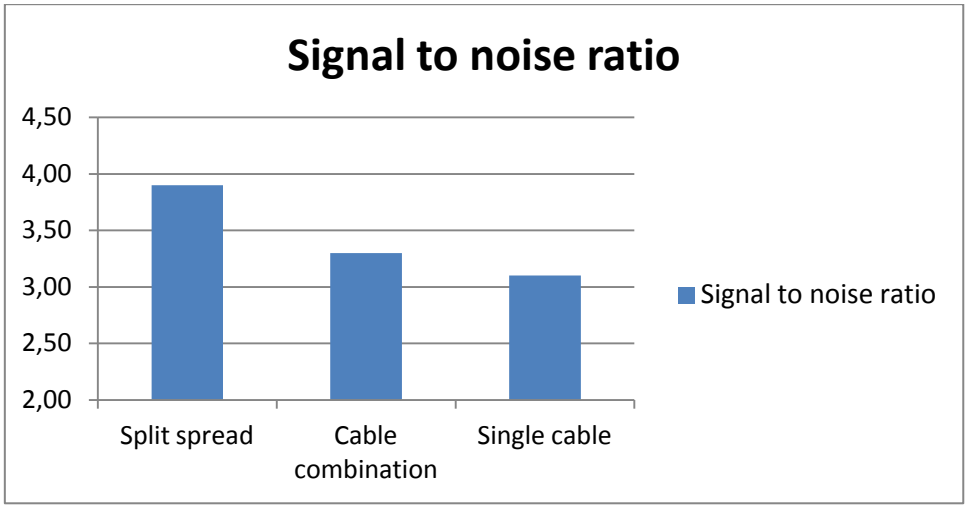

Figure 6 - 1: *Difference in signal to noise ratio between the different methods used for the survey. Both the single cable and the cable combination seismic are acquired in high tide and with vessel direction of 296 degrees. The split spread are combination of the two cable combination seismic volumes acquired in high tide.*

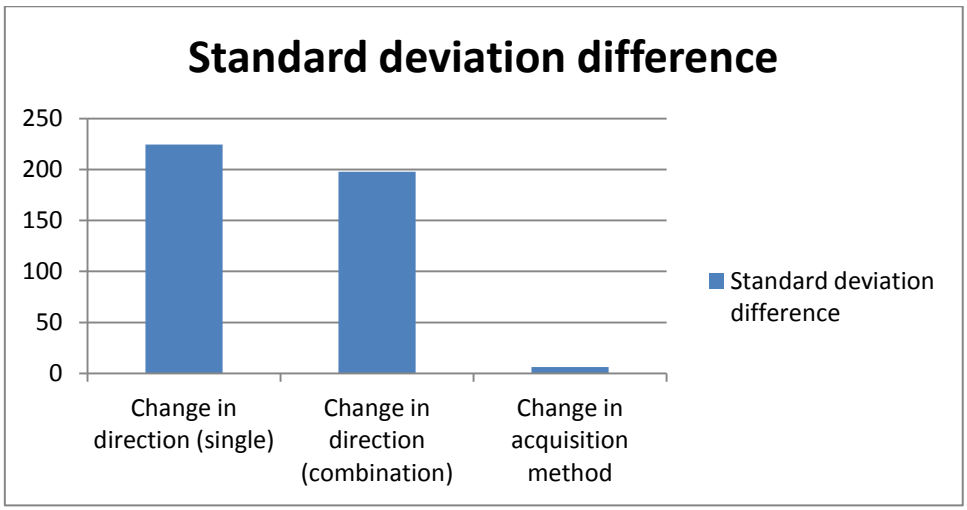

Figure 6 - 2: *Difference in standard deviations regarding change in direction for both single cable and cable combination inversions, and also the change in acquisition method as input for the inversion volumes. Figure based on the results found in table 4-2 and 4-4.*

Inversions were also performed with two different weight factors on the background model, to illustrate the changes for high and low weight factors on the inversions. These weight factors were applied to the inversion process for inversions based on both acquisition methods. The results indicate that the changes in weight factor are more or less similar for both single cable and cable combination inversions, and no significant difference were found.

Based on the datasets used in this work, the experiments have resulted in verification of various parameters that influence the inversion volumes significantly. Experiments indicate that the cable combination acquisition method has minor influence on the inversion process. There are other parameters that were identified to have a larger impact;

- Acquisition direction
- Fold (split spread)
- Feathering of the receiver cables

All these parameters have a larger impact on the inversion than the cable combination acquisition method. The work done has resulted in the verification of these changes and also has indicated that the change in the inversion volume due to a change in the acquisition method has no significant effect.

Works Cited

Berkhout A. J. Seismic resolution [Book]. - London - Amsterdam : Pergamon press, 1984. - Vol. 12.

Christoffersen K. R. [et al.] Continous History Matching a HPHT Gas Condensate Field during the First Two Years of Production [Journal]. - [s.l.] : SPE International, 2008.

Dyrnes H. Inversion of 2D seismic data from the Kristin Field in the Norwegian Sea acquired with an over/under cable combination streamer [Report]. - Trondheim : NTNU, 2011.

Geomatic E Notes [Online] // enotes.com. - 2009. - 28 April, 2012. - http://www.enotes.com/topic/IRAP_RMS_Suite.

Halliburton Landmark [Online] // Halliburton.com. - Haliburton, February 2008. - April 28, 2012. - http://www.halliburton.com/public/landmark/contents/Data_Sheets/web/H05283.pdf.

Hampson-Russell Hampson Russell Assistant [Document from program]. - [s.l.] : CGG Veritas, 2009.

Hampson-Russell Theory of the STRATA program [Journal]. - [s.l.] : CGG Veritas, 1999.

Henry S. G. searchanddiscovery.com [Online] // Understanding the Seismic Wavelet. - Geolearn, 2001. - April 26, 2012.

Hill D., Combee L. and Bacon J. Over/under acquisition and data processing: the next quantum leap in seismic technology? [Journal]. - [s.l.] : First Break, 2006. - Vol. 24.

Ikele L. and Amundsen L. Petroleum Seismology: Chapter 4 [Online] // petroleumgeophysics.com. - Petroleum Geophysics. - April 30, 2012. - http://petroleumgeophysics.com/images/Chapter-4.

Ikele L. and Amundsen L. petroleumgeophysics.com [Online] // Petroleum Seismology. - Petroleum Seismology. - April 26, 2012. - http://petroleumgeophysics.com/images/Chapter-4.

Kvale E. P. Tidalites [Online] // Access Science. - 2008. - http://accessscience.com/content/Tidalites/696800.

Langridge A. Depth Imaging Data Processing Report [Report]. - Stjørdal : Statoil, 2010.

Langridge Andrew Cable Combination spectrum [Interview]. - April 19, 2012.

MatLab [Online] // MatLab: The Language of Technical Computing. - MathWorks, 2012. - April 29, 2012. - http://www.mathworks.se/products/matlab/.

Moldoveanu N., Combee L. and Egan M. Over/under towed-streamer acquisition: A method to extend seismic bandwidth to both higher and lower frequencies [Journal]. - [s.l.] : The Leading Edge, 2007.

NPD NPD factpages [Online] // Norwegian Petroleum Directorate. - Norwegian Petroleum Directorate, May 29, 2002. - April 30, 2012. - http://factpages.npd.no/ReportServer?/FactPages/PageView/wellbore_exploration&rs:Command=Render&rc:Toolbar=false&rc:Parameters=f&NpdId=2849&IpAddress=129.241.222.246&CultureCode=nb-no.

NPD The NPD`s Fact-pages [Online] // npd.no. - Norwegian Petroleum Directorate, April 24, 2012. - April 24, 2012. - http://www.npd.no/engelsk/cwi/pbl/en/index.htm.

PGS GeoStramer GS - The Ghost Free Solution [Article] // TECH LINK. - [s.l.] : PGS, 2011. - 4. - Vol. 11.

Quin J. G. [et al.] Sedimentology and unexpected pressure decline: the HP/HT Kristin Field [Journal]. - Stjørdal : Statoil, 2010.

Sah S. L. Encyclopedia of Petroleum Science and Engineering [Book]. - Dehli : Gyan Publishing House, 2003. - Vol. 1.

Statoil statoil.com [Online]. - Statoil ASA, September 3, 2007. - April 26, 2012. - http://www.statoil.com/en/ouroperations/explorationprod/ncs/kristin/pages/default.aspx.

Technology Offshore Kristin Deepwater Project [Online] // offshore-technology.com. - Statoil, September 3, 2007. - April 26, 2012. - http://www.offshore-technology.com/projects/kristin/.

Weisstein Eric W. Least Squares Fitting [Online] // A Wolfram Web Resource. - MathWorld. - April 29, 2012. - http://mathworld.wolfram.com/LeastSquaresFitting.html.

XSGeo XSGeo.com [Online] // Excess Geophysics. - Domains and Transforms, 1999. - April 26, 2012. - http://www.xsgeo.com/course/basic.htm.

Y. Quan J. M. Harris Stanford University Education [Online] // pangea.stanford.edu. - Geophysics Department. - April 26, 2012. - http://pangea.stanford.edu/~quany/StochasticSeismicInv_withRef.pdf.

Zweigel P. [et al.] International Geological Congress [Online] // cprm.gov.br. - Statoil, August 14, 2009. - April 27, 2012. - http://www.cprm.gov.br/33IGC/1324729.html.

Table of Figures

List of Tables

Appendix

A - Seismic

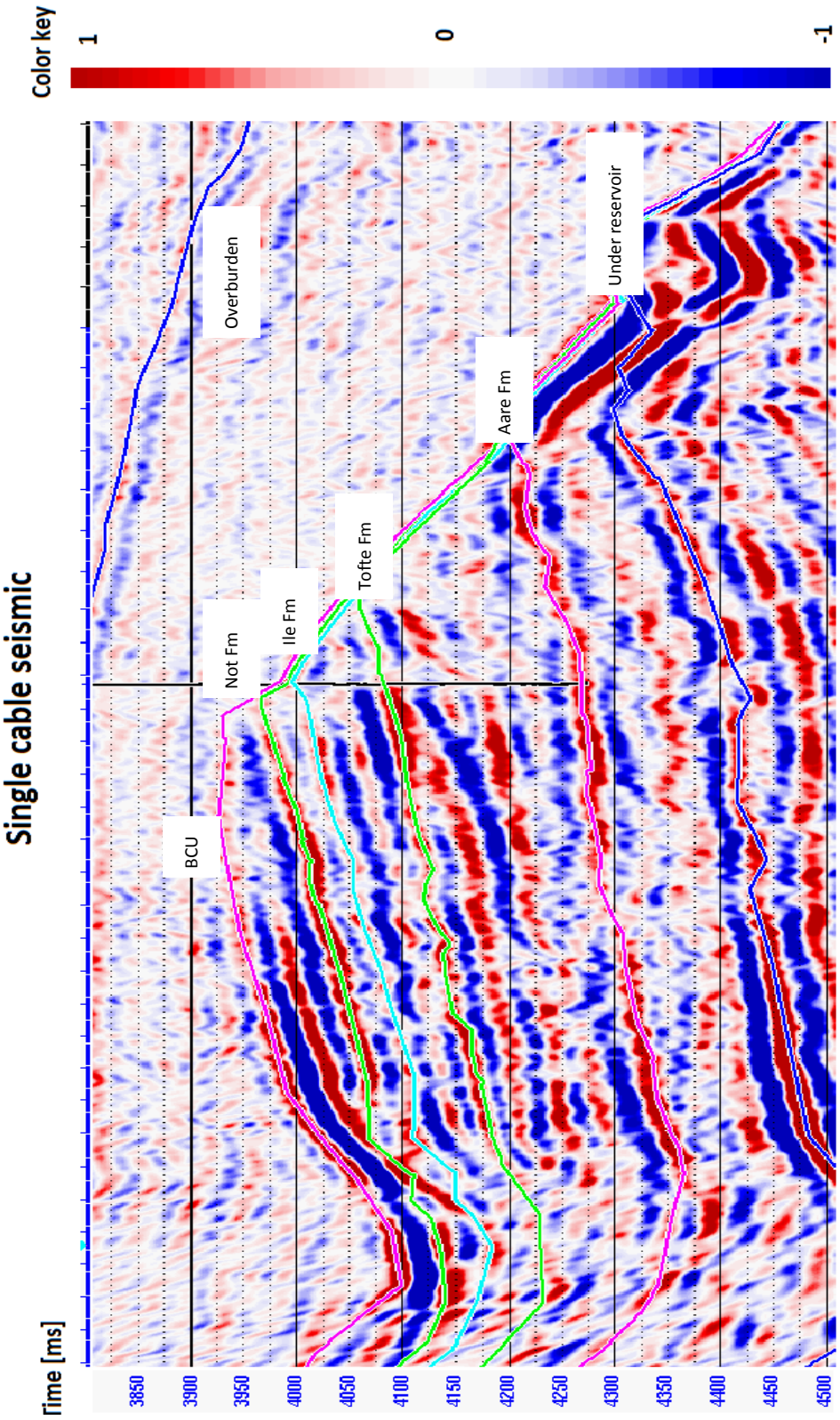

Figure A - 1: *Single cable seismic with vessel direction of 296 degrees and acquired in high tide.*

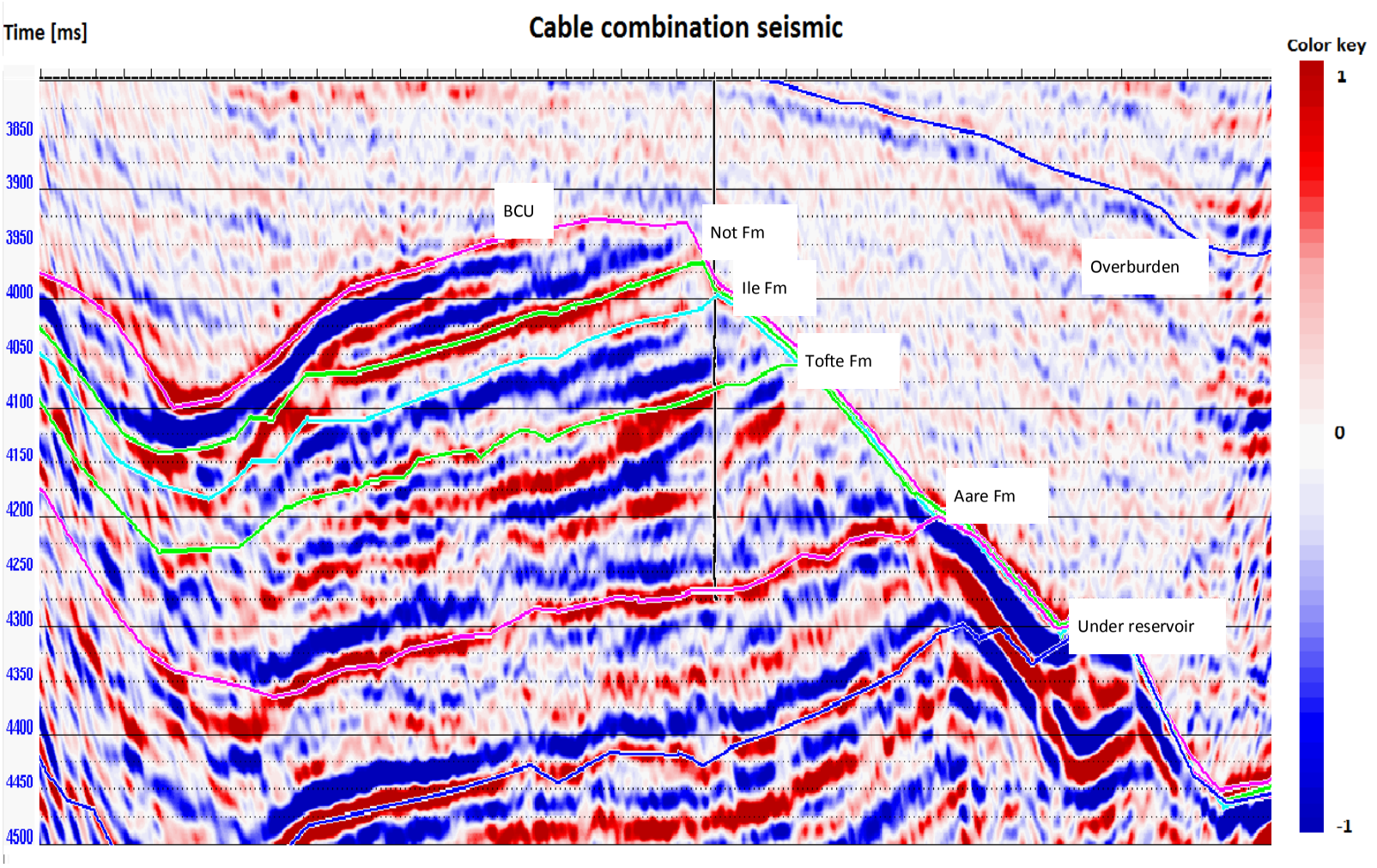

Figure A - 2: *Cable combination seismic with vessel direction of 296 degrees and acquired in high tide.*

B – Inversion

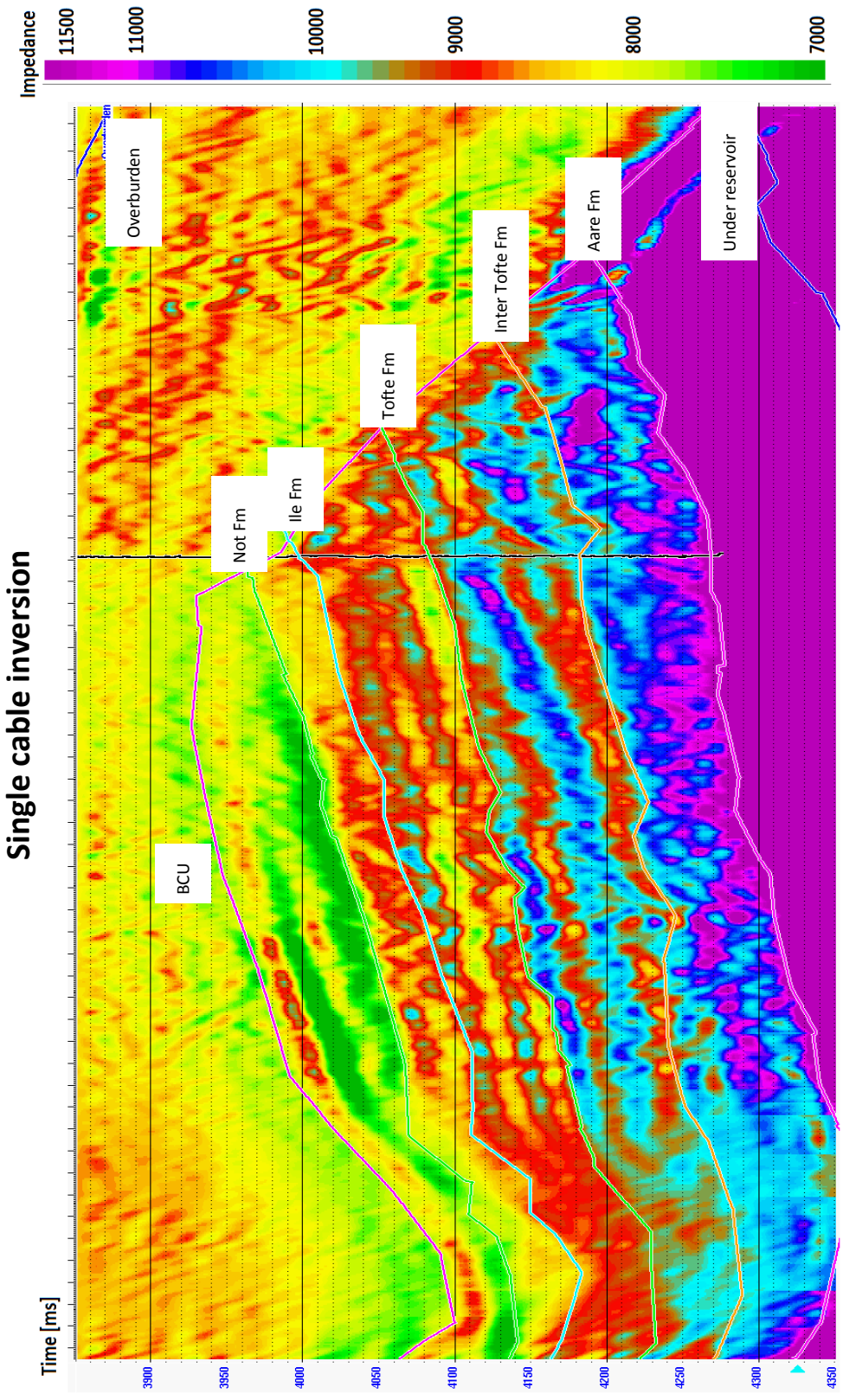

Figure B - 1: *An inversion volume with input seismic shown in figure A-1. Single cable inversion.*

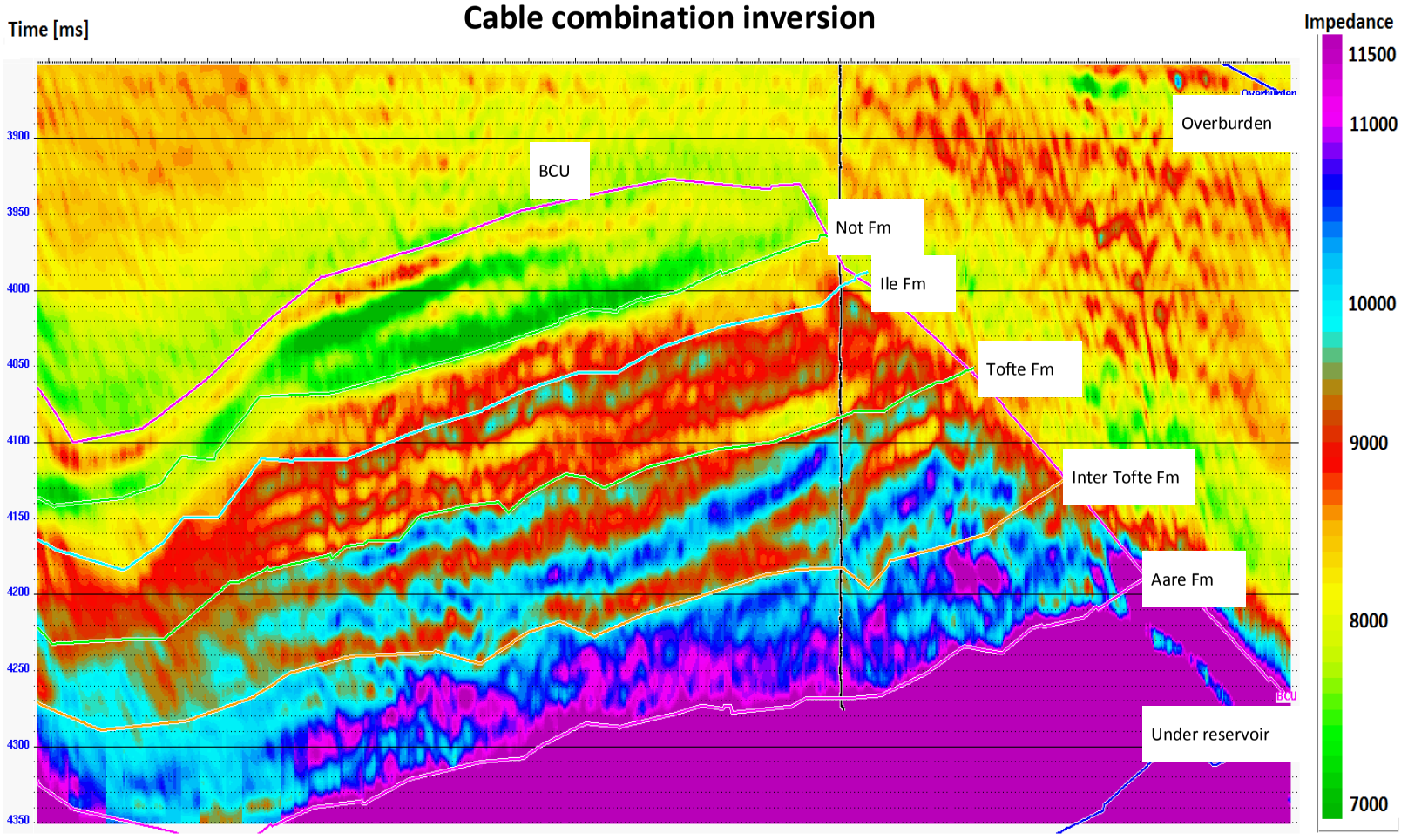

Figure B - 2: *An inversion volume with input seismic shown in figure A-2. Cable combination inversion.*

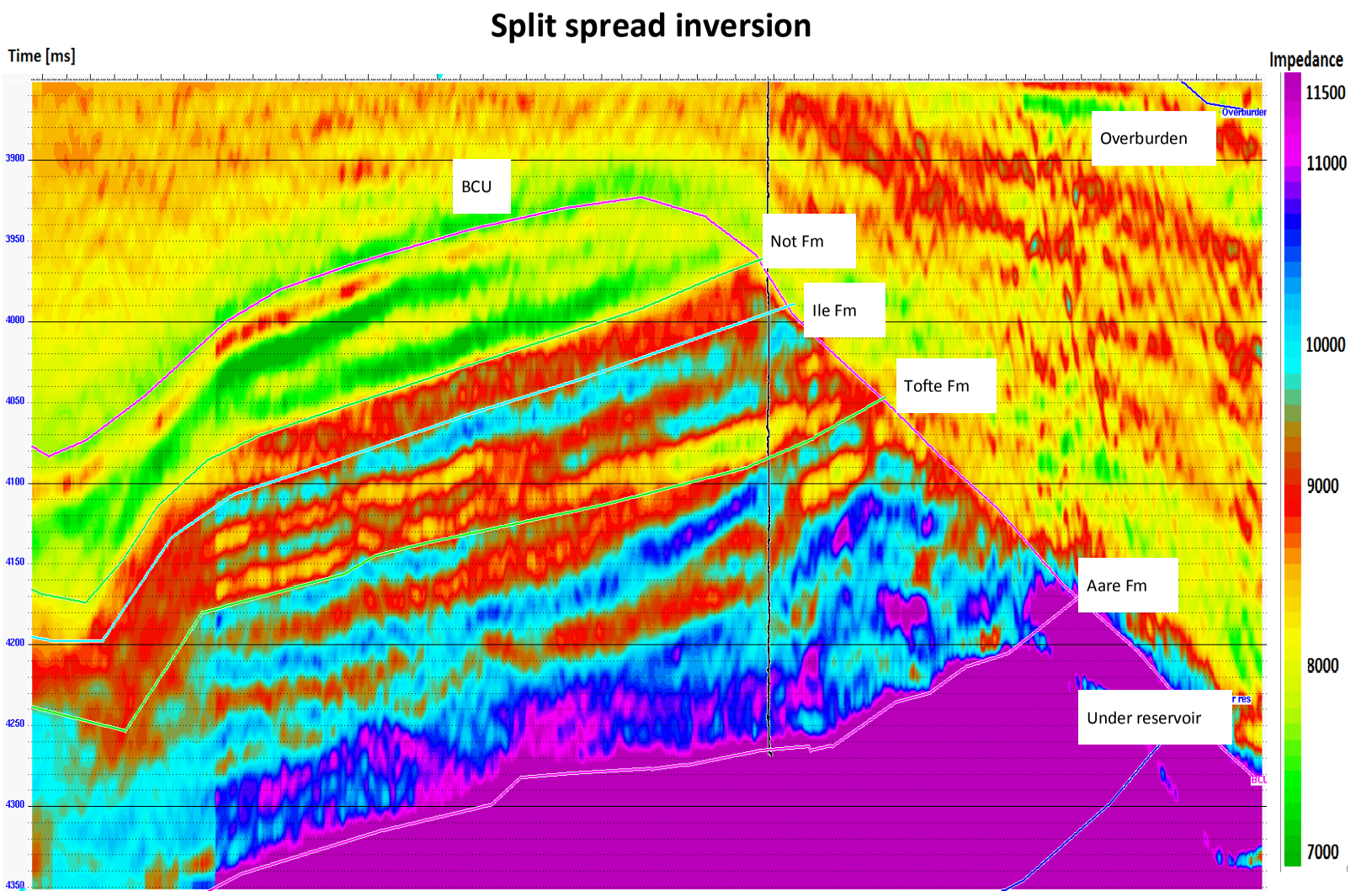

Figure B - 3: *An inversion volume with input seismic based on the split spread method. Split spread inversion.*

C – Matlab codes

In this appendix we have added 4 different codes which are important for the work done. These are;

1. Code for plotting and calculating standard deviation and mean
2. Code for plotting two different wavelets and the difference between them
3. Code for the difference in amplitude spectra
4. Code for checking the vertical resolution

1. *Plotting, standard deviation and mean*

```
% The program was developed to quantify the difference between
% cable combination inversion and single cable inversion.
%
% In this specific code, the user wants to quantify the difference
% between inversion with 1% weight on the data (seismic) to 80% weight
% on the data (seismic), and compare the results for both single cable
% inversion and cable combination inversion.
%
% The red line in the figures created on the crossplots are linear
% regression with minimized squared error. The blue line on top and under
% the linear regression line (LR) is then LR +/- standard deviation of
% (X-Y);
%
%   - Red line:     LR
%   - Blue lines:   LR +/- std (X-Y)
%
% The mean and standard deviation with increasing trace line is also
% plotted. Since the inversion is created only in the reservoir section,
% and the traces consists of 700 traces in the X-line direction, we only
% have 700 traces in the plot.
%
% The reason why we have 4 plots on the inversion difference, is based on
% the fact that we are also comparing the results from the different
% acquisition types against each other. Here are the 4 different plots in
% figure 1;
%
%   1 - Single1(X) vs Single80(Y)
%   2 - Comb1(X) vs Comb80(Y)
%   3 - Single1(X) vs Comb1(Y)
%   4 - Single80(X) vs Comb80(Y)
%
% Single1 = Single cable inversion 1% weight factor on the seismic
% Single80 = Single cable inversion 80% weight factor on the seismic
% Comb1 = Cable combination inversion 1% weight factor on the seismic
% Comb80 = Cable combination inversion 80% weight factor on the seismic
%
% The code is specified for 2 specific inputs, and is not dynamic.
%
%
% The code was created by
% Haakon Dyrnes
% For use in the master`s thesis
% April, 2012


%% Clearing all parameters and closing all open files in MatLab
clear all; close all;


%% Reading the files
fid = fopen('H:\MASTER\Exports\02_001_080','r');
for i=1:14                                          % Skip 14 lines
    dum = fgetl(fid);
end
A = fscanf(fid,'%f %f %d %d',[4 inf])';


fid2 = fopen('H:\MASTER\Exports\03_001_080','r');
```

```
for i=1:14                                                  % Skip 14 lines
    dum = fgetl(fid2);
end
A2 = fscanf(fid2,'%f %f %d %d',[4 inf])';



%% Number of traces
ntraces=701;
nt=126;


%% Mean and standard deviation
Mean1=zeros(ntraces,1);
Mean2=zeros(ntraces,1);
Mean3=zeros(ntraces,1);
Mean4=zeros(ntraces,1);

Std1=Mean1;
Std2=Mean1;
Std3=Mean1;
Std4=Mean1;



for i=1:ntraces
Mean1(i)=mean(A((((i-1)*nt+1):(i*nt)),2) - A((((i-1)*nt+1):(i*nt)),1));
Std1(i)=std(A((((i-1)*nt+1):(i*nt)),2) - A((((i-1)*nt+1):(i*nt)),1));
end

for i=1:ntraces
Mean2(i)=mean(A2((((i-1)*nt+1):(i*nt)),2) - A2((((i-1)*nt+1):(i*nt)),1));
Std2(i)=std(A2((((i-1)*nt+1):(i*nt)),2) - A2((((i-1)*nt+1):(i*nt)),1));
end

for i=1:ntraces
Mean3(i)=mean(A2((((i-1)*nt+1):(i*nt)),1) - A((((i-1)*nt+1):(i*nt)),1));
Std3(i)=std(A2((((i-1)*nt+1):(i*nt)),1) - A((((i-1)*nt+1):(i*nt)),1));
end

for i=1:ntraces
Mean4(i)=mean(A2((((i-1)*nt+1):(i*nt)),2) - A((((i-1)*nt+1):(i*nt)),2));
Std4(i)=std(A2((((i-1)*nt+1):(i*nt)),2) - A((((i-1)*nt+1):(i*nt)),2));
end

%% Mean
Mean01=mean(Mean1);
Mean02=mean(Mean2);
Mean03=mean(Mean3);
Mean04=mean(Mean4);


%% Sum of squared mean
Meanergy1=sum(Mean1.^2);
Meanergy2=sum(Mean2.^2);
Meanergy3=sum(Mean3.^2);
Meanergy4=sum(Mean4.^2);
```

```
%% The mean of the absolute value of the mean
Meanabs1=mean(abs(Mean1));
Meanabs2=mean(abs(Mean2));
Meanabs3=mean(abs(Mean3));
Meanabs4=mean(abs(Mean4));


%% Standard deviation
Std01=std(Std1);
Std02=std(Std2);
Std03=std(Std3);
Std04=std(Std4);


%% Defining the parameters
X=A(:,1);
Y=A(:,2);
X2=A2(:,1);
Y2=A2(:,2);


%% Setting sigma
sigma=0.1;


%% Computing the slope and intercept
[a,b]=polyfit(X,Y,2);
Output=polyval(a,X);
Correlation=corrcoef(Y, Output);
[a1,da1]=linreg(X,Y,sigma*Y);
Standard_Deviation1=std(Y-X);
The_Mean1=mean(Y-X);

[c,d]=polyfit(X2,Y2,2);
Output2=polyval(c,X2);
Correlation2=corrcoef(Y2, Output2);
[a2,da2]=linreg(X2,Y2,sigma*Y2);
Standard_Deviation2=std(Y2-X2);
The_Mean2=mean(Y2-X2);

[e,f]=polyfit(X,X2,2);
Output3=polyval(e,X);
Correlation3=corrcoef(X2, Output3);
[a3,da3]=linreg(X,X2,sigma*X2);
Standard_Deviation3=std(X2-X);
The_Mean3=mean(X2-X);

[g,h]=polyfit(Y,Y2,2);
Output4=polyval(g,Y);
Correlation4=corrcoef(Y2, Output4);
[a4,da4]=linreg(Y,Y2,sigma*Y2);
Standard_Deviation4=std(Y2-Y);
The_Mean4=mean(Y2-Y);


%% Crossplot, mean and standard deviation
figure(1);
subplot(221), plot(Mean1, 'g-')%,hold on, plot(Mean2, 'black-');
```

```
    AX=title('Mean');
    LEG=findobj(AX,'type','text');
    set(LEG,'FontSize',14);
    grid;
    axis([0,710,-100,100]);
    xlabel ({'Trace number';['Mean =',num2str(Mean01)]});
    ylabel ({'Single cable';'1% vs 80%'});
subplot(222), plot(Std1, 'b-')%, hold on, plot(Std2, 'r-');
    AX=title('Standard Deviation');
    LEG=findobj(AX,'type','text');
    set(LEG,'FontSize',14);
    grid;
    axis([0,710,0,1000]);
    xlabel ({'Trace number';['Standard Deviation =',num2str(Std01)]});
    ylabel ({'Acoustic';'Impedance'});
subplot(223), plot(Mean2, 'g-');
    %title('Mean');
    grid;
    axis([0,710,-100,100]);
    xlabel ({'Trace number';['Mean =',num2str(Mean02)]});
    ylabel ({'Cable comb.';'1% vs 80%'});
subplot(224), plot(Std2, 'b-');
    %title('Standard Deviation');
    grid;
    axis([0,710,0,1000]);
    xlabel ({'Trace number';['Standard Deviation =',num2str(Std02)]});
    ylabel ({'Acoustic';'Impedance'});

figure(2);
subplot(221), plot(Mean3, 'g-')%,hold on, plot(Mean2, 'black-');
    AX=title('Mean');
    LEG=findobj(AX,'type','text');
    set(LEG,'FontSize',14);
    grid;
    axis([0,710,-100,100]);
    xlabel ({'Trace number';['Mean =',num2str(Mean03)]});
    ylabel ({'Comb. vs single';'1%'});
subplot(222), plot(Std3, 'b-')%, hold on, plot(Std2, 'r-');
    AX=title('Standard Deviation');
    LEG=findobj(AX,'type','text');
    set(LEG,'FontSize',14);
    grid;
    axis([0,710,0,1000]);
    xlabel ({'Trace number';['Standard Deviation =',num2str(Std03)]});
    ylabel ({'Acoustic';'Impedance'});
subplot(223), plot(Mean4, 'g-');
    %title('Mean');
    grid;
    axis([0,710,-100,100]);
    xlabel ({'Trace number';['Mean =',num2str(Mean04)]});
    ylabel ({'Comb. vs single';'80%'});
subplot(224), plot(Std4, 'b-');
    %title('Standard Deviation');
    grid;
    axis([0,710,0,1000]);
    xlabel ({'Trace number';['Standard Deviation =',num2str(Std04)]});
    ylabel ({'Acoustic';'Impedance'});

figure(3);
subplot(121), plot(X,Y,'g.');
    hold on
```

```
    plot(X,a1(2)*X+a1(1),'b-');
    plot(X,a1(2)*X+a1(1)-std(X-Y),'r-');
    plot(X,a1(2)*X+a1(1)+std(X-Y),'r-');
    grid;
    AX=title('Inversion Single Cabel');
    LEG=findobj(AX,'type','text');
    set(LEG,'FontSize',14);
    xlabel ({'1% weight factor';['Standard Deviation =',num2str(Std01)]});
    ylabel('80% weight factor');
    legend('Crossplot','Linear regression (LR)','LR +/- std(X-Y)');
    axis([5000,30000,5000,30000]);
subplot(122), plot(X2,Y2,'g.');
    hold on
    plot(X2,a2(2)*X2+a2(1),'b-');
    plot(X2,a2(2)*X2+a2(1)-std(X2-Y2),'r-');
    plot(X2,a2(2)*X2+a2(1)+std(X2-Y2),'r-');
    grid;
    AX=title('Inversion Cable Combination');
    LEG=findobj(AX,'type','text');
    set(LEG,'FontSize',14);
    xlabel ({'1% weight factor';['Standard Deviation =',num2str(Std02)]});
    ylabel('80% weight factor');
    legend('Crossplot','Linear regression (LR)','LR +/- std(X-Y)');
    axis([5000,30000,5000,30000]);

figure(4);
subplot(121),plot(X,X2,'g.');
    hold on
    plot(X,a3(2)*X+a3(1),'b-');
    plot(X,a3(2)*X+a3(1)-std(X-X2),'r-');
    plot(X,a3(2)*X+a3(1)+std(X-X2),'r-');
    grid;
    AX=title('Inversion 1% weight factor');
    LEG=findobj(AX,'type','text');
    set(LEG,'FontSize',14);
    xlabel ({'Single Cable';['Standard Deviation =',num2str(Std03)]});
    ylabel('Cable Combination');
    legend('Crossplot','Linear regression (LR)','LR +/- std(X-Y)');
    axis([5000,30000,5000,30000]);
subplot(122), plot(Y,Y2,'g.');
    hold on
    plot(Y,a4(2)*Y+a4(1),'b-');
    plot(Y,a4(2)*Y+a4(1)-std(Y-Y2),'r-');
    plot(Y,a4(2)*Y+a4(1)+std(Y-Y2),'r-');
    grid;
    AX=title('Inversion 80% weight factor');
    LEG=findobj(AX,'type','text');
    set(LEG,'FontSize',14);
    xlabel ({'Single Cable';['Standard Deviation =',num2str(Std04)]});
    ylabel('Cable Combination');
    legend('Crossplot','Linear regression (LR)','LR +/- std(X-Y)');
    axis([5000,30000,5000,30000]);
```

2. *Wavelet difference*

```
% The code was developed to illustrate the difference between two different
% wavelets, respectively between wavelets from a seismic line acquired
% with a single cable receiver and a seismic line acquired with a cable
% combination receiver.
%
% The code have input data from a wavelet plot in Hampson-Russell STRATA,
% and uses cubic interpolation between the plot coordinates to make a
% smoother wavelet.
%
% The code is specified for 2 specific inputs, and is not dynamic.
%
%
% The code was created by
% Haakon Dyrnes
% For use in master thesis
% April, 2012


%% Clearing all parameters and closing all open files in MatLab
clear all; close all;


%% Reading the files
fid = fopen('H:\MASTER\MATLAB\wave_004_02.asc','r');
for i=1:26                                          % Skip 26 lines
    dum = fgetl(fid);
end
A = fscanf(fid,'%f',[1 inf])';


fid2 = fopen('H:\MASTER\MATLAB\wave_004_03.asc','r');
for i=1:26                                          % Skip 26 lines
    dum = fgetl(fid2);
end
A2 = fscanf(fid2,'%f',[1 inf])';


%% Creating a time-matrix
time=-96;
for i=1:1:50
    A(i,2)=time;
    A2(i,2)=time;
    time=time+4;
end




%% Refine the data
Time=A(:,2);
Time=linspace(-96,100,50);
Time2=A2(:,2);
Time2=linspace(-96,100,50);

nTime=linspace(-96,100,785);
```

```
nTime2=linspace(-96,100,785);

Wave=A(:,1);
Wave2=A2(:,1);

nWave=interp1(Time,Wave,nTime,'cubic');
nWave2=interp1(Time2,Wave2,nTime2,'cubic');

B=zeros(length(nWave),2);
B2=zeros(length(nWave2),2);

for i=1:length(nWave)
    B(i,1)=nWave(i);
    B2(i,1)=nWave2(i);
    B(i,2)=nTime(i);
    B2(i,2)=nTime2(i);
end



%% Find the positive values and negative values
nA=zeros(size(B));
nA2=zeros(size(B2));

indpos=find(nWave>=0);
indneg=find(nWave<0);
indpos2=find(nWave2>=0);
indneg2=find(nWave2<0);

nA(:,2)=nTime;
nA2(:,2)=nTime2;
nA(indpos,1)=nWave(indpos);
nA2(indpos2,1)=nWave2(indpos2);
nA(1,1)=0;
nA(length(nA),1)=0;
nA2(1,1)=0;
nA2(length(nA2),1)=0;



%% Plot the data
hf=fill(nTime2,nA2(:,1),'r');
    set(hf,'FaceAlpha',0.5);
    hold on;
plot(nTime2,nWave2,'r');
    fill(nTime,nA(:,1),'black');
    hold on
plot(nTime,nWave,'black');
    grid
    AX=title('Wavelet');
    LEG=findobj(AX,'type','text');
    set(LEG,'FontSize',14);
    xlabel('Time [ms]','fontsize',12), ylabel('Amplitude','fontsize',12);
    legend('Cable Combination','Response','Single Cable','Response');
```

3. *Difference in amplitude spectra*

```
% The program was developed to quantify the difference between the
% amplitude spectra from cable combination and single cable seismic.
%
% The code load 2 different amplitude spectra extracted from the Hampson
% Russell software package, STRATA, and plots the two different spectra on
% top of each other to investigate the differences between them.
%
% The code is specified for 2 specific inputs, and is hence not dynamic.
%
%
% The code was created by
% Haakon Dyrnes
% For use in the master`s thesis
% April, 2012


%% Reading the files
fid = fopen('H:\MASTER\Exports\Amp_spec_HR_00303','r');
for i=1:7                                           % Skip 14 lines
    dum = fgetl(fid);
end
A = fscanf(fid,'%f %f',[2 inf])';             % Read the rest of it

fed = fopen('H:\MASTER\Exports\Amp_spec_HR_00302','r');
for j=1:7                                           % Skip 14 lines
    dum2 = fgetl(fed);
end
A2 = fscanf(fed,'%f %f',[2 inf])';             % Read the rest of it



%% Setting the parameters

X=A(:,1);
Y=A(:,2);

X2=A2(:,1);
Y2=A2(:,2);



%% Refine the data

Notation=A(:,1);
Notation=linspace(0,125,131);

Notation2=A2(:,1);
Notation2=linspace(0,125,131);

nNotation=linspace(0,125,1001);
nNotation2=linspace(0,125,1001);

Frequency=A(:,2);
Frequency2=A2(:,2);
```

```
nFrequency=interp1(Notation, Frequency, nNotation, 'cubic');
nFrequency2=interp1(Notation2, Frequency2, nNotation2, 'cubic');

B=zeros(length(nFrequency),2);
B2=zeros(length(nFrequency2),2);

for i=1:length(nFrequency)
    B(i,1)=nNotation(i);
    B2(i,1)=nNotation2(i);
    B(i,2)=nFrequency(i);
    B2(i,2)=nFrequency2(i);
end




%% plot
figure;
    hold on;
    plot(B(:,1),B(:,2),'black-')
    plot(B2(:,1),B2(:,2),'r-');
    grid;
    axis([0,50,0,100000]);
    h_legend=legend('Cable Combination', 'Single Cable');
    set(h_legend,'FontSize',12);
    xlabel('Frequency [Hz]','FontSize',12);
    ylabel('Amplitude','FontSize',12);
    axes('Position',[0 0 1 1],'Xlim',[0 1],'Ylim',[0
1],'Box','off','Visible','off','Units','normalized', 'clipping' , 'off');
    text(0.5, 0.99,{'Amplitude
Spectrum';'Comparison'},'HorizontalAlignment'
,'center','VerticalAlignment', 'top','FontSize',14);
```

4. *Difference in vertical resolution*

```
% The code was developed to illustrate the difference in vertical
% resolution between 2 different wavelets. The wavelets is extracted from
% the Hampson Russell software package, STRATA, and is used to indicate
% changes in seismic due to two different acquisition methods, respectively
% using single cable receivers and the cable combination receivers.
%
% Because of the coarseness of the wavelet points from Hampson Russell, the
% code uses cubic interpolation to make the wavelets smoother.
%
% By adding a matrix with only zeroes, we are adding reflection
% coefficients to the matrix illustrating a pinch-out. The reflection
% coefficients are then convolved with the wavelet to illustrate the
% response given the two different wavelets. The area where we no longer
% can observe two responses, but move to one response, is the response
% where we have the critical point for the vertical resolution.
%
% The code is specified for 2 specific inputs, and is not dynamic.
%
%
% The code was created by
% Haakon Dyrnes
% For use in the master`s thesis
% April, 2012


%% Clearing all parameters and closing all open files in MatLab
clear all; close all;


%% Reading the files
fid = fopen('H:\MASTER\MATLAB\wave_003_02.asc','r');
for i=1:26                                          % Skip 26 lines
    dum = fgetl(fid);
end
A = fscanf(fid,'%f',[1 inf])';


fid2 = fopen('H:\MASTER\MATLAB\wave_003_03.asc','r');
for i=1:26                                          % Skip 26 lines
    dum = fgetl(fid2);
end
A2 = fscanf(fid2,'%f',[1 inf])';


%% Creating a time-matrix
time=-96;
for i=1:1:50
    A(i,2)=time;
    A2(i,2)=time;
    time=time+4;
end
```

```
%% Refine the data
Time=A(:,2);
Time=linspace(-96,100,50);
Time2=A2(:,2);
Time2=linspace(-96,100,50);

nTime=linspace(-96,100,197);
nTime2=linspace(-96,100,197);

Wave=A(:,1);
Wave2=A2(:,1);

nWave=interp1(Time,Wave,nTime,'cubic');
nWave2=interp1(Time2,Wave2,nTime2,'cubic');

B=zeros(length(nWave),2);
B2=zeros(length(nWave2),2);

for i=1:length(nWave)
    B(i,1)=nWave(i);
    B2(i,1)=nWave2(i);
    B(i,2)=nTime(i);
    B2(i,2)=nTime2(i);
end

B(1,1)=0;
B(length(B),1)=0;
B2(1,1)=0;
B2(length(B2),1)=0;


%% Creating the matrix

R=zeros(306,100);
R(105,:)=1;
R2=zeros(306,100);
R2(105,:)=1;

for i=1:100
    R(105+i,i)=1;
end

for i=1:100
    R2(105+i,i)=1;
end

w=nWave';
w2=nWave2';

Seis=convn(R,w,'same');
Seis2=convn(R2,w2,'same');

figure;
    hold on;
        for i=1:100
            plot(i*ones(306,1)+0.0001*Seis(:,i),1:306)
        end
    set(gca,'ydir','reverse')
    %grid(gca,'minor');
```

```
    box on;
    axis tight
    xlabel({'';'Time [ms]'},'FontSize',12);
    h_legend=legend('Single cable response');
    set(h_legend,'FontSize',12);
    axes('Position',[0 0 1 1],'Xlim',[0 1],'Ylim',[0
1],'Box','off','Visible','off','Units','normalized', 'clipping' , 'off');
    text(0.5, 0.99,{'Response of a pinch-out [Single Cable]';'Zero-phase
wavelet'},'HorizontalAlignment' ,'center','VerticalAlignment',
'top','FontSize',14);


figure(2);
    hold on;
        for i=1:100
            plot(i*ones(306,1)+0.0001*Seis2(:,i),1:306)
        end
    set(gca,'ydir','reverse')
    %grid(gca,'minor');
    box on;
    axis tight
    xlabel({'';'Time [ms]'},'FontSize',12);
    h_legend=legend('Cable Combination response');
    set(h_legend,'FontSize',12);
    axes('Position',[0 0 1 1],'Xlim',[0 1],'Ylim',[0
1],'Box','off','Visible','off','Units','normalized', 'clipping' , 'off');
    text(0.5, 0.99,{'Response of a pinch-out [Cable Combination]';'Zero-
phase wavelet'},'HorizontalAlignment' ,'center','VerticalAlignment',
'top','FontSize',14);


figure(3);
    hold on;
        for i=1:100
            plot(i*ones(306,1)+0.0001*Seis2(:,i),1:306,'b')
            plot(i*ones(306,1)+0.0001*Seis(:,i),1:306,'r')
        end
    set(gca,'ydir','reverse')
    %grid(gca,'minor');
    box on;
    axis tight
    xlabel({'';'Time [ms]'},'FontSize',12);
    h_legend=legend('Cable Combination response','Single Cable response');
    set(h_legend,'FontSize',12);
    axes('Position',[0 0 1 1],'Xlim',[0 1],'Ylim',[0
1],'Box','off','Visible','off','Units','normalized', 'clipping' , 'off');
    text(0.5, 0.99,{'Response of a pinch-out [Compared]';'Zero-phase
wavelets'},'HorizontalAlignment' ,'center','VerticalAlignment',
'top','FontSize',14);
```